On the coupling of noisy processes in biology to produce functional phenotypic variability

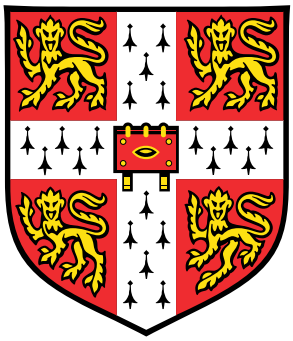

Om Patange

Department of Biochemistry
University of Cambridge

This dissertation is submitted for the degree of
Doctor of Philosophy

Gonville and Caius College September 2018

Declaration

I hereby declare that except where specific reference is made to the work of others, the contents of this dissertation are original and have not been submitted in whole or in part for consideration for any other degree or qualification in this, or any other university. This dissertation is my own work and contains nothing which is the outcome of work done in collaboration with others, except as specified in the text and Acknowledgements. This dissertation contains fewer than 60,000 words including appendices, bibliography, footnotes, tables and equations and has fewer than 150 figures.

Om Patange
September 2018

Abstract

Noise is ubiquitous in biology. Recent studies have demonstrated that both gene expression and physiological processes, such as growth, can be noisy. The cell-to-cell variation resulting from this stochasticity has been implicated in survival strategies for bacterial populations. However, it remains unclear how single cells couple gene expression with growth to implement these strategies. In this thesis we show how noisy expression of a key stress response regulator, RpoS, allows *E. coli* to modulate its noisy growth dynamics to survive future adverse environments. We first demonstrate that single cells in bulk, exponential phase cultures have heterogeneous *rpoS* expression. Combining microfluidics and time-lapse microscopy we reveal multi-generation RpoS activity pulses are responsible for this heterogeneity. We next show that RpoS and growth have stochastic dynamics and are anti-correlated. With a stochastic simulation of chemical reactions coupled to a deterministic cell growth model we show that a mutual inhibition loop between RpoS activity and growth rate is sufficient to capture the observed dynamics. We test our model by performing experimental perturbations and find good agreement between theory and experiment. Next, we demonstrate the functionality of this phenotypic variability by using the microfluidic platform to apply a short, intense period of oxidative stress. By tracking cells prior to the stress and testing for survival after the stress we reveal that *E. coli* prepare for sudden stressful events by entering prolonged periods of slow growth mediated by RpoS. This dynamic phenotype is captured by the RpoS-growth feedback model. Our synthesis of noisy gene expression, growth, and survival paves the way for further exploration of functional phenotypic variability.

I dedicate this thesis to my mother.

Acknowledgements

First and foremost I thank my supervisor, James Locke. I am grateful that he hired me in the first place and has accommodated my odd working habits since. James is a constant source of clever ideas and hypotheses, indeed one such hypothesis sparked this entire project. James is always generous with his time and resources. I learned to appreciate subtleties in data, both of mine and others, by observing him work. It is a joy to work with him.

I was generously supported by a PhD Scholarship from Microsoft Research and co-supervised by Andrew Phillips. I thank Andrew for valuable discussions as well as for giving me the opportunity to intern at Microsoft Research. Working with my old mentor and friend Paul Grant on spatial patterning of bacteria was a pleasure. I thank Paul for patiently teaching me molecular biology and mentoring my transition to biology, and Jim Haseloff for allowing me the time to make the transition in his lab when I first arrived in Cambridge.

The Sainsbury Laboratory has been an incredible environment to work in. I was able to pursue research on bacteria despite being in a plant sciences institute. I thank all the staff and researchers for making work at the SLCU so pleasant. Douglas Griffith was a great help doing much of the molecular biology and challenging me with insightful questions. Casandra Villava took up the torch after Douglas, adding her own flair and cheer. This project would have taken much longer to complete without both of their help. Chris Schwall patiently showed me the tools available for single-cell research in the Locke lab during my first year. Chris then boldly established the microfluidics facilities at the SLCU, which I gladly took advantage of. I thank Pau Formosa-Jordan for his wonderful company, especially in the late hours at the lab, and for taking the time to listen and debate some of my more outlandish thoughts. Bruno Martins has been a constant source of inspiration in the way he does science. I am always glad to have his company. For several years I had the privilege of being deskmates with Niall Murphy. His childlike wonder at all things interesting was motivational. I thank all members of the Locke group, past and present, for their friendship and stimulating discussion.

My family has been a pillar of support throughout my life. I would not have had the courage, nor the inclination, to move countries and start work in a foreign field without the lessons my parents imparted to me. I thank them for everything. I am proud of my little sister. Her adventurous spirit and mature sensibility are an inspiration to me.

I thank my college, Gonville and Caius, for providing an intellectually stimulating environment outside of the lab. I am grateful for all the friendships I made dining in Hall so often and at my home in college, Cobwebs. I cherish my friends in the Old Science Society, especially Sasha Blackwell, Patrick Diaz, and Michael Kosicki. Participation in Old Science has furnished me with as much a breadth of education in biology as my PhD has provided depth. Our weekend coffee shop meetings have been a highlight of my time here.

Cambridge has transformed me in many wonderful ways. I transitioned from a physicist studying inanimate matter to one studying animate matter here. Under the guidance of the coaches at Crossfit Cambridgeshire I metamorphised from obese to not. Thank you Lee, James, Phill, and Josh!

Perhaps most surprising of all my transformations, and most wonderful of all, I fell in love. I cannot imagine life without Giulia. I thank her for putting up with all the trials and tribulations that have been involved in producing this thesis and for her loving support. I look forward to our post-thesis future :D.

I gratefully acknowledge that I downloaded the template for this report from the Cambridge University Engineering Department; the template was authored by Krishna Kumar.

The results in this thesis are an expanded version of a paper published in *Nature Communications* (doi: 10.1038/s41467-018-07702-z) and available as a preprint on bioRxiv (doi: 10.1101/265801), prepared in collaboration with Christian Schwall, Matt Jones, Casandra Villava, Douglas Griffith, Andrew Phillips, and James Locke. Matt Jones submitted some of these results as part of his Part III Systems Biology thesis. The data presented in Chapter 6 was prepared in collaboration with Alex Bailey, which he also prepared as part of his Part III Systems Biology thesis. Both of these theses were under my co-supervision with James Locke. Some strains used in this thesis were kind gifts of Kenn Gerdes and Herb Schellhorne. The pDR111 plasmid was a kind gift of David Rudner. JT Saul and Suckjoon Jun provided a mould to create the Mother Machine microfluidic devices, via Chris Schwall. I am grateful to all of my collaborators. I thank James Locke, Pau Formosa-Jordan, and Giulia Arsuffi for critically reading my thesis. Finally, I thank Pietro Cicuta and Jordi Garcia-Ojalvo for a stimulating and thorough *viva voce*. I am grateful for all their suggestions on ways to improve this thesis.

Table of contents

List of figures

List of tables

Chapter 1

Introduction

1.1 Noise in biology

1.1.1 What is noise?

Colloquially, noise is what you hear but would rather not - such as the voices and music in a cafe other than the sound of your conversation partner. More precisely, noise, or stochasticity, is the random variation in a process. When a song plays on a speaker, noise is the vibration of the membrane in addition to that needed to make the sound of the notes (Fig. 1.1). In this thesis, we explore noise in biology and its role in generating functional phenotypic variability.

1.1.2 Functional phenotypic variability

What is a phenotype? It is the form and function of an organism. It is the shape of the Finches' beaks, the five fingers on our hands, the ability to write poetry and analyse the universe with mathematics. In contrast, a genotype is simply the sequence of nucleotides comprising an organism's genetic material, its genome.

The phenotype of organisms can vary due to changes in their genomes arising from procesess such as mutation and recombination. Evolution can act on this phenotype to propagate or abolish the genome. The modern synthesis has established this central role of genotypic variability in evolution [1]. In contrast, a single genome can give rise to many phenotypes. This is apparent in the development of multicellular organisms with differentiated cell types [2, 3]. The same genome can also give rise to varied phenotypes in response to environmental cues [4, 5]. Another category of phenotypic variability, and the main focus of this thesis, can arise from stochastic molecular interactions, leading to, for instance, stochastic gene expression. That is, considering a population of undifferentiated, clonal cells in a constant environment, individual cells may still have different phenotypes. Phenotypic variability due to stochastic molecular processes has been observed in a wide range

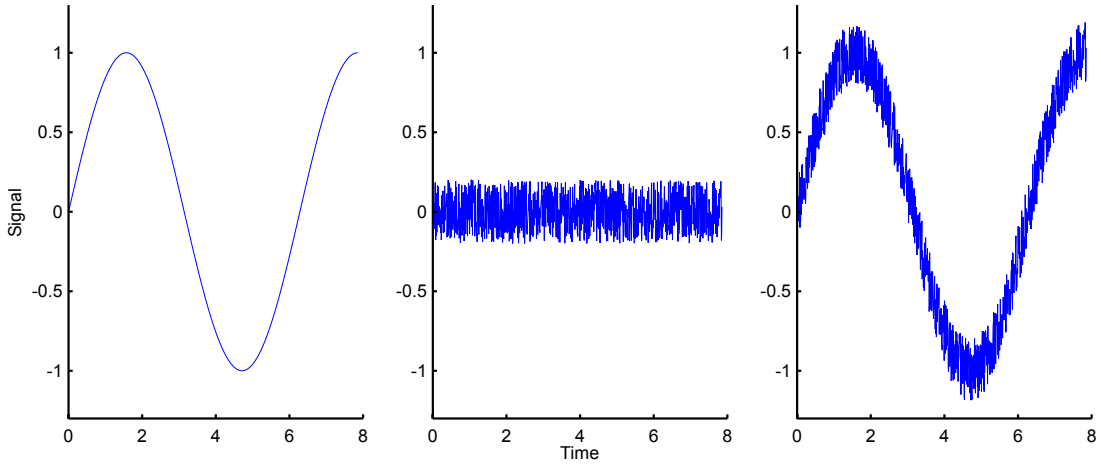

Fig. 1.1 Illustration of noise on a signal. From left to right are signal, noise, and signal+noise. The signal is a simple sinusoid representing a single note of sound. The noise is random numbers drawn from a uniform distribution from -0.2 to 0.2. The signal+noise is representative of a noisy signal.

of cells including archaea [6], bacteria [7–13], funghi [14, 15], animals [16], and plants [17]. Similarly, multicellular organisms have also been shown to exhibit stochastic phenotypic variability between individuals including in funghi [18], animals [19], and plants [20, 21], although the mechanisms of variability are less well understood than in the case of single cells.

Phenotypic variability has been shown to be functional as well [22, 23]. For instance, *Lactococcus lactis* prepare for different sugar environments heterogeneously [11], and *Staphylococcus pyogenes* infections persist against penicillin treatment phenotypically [7] as do *Escherichia coli* [8]. The tuberculosis causing bacteria, *Mycobacterium tuberculosis*, have also been shown to avoid the effects of antibiotics phenotypically [24]. Engineered yeast that are able to switch between two metabolic phenotypes have been shown to survive in fluctuating environments matching the phenotype switching rates [15]. More complex eukaryotic organisms also have been shown to use stochasticity. Desert plants have been shown to vary their germination times to save seeds for potentially better growing environments [20]. Cancer cells evade death by chemotherapy by entering different phenotypic states [16].

The most prominent example of the functional use of noise is, perhaps, that of bet-hedging by bacteria. Bet-hedging is a strategy wherein populations of organisms distribute the costs and benefits of different phenotypes over subpopulations to improve their fitness to unpredictable environments [23, 25]. During the course of World War II Joseph Bigger investigated why penicillin treatment sometimes failed to clear patients of a *Staphylococcus* infection [7]. By treating *in vitro* cultures with penicillin under various growth conditions he discovered that a small fraction of cells were entering a non-dividing state that was less

susceptible to the drug. He termed the cells persisters, distinct from resistant cells. For persisters gave rise to progeny that were susceptible to drug treatment, indicating a lack of resistance mutation. Decades later, a modern microfluidics experiment, using *E. coli*, showed that single cells in a growing population were entering this phenotypic protective state [8]. By partitioning their population into a growth arrested, protected state and a fast growing, susceptible state, the bacteria hedge their bets against future antibiotic attack while still taking advantage of nurturing environments.

1.1.3 Single-cell approaches reveal noisy bacteria

Single-cell approaches have been essential for revealing the role of noise in biology, as bulk studies can mask dynamic and heterogeneous gene expression [26]. Single cells can be examined in isolation or as members of a colony. In isolation, the autonomous behaviour of cells can be investigated, absent of cell-to-cell interaction [27–29]. Considering single cells in a collection can allow the interrogation of emergent phenomena, such as those arising by mechanical coupling [30, 31], chemical interaction [32–34], or even electrical coupling [35].

Single-cell techniques

Heroic workers in the past investigated single-cell heterogeneity by diluting cultures to single cells and observing the resulting populations [36]. Subsequently, techniques such as flow cytometry and single-cell RNAseq have been used [37]. While these methods can reveal heterogeneity in a population, they do so at a single point in time. More recently, single-cell microscopy techniques have been developed to track gene expression via fluorescent reporters, which have revealed rich dynamics [38–40]. For example, *Bacillus subtilis* has been found to respond to stress using frequency modulated stochastic pulses of a key transcriptional regulator, σ^B [39]. These early time-lapse studies were limited in the durations of experiments since the culturing method resulted in cells growing in 3D microcolonies, negating the single-cell advantage. The ability to culture cells in patterned, soft, polymer microfluidic devices allowed single cells to be tracked over many generations [41]. The earliest device confined cells in linear grooves, which would eventually fill up with the newly grown cells [8]. Later devices improved on this design by allowing cells to be washed away by a flow of media that also supplied the confined cells [42, 43].

Mother Machine

Of particular importance for this thesis is the microfluidic device known as the Mother Machine [27]. It was invented by the team of Suckjoon Jun to investigate a classic problem in bacteriology - do *E. coli* age? In particular Jun sought to discover if there was a prefered pole

of the bacteria that would collect detritus from the cell and eventually die, or whether the two poles of *E. coli* were symmetric. They solved the problem by, in principle, reducing a test tube in size such that it could fit a single cell at the bottom. This cell was then constantly supplied with fresh media and observed with time-lapse microscopy allowing Jun to interrogate many generations of cells. They found the cells divide symmetrically [27]. Jun went on to discover that *E. coli* divide using the so-called adder rule, dividing once they have added a fixed volume since their last division [44]. The Mother Machine is now widely used to discover phenomena that become apparent only when processes are considered over extended periods of time encompasing many cell divisions [28, 45, 46, 29].

1.1.4 The molecular origin of noisy gene expression

The pervasiveness of noisy gene expression lies in its origin. It arises from the random collisions due to thermal fluctuations of small concentrations of regulators, polymerases, and nucleic acids in cells [47–50]. Consider the process of transcription of a gene. An RNA polymerase molecule must collide with a stretch of DNA tens of base pairs long, in the correct orientation, to initiate transcription. There may be only one copy of this bit of DNA, and a handful of RNAP available for this task (Tab. 1.1 and Fig. 1.2). Thus, the interaction of these two types of particles will be inherently stochastic. There are a host of other molecular processes that could also lead to stochastic phenotypic variability. In the hypothetical scenario where precise numbers of protein products were made for each gene, it could still be the case that variation in the concentration of small particles such as metabolites and ions could lead to variable phenotypes from cell-to-cell. In this thesis, we focus on variability arising from stochastic gene expression and lump these other possible sources of noise into gene expression.

A high-throughput approach was recently used to show that genes in *E. coli* were, in fact, noisy [51] (Fig. 1.3). Taniguchi *et al.* found the variation in numbers of mRNA and proteins scaled inversely with the numbers of these molecules for each gene. This would be expected if the noise arose from thermal fluctuations in the processes of transcription and translation ('intrinsic noise limit' in Fig. 1.3). For proteins expressed in large numbers, where noise might be expected to be low, they found a lower limit of noise, which they termed the 'extrinsic noise limit'. This limit likely arises from fluctuations in the concentrations of key components of the cell governing its physiology, such as metabolic enzymes, metabolites, and polymerases.

1.1.5 Modelling noise mathematically

Mathematical models in science allow one to encode assumptions about physical systems with precision. With tools from mathematics, one can then test the consequences of the assumptions, often in ways that would be impossible with descriptive, qualitative models.

Table 1.1 Numbers involved in the Central Dogma operating in *E. coli* [52]

Molecule	Number per cell	Concentration	Number per gene
Genes	~4,500	-	-
RNAP	~8,000	~8 mM	~2
Active RNAP	~2,000	~2 mM	< 1
Ribosomes	~50,000	~50 mM	~10

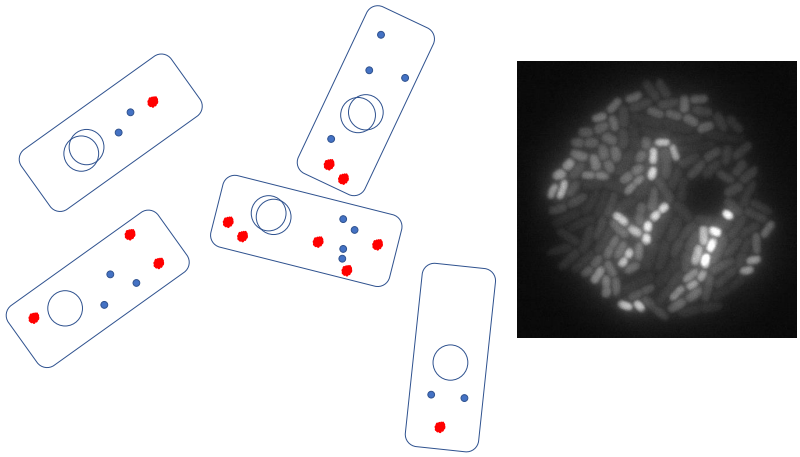

Fig. 1.2 Schematic of the source of noise and illustration of its existence. The schematic on the left represents the small copy number of genes (chromosomes represented as circles) and the resulting mRNA (blue dots) leading to heterogeneous expression of a protein (red dots). On the right is an example of a microcolony of clonal *E. coli* cells with heterogeneous gene expression.

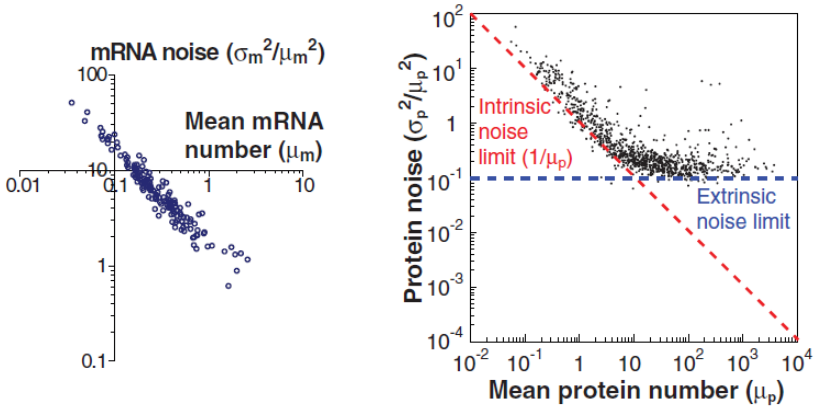

Fig. 1.3 Many genes in *E. coli* are noisy, figure adapted from [51], with permission. Each dot represents a gene. Noise in both mRNA and protein number scales inversely with molecule number. At large protein number there is a lower limit to the observed noise.

However, for such a theoretical endeavour to be fruitful the appropriate elements of the physical system must be ignored, both to produce a tractable model as well as to generate insights on the dominant mechanisms underlying observations. For instance, in developing the theory of gravity, Newton chose to ignore the heterogeneous composition of celestial bodies, in fact he chose to ignore their finite extent as well! By reducing objects as large as the Earth and the Sun to infinitesimal points, he encoded the assumption that the value of a single quantity the objects posses, their masses (m), together with the distance separating them (r), was sufficient to explain the force of attraction between the two objects [1]:

$$F_G = \frac{G \cdot m_1 \cdot m_2}{r^2} \tag{1.1}$$

Biology is a complex phenomenon, with many details amenable to mathematical treatment [54]. In the past, workers have gleaned insights with mathematics at various levels of details spanning the atomic to the ecological scales. The theory of x-ray scattering off atoms led to the identification of the atomic nature of genes [55, 56] and the discovery of the structure of DNA [57–59]. Ignoring the detailed interactions of molecules, Turing focused instead on abstract networks of molecular interactions coupled with diffusion to demonstrate the chemical basis of morphogenesis [60]. Turing showed that instead of blurring the boundaries between domains, as would be expected of a diffusive process alone, his system could give rise to domains with sharp boundaries [60, 61]. Hodgkin and Huxley reduced the details of ion pumps and membrane potentials to a simple lumped-element electrical circuit, which they analysed to explain the way in which neurons transmit information [62]. Lotka modelled the population sizes of a plant species and an animal species consuming the plant with simple differential equations [63]. By analysing these equations he showed the populations can continue to oscillate in size indefinitely [63].

In this thesis we want to encode our assumptions on the coupling of two noisy processes in a mathematical model. Given the molecular origin of noise in biology we will naturally choose to model chemical reactions. However, there are several levels of details that we must choose to consider or ignore. Should we consider molecular collisions and model the orientation of molecules to determine the fate of the reaction; or simply use an abstract reaction rate? Should we consider all the steps of the Central Dogma, transcription, translation, and their regulation; or should we lump these steps into an effective protein production step? Should we consider the spatial extent in which all of these chemical reactions happen; or should we ignore the spatial dimension and consider only the time evolution?

In Chapter 4 we shall choose to largely ignore the spatial dimension and lump the process of gene expression into abstract chemical reactions. There are several ways to formally express these assumptions, each with its pros and cons [64]. In the limit of high concen-

[1] See Chapter 9, Volume 1 of the Feynman Lectures for another, similar, example of Newton's genius for ignoring the right details [53].

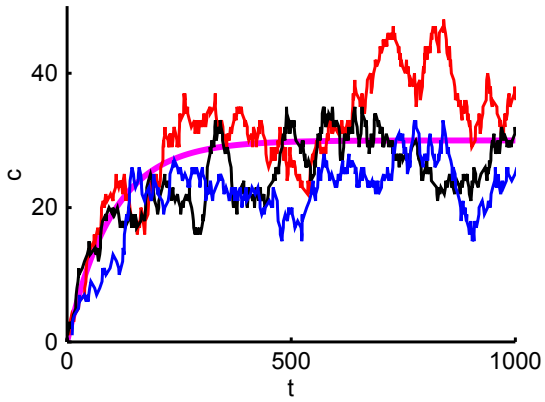

Fig. 1.4 Deterministic versus stochastic simulation illustration. The magenta line is the solution to Eq 1.2 presented in the text, with $k_p = 0.3$ and $k_d = 0.01$. The blue, black, and red traces are three separate simulations from the Gillespie algorithm for the same parameters.

trations of molecules, the appropriate formalism is a deterministic ordinary differential equation, for example:

$$\frac{dc}{dt} = k_p - k_d \cdot c \tag{1.2}$$

This equation represents the concentration (c) of a molecular species increasing at a constant rate k_p and decreasing at a rate dependent on the current concentration $k_d \cdot c$. Equation 1.2 has an analytical solution, $c(t) = \frac{k_p}{k_d}(1 - e^{-k_d t})$, making further analysis straightforward. For instance, we can read off the solution that the steady state concentration will be $\frac{k_p}{k_d}$ and will be reached in a characteristic time $\frac{1}{k_d}$ (see Fig. 1.4). However, it fails to capture the stochastic fluctuations that arise in the limit of low concentrations.

One approach to solve this problem is to add a noise term to the ordinary differential equation, η, to produce a stochastic differential equation:

$$\frac{dc}{dt} = k_p - k_d \cdot c + \eta \tag{1.3}$$

Alternatively, instead of modelling the concentration of the molecule, one can model the *probability*, P_m, that the molecule will be present in a given number (m), using the Chemical Master Equation (CME) [64]:

$$\frac{dP_m}{dt} = k_p \cdot [P_{m-1} - P_m] + k_d \cdot [(m+1) \cdot P_{m+1} - m \cdot P_m] \tag{1.4}$$

Both of these formulations have analytical solutions for the simple example used here. However, for slightly more complicated situations, for example, involving more chemical reactions, the analytical solutions are challenging to find. We must then rely on numerical techniques to find approximate solutions to these differential equations.

In the 1970s Daniel Gillespie formulated the Stochastic Simulation Algorithm (SSA, or Gillespie algorithm) [65, 47] as an alternative, exact solution to the CME. Instead of modelling the probability of a number of molecules existing at a given time, the Gillespie algorithm directly simulates trajectories of molecule numbers resulting from the chemical reactions (see Fig. 1.4). Starting with an initial number of molecules, the algorithm uses a uniform random number, r_1, to simulate the exponentially distributed probability of the time to next reaction, $P(\tau) = a_0 \exp(-a_0\tau)$, giving τ:

$$\tau = \frac{1}{a_0} \ln \frac{1}{r_1} \tag{1.5}$$

where a_0 is the sum of all reaction propensities; $a_0 = k_p + m * k_d$ in the simple case above. The algorithm uses a second uniform random number, r_2, to simulate the probability distribution of which reaction happens next, $P(i^{th}\text{reaction}) = a_i/a_0$, where $a_1 = k_p$ and $a_2 = m * k_d$ in the above example. The μ^{th} reaction is chosen such that:

$$\sum_{i=1}^{\mu-1} a_i < r_2 a_0 \leq \sum_{i=}^{\mu} a_i \tag{1.6}$$

The statistics calculated from all such trajectories are an exact representation of the probability evolution captured in the CME. We chose to use the Gillespie algorithm in this thesis in combination with a cellular growth model, described in detail in Chapter 4.

1.2 Model system to study coupling of noisy processes

Escherichia coli is an ideal model organism in which to study how noisy processes might couple to produce functional phenotypic variability. Its genome, genetics and biochemistry have been well characterized and molecular biology techniques to manipulate *E. coli* are mature [66]. As we have seen in Section 1.1.4, genes in *E. coli* are known to be noisy. Furthermore, the stress response system of *E. coli* has been carefully studied for decades [67, 68], and we will show in Chapter 3 that its regulation is noisy. In recent times, *E. coli* has been a preferred organism to explore dynamic phenomena at the single-cell level [8, 69, 27, 70, 45, 44, 71, 46]. These studies have revealed, among other things, that *E. coli* growth is noisy [70, 71]. In this thesis we will study how the noisy stress response of *E. coli* can couple with its noisy growth to produce a functional phenotype (Fig. 1.5).

1.2.1 *E. coli* general stress response system, RpoS

E. coli must defend against many stresses in its environment, such as oxidative stress, acid stress, osmotic stress, heat shock, *etc.* [67]. It has evolved systems that sense and protect it from these dangers. For example, the catalase gene, *katG*, is expressed in the presence of

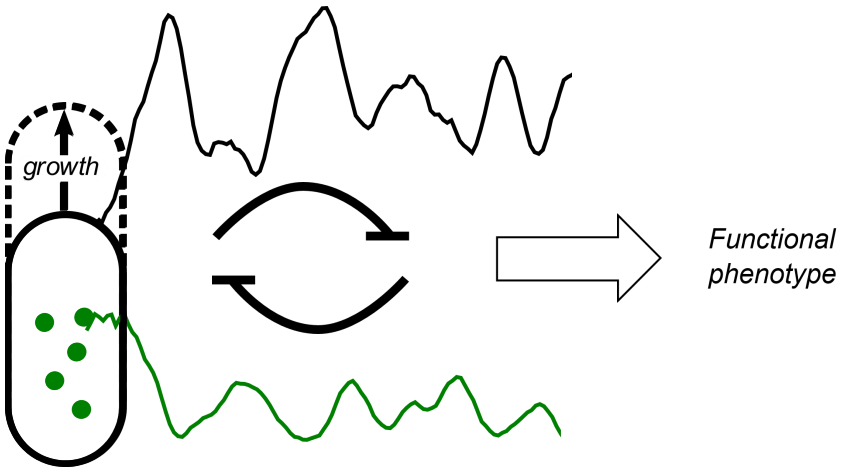

Fig. 1.5 Graphical Abstract. In this thesis we will show how noisy growth and noisy gene expression can couple to generate a functional phenotype.

oxidative stress, and upregulated by the sensory OxyR system [72, 73]. In addition to specific responses, *E. coli* has evolved a general stress response system, regulated by the gene *rpoS* [74]. This gene was discovered several times as the regulator of response to specific stresses (see Timeline in Table 1.2). However, in the 90's RpoS was recognised as a master regulator of the general stress response system [75]. When RpoS levels are high, many genes are activated allowing the cells to survive multiple stresses (Fig. 1.6). For example, the catalase gene, *katE*, is under RpoS control [76], as is a system for protection against osmotic stress [77]. Functionally, the status of RpoS as a master regulator was established when it was shown that induction of RpoS by one stress subsequently enhanced the cells' ability to survive a different stress (Fig. 1.7) [77].

The molecular nature of RpoS also reflects its role as a master regulator. It is an alternative sigma factor [78]. Sigma factors are a component of the RNA polymerase holoenzyme that recognise and bind to the promoter region of genes [74], thus regulating the transcriptional activity of the cell (Fig 1.6). *E. coli* has a primary, housekeeping sigma factor, σ^{70}, which promotes the transcription of gene essential for processes such as growth, replication, and metabolism [79]. There are six alternative sigma factors. Five are responsible for upregulating genes necessary for survival against specific stresses (Tab. 1.3). RpoS is the primary alternative sigma factor, responsible for upregulating a large, general stress response regulon [79].

In the seminal study that identified *rpoS* as the master stress response regulator, RpoS expression was induced by starving cells of carbon [75]. Similarly, when cells are depleted of resources, in stationary phase, RpoS expression is induced (***rpoS***: **R**NA **po**lymerase, sigma **S** = Starvation or Stationary phase [75], see Figure 1.8). In contrast, when an *E. coli* culture is started, after a lag phase, cells enter exponential phase due to the abundance of resources,

Table 1.2 Timeline of key discoveries related to RpoS

1953	Structure of DNA discovered [57–59]
1959-61	RNA polymerase discovered [82]
1969	Discovery of sigma factors [83]
1984-5	*rpoS* discovered as *katF* [84, 85]
1986	Many genes upregulated in carbon starved *E. coli* [86] and *rpoS* discovered as *appR* [87]
1988	Starved cells heat shock and H_2O_2 resistant [88]
1989	*katF* sequenced, found to have high homology to sigma factors [78]
1991	*rpoS* named and discovered to be identical to *katF* and *appR* [75]
1993	*rpoS* cloned [89] and induced RpoS shown to protect against different subsequent stress [77]
1994	RpoS regulated at every level [90]
1995	RpoS purified, resulting reconsituted RNAP holoenzyme transcribed *in vitro* [91]

where the population increases directly proportional to the number of cells already present. In this scenario, very little RpoS is expressed, while σ^{70} expression is high (Fig. 1.8) [80]. However, RpoS expressed in exponential phase has been shown to be functional [81]. In this thesis, the first noisy process we consider is the expression of RpoS in exponential phase cells.

1.2.2 *E. coli* grows noisily

The second process we consider is the growth of the cell. The growth of *E. coli* and related bacteria has been a subject of investigation for more than a century. Early work revealed the different phases of growth of *E. coli* populations such as exponential and stationary phase [92, 93] (Fig. 1.8). In the middle of the 20^{th} century work turned to carefully growing cells in steady state in exponential phase [94]. Robust phenomenology about populations of cells was revealed by this work, such as the principle that the average mass of cells is an exponential function of the growth rate of the population [95]. Such phenomena have been investigated and confirmed at the single-cell level in recent studies (see Sec. 1.1.3).

However, and most importantly for this thesis, the recent single-cell investigations have revealed wide-spread heterogeneity in the growth of cells - both between cells in a population and in time for single cells [44, 70, 71]. For instance, using the Mother Machine

Table 1.3 The sigma factors of *E. coli* [66]

Sigma factor	Synonyms	Function
σ^{70}	*rpoD*, σ^{D}	Primary, housekeeping sigma factor
rpoS	σ^{38}, σ^{S}, *katF, appR, otsX, adrB, csi2, dpeB, nur*	Main secondary sigma factor, governs general stress response
σ^{E}	σ^{24}	Extreme heat shock
σ^{F}	σ^{28}, *fliA*	Flagella production
σ^{H}	σ^{32}, *rpoH*	Heat shock
σ^{N}	σ^{54}, *rpoN*	Nitrogen limitation
fecI	σ^{19}	Iron transport

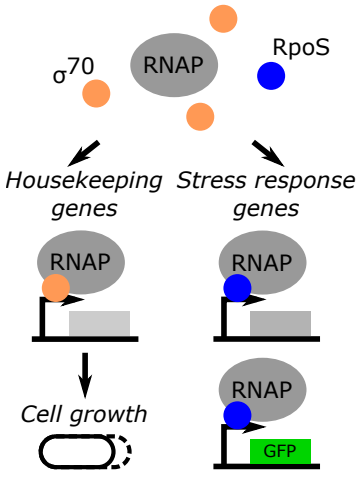

Fig. 1.6 Schematic of the role of sigma factors σ^{70} and RpoS in promoting growth and activation of the stress response regulon, respectively. Also illustrated is the RpoS reporter, a transcriptional fusion to a stress response promoter (see Fig. 2.1 in Sec. 2.1.3).

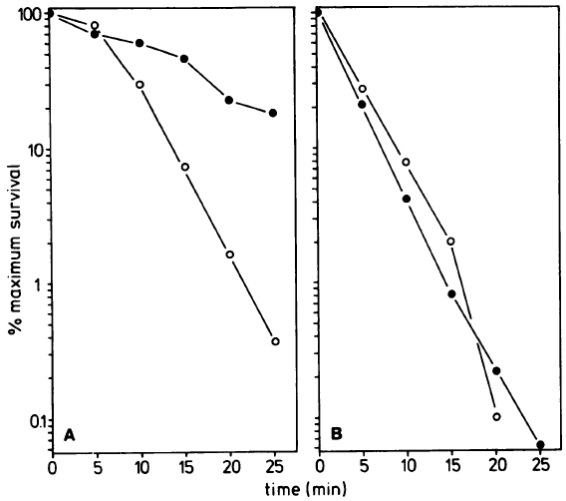

Fig. 1.7 Literature data showing enhanced survival after RpoS induction. This is figure 4 of reference [77], reproduced with permission. The original caption reads: "Osmotic induction of H_2O_2 resistance. Strains MC4100 (A) and RH90 (B), grown for 90 min in the presence (solid circle) or absence (open circle) of 0.3 M NaCl, were exposed to 15 mM H_2O_2. Viable cell numbers were determined as CFU by plating appropriately diluted aliquots on LB plates." A is *WT* and B is Δ*rpoS*. In addition to generality of the RpoS stress response, this figure indicates that Δ*rpoS* cells are more susceptible than WT cells to oxidative stress in exponential phase. Consider the open circles and compare survival percent from Figure A (*WT*) and B (Δ*rpoS*) at 20 minutes. Our single-cell analysis in Chapter 5 sheds light on the details of this difference in survival.

microfluidic device, Taheri-Araghi *et al.* showed that the average size of new-born *E. coli* cells is an exponential function of the population growth rate, as would be expected (see Fig. 1.9a) [95, 44]. However, the individual cells comprising the average come from a wide distribution that does not obey the same exponential relation to population growth rate (1.9a) [44]. Similarly, one might expect the growth rate of *E. coli* to be inversely proportional to the time the cells take to divide. Indeed, Kennard *et al.* found this to be the case for averages of single-cell data [71] (see Fig. 1.9b). However, they found individual cells deviated strongly from this population trend, especially at fast growth rates [71] (Fig. 1.9b). Kiviet *et al.* explicitly illustrated that the growth rate of a single *E. coli* cell can fluctuate in time as a consequence of metabolic stochasticity [70] (see Fig. 1.9c). This is remarkable since a physiological process such as growth is the product of many genes and metabolites, many of which will be regulated and be present in large numbers. Considering much longer time scales, Tanouchi *et al.* observed oscillations in cell size along individual lineages with a period on the order of 10 generations [45]. They found a phenomenological model of future length being linearly proportional to current lenght with the addition of a noise term captured their data [45]. The phenomenon of noisy growth has been observed more widely as well, including in archea [6] and *B. subtilis* [12].

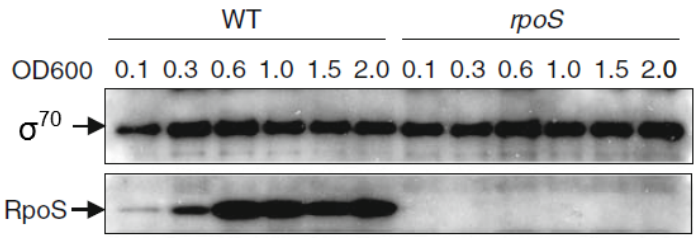

(a)

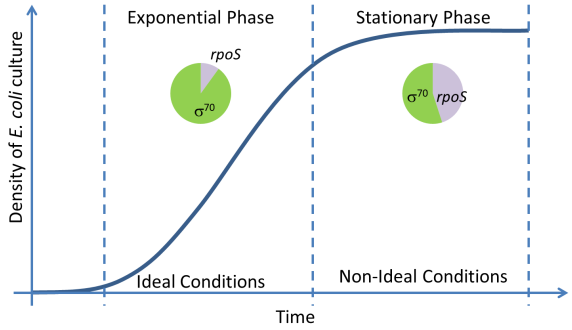

(b)

Fig. 1.8 Bulk culture data showing exponential phase cells express low levels of RpoS. a) Western blot analysis, adapted from [80], with permission, shows *rpoS* levels increasing as cells transition from exponential phase to stationary phase. b) A schematic representation of the data. The solid line represents the growth curve of a bulk culture of *E. coli*, the pie charts represent the fraction of the sigma factors present in bulk cultures in the two growth phases.

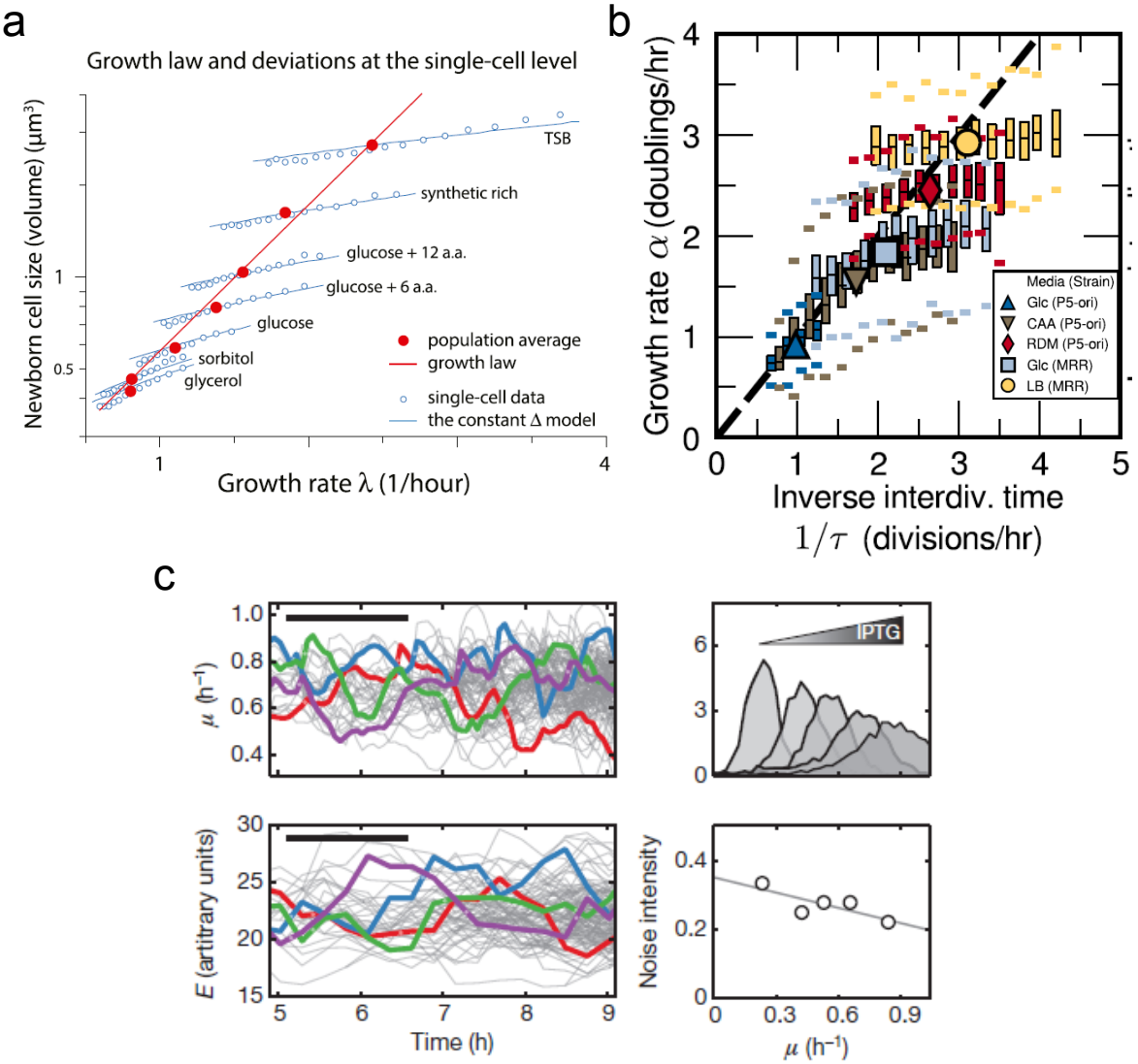

Fig. 1.9 Literature data showing noisy *E. coli* growth. a, Taheri-Araghi *et al.* showed single cells follow a classic bacterial growth law on average (red line and poitns), but diverge from it in detail, exhibiting single-cell heterogeneity (blue circles). Figure adapted from [44], with permission. The different growth rates were achieved by changing media conditions. b, Kennard *et al.* showed that growth rate and the time cells take to divide are inversely proportional on average (large symbols), but heterogeneous at the single-cell level (box plots). Figure adapted from [71], with permission. The different colours represent different growth conditions and strains used. c, Kiviet *et al.* showed that single cells can have noisy growth (μ) and gene expression (E) in time that arises from stochasticity in the cell metabolism. Figure adapted from [70], with permission. The figure shows single-cell traces on the left, growth rate histograms on the top right and coefficients of variation ('Noise intensity') for various growth rates. The growth rate was controlled by an IPTG inducible *lac* operon and feeding cells with lactuolose, a lactose analogue.

1.3 Outline of thesis

Populations of *E. coli* in exponential phase have been shown to express small amounts of functional RpoS [75, 80]. However, these studies were of bulk cultures, which can mask single-cell phenotypes. Here we take a single-cell approach to uncover heterogeneous expression of RpoS in exponential phase *E. coli* [38]. We reveal the pulsatile dynamics that give rise to RpoS heterogeneity by tracking single cells over many generations in the Mother Machine microfluidic device [27]. Using modelling [47, 96] and experiments, we show that RpoS and growth rate are coupled in a mutual inhibition feedback loop and this coupling gives rise to the RpoS pulses. Finally, we demonstrate that the function of this coupling of gene expression and growth rate is to allow *E. coli* to survive sudden stress. Below is an outline of how these results are presented in the thesis.

Chapter 3: Stochastic RpoS expression

In the first chapter we use a single-cell imaging protocol to interrogate *E. coli* grown in standard bulk culture. By using a variety of control experiments we show robustly that RpoS is heterogeneously expressed by a population of exponential phase cells. We next investigate *E. coli* cells using microfluidics and time-lapse microscopy. By following single cells over many generations we identify pulsatile RpoS activity as the source of the heterogeneity. We also observe that the growth rate of cells is widely distributed and is anti-correlated with RpoS activity.

Chapter 4: RpoS-growth mutual inhibition

To understand how these stochastic dynamics arise, in this chapter we turn to mathematical modelling. We use a standard Gillespie algorithm to model stochastic chemical reactions, but add that these reactions happen inside growing cells. With this coupled simulation we reveal that RpoS and growth are in a mutual inhibition feedback loop. We test this conclusion by experimentally perturbing both RpoS levels and population growth rates.

Chapter 5: Function of heterogeneous RpoS and noisy growth

In the final results chapter, we reveal the function of the phenotypic variability uncovered in the previous two chapters. We find that *E. coli* use high RpoS activity and slow growth to allow a subpopulation of cells to survive sudden stressful events. We reveal that the dynamic role of RpoS in *WT* cells is to prolong the time cells remain in the slow growing state, and so enhance survival.

Chapter 2

Materials and Methods

2.1 Strains and Growth Conditions

2.1.1 Strains

Table 2.1 List of strains.

Strain name	Genotype or description	Construction procedure	Source
MG1655*	*WT* of reporter library [97]		Yale CGSC (CGSC # 6300 and 7740), and gift of Kenn Gerdes
MG1655+bolA	Same as MG1655; P_{bolA}-*GFP, Kan*^{r}	Reporter plasmid P_{bolA}-*GFP, Kan*^{r} [97] in MG1655	Reporter library [97] and this work
MG1655+blc	Same as MG1655; P_{blc}-*GFP, Kan*^{r}	Reporter plasmid P_{blc}-*GFP, Kan*^{r} [97] in MG1655	Reporter library [97] and this work
MG1655+poxB	Same as MG1655; P_{poxB}-*GFP, Kan*^{r}	Reporter plasmid P_{poxB}-*GFP, Kan*^{r} [97] in MG1655	Reporter library [97] and this work
MG1655+rpsL	Same as MG1655; P_{rpsL}-*GFP, Kan*^{r}	Reporter plasmid P_{rpsL}-*GFP, Kan*^{r} [97] in MG1655	Reporter library [97] and this work
MG1655+lacI	Same as MG1655; P_{lacI}-*GFP, Kan*^{r}	Reporter plasmid P_{lacI}-*GFP, Kan*^{r} [97] in MG1655	Reporter library [97]

MGChrPbolA	Same as MG1655 with chromosomally integrated P_{bolA}-*GFP*, *Kan*^{r}	Used Red/ET system and PCR product amplified from reporter plasmid P_{bolA}-*GFP*, *Kan*^{r} [97]	This work
DrpoS*	MG1655 with Δ*rpoS::Kanr*	Used a PCR product from Keio collection Δ*rpoS* strain [98]	This work
DrpoSF-	Same as DrpoS, markerless	FLPe recombinase	This work
DrpoSF-+bolA	Same as DrpoSF-; P_{bolA}-*GFP*, *Kan*^{r}	Reporter plasmid P_{bolA}-*GFP*, *Kan*^{r} [97] in DrpoSF-	This work
DrpoSF-+blc	Same as DrpoSF-; P_{blc}-*GFP*, *Kan*^{r}	Reporter plasmid P_{blc}-*GFP*, *Kan*^{r} [97] in DrpoSF-	This work
DrpoSF-+poxB	Same as DrpoSF-; P_{poxB}-*GFP*, *Kan*^{r}	Reporter plasmid P_{poxB}-*GFP*, *Kan*^{r} [97] in DrpoSF-	This work
DrpoSF-+rpsL	Same as DrpoSF-; P_{rpsL}-*GFP*, *Kan*^{r}	Reporter plasmid P_{rpsL}-*GFP*, *Kan*^{r} [97] in DrpoSF-	This work
DrpoSF-+lacI	Same as DrpoSF-; P_{lacI}-*GFP*, *Kan*^{r}	Reporter plasmid P_{lacI}-*GFP*, *Kan*^{r} [97] in DrpoSF-	This work
DrpoSF-ChrPbolA	Same as DrpoSF- with chromosomally integrated P_{bolA}-*GFP*, *Kan*^{r}	Used Red/ET system and PCR product amplified from reporter plasmid P_{bolA}-*GFP*, *Kan*^{r} [97]	This work
MGmCherry	Same as MG1655, with *rpoS::mCherry* chromosomally integrated, replacing *rpoS*	-	Gift of Kenn Gerdes
MGmCherry+bolA	Same as MGmCherry; P_{bolA}-*GFP*, *Kan*^{r}	Reporter plasmid P_{bolA}-*GFP*, *Kan*^{r} [97] in MGmCherry	This work
MG1655+bolASpec	Same as MG1655; P_{bolA}-*GFP*, *Spec*^{r}	Reporter plasmid P_{bolA}-*GFP*, *Kan*^{r} [97] in MG1655, with antibiotic switched from *Kan*^{r} to *Spec*^{r}	This work
DrpoSF-+bolASpec	Same as DrpoSF-; P_{bolA}-*GFP*, *Spec*^{r}	Reporter plasmid [97] in DrpoSF-, with antibiotic switched from *Kan*^{r} to *Spec*^{r}	This work

PDC47	Same as MG1655 with markerless $\Delta relA$ and $\Delta spoT::cat$	-	Gift of Kenn Gerdes [99]
PDC47+bolA	Same as PDC47 with P_{bolA}-*GFP*, Kan^r	Reporter plasmid P_{bolA}-*GFP*, Kan^r [97] in PDC47	This work
BW25113	*WT* of knockout library [98]		Yale CGSC # 7636
KDr	Same as BW25113 with $\Delta rpoS::Kan^r$	-	From Keio collection [98]
KDr+bolASpec	Same as KDr with P_{bolA}-*GFP*, $Spec^r$	Reporter plasmid P_{bolA}-*GFP*, Kan^r [97] in KDr, with antibiotic switched from Kan^r to $Spec^r$	This work
DrelA	Same as BW25113 with $\Delta relA::Kan^r$	-	From Keio collection [98] (plates 53 and 54)
DrelA+bolA	Same as DrelA with P_{bolA}-*GFP*, $Spec^r$	Reporter plasmid P_{bolA}-*GFP*, Kan^r [97] in DrelA, with antibiotic switched from Kan^r to $Spec^r$	This work
MC4100DE3 (pRPOS)	MC4100 *WT*, expressing T7 RNA polymerase, contains IPTG-inducible RpoS construct, Amp^r	-	Gift of Herb Schellhorn [81]
MC4100DE3 (pRPOS)+bolA	Same as MC4100DE3 (pRPOS); P_{bolA}-*GFP*, Kan^r	Reporter plasmid P_{bolA}-*GFP*, Kan^r [97] in MC4100DE3 (pRPOS)	This work
HS1600DE3 (pRPOS)	Same as MC4100DE3 except *rpoS13::Tn10*	-	Gift of Herb Schellhorn [81]
HS1600DE3 (pRPOS)+bolA	Same as HS1600DE3 (pRPOS); P_{bolA}-*GFP*, Kan^r	Reporter plasmid P_{bolA}-*GFP*, Kan^r [97] in HS1600DE3 (pRPOS)	This work

*Isolate CGSC #6300 was used as the parent strain for Mother Machine experiments due to superior loading properties. For liquid culture experiments we used isolates CGSC #6300 and CGSC #7440, from the Stock Centre, isolates from the Reporter library [97], and an isolate that was a kind gift of Prof. Kenn Gerdes.

2.1.2 Media

M9 (1xM9 Salts, 2mM $MgSO_4$, 0.1 mM $CaCl_2$; 5xM9 Salts 34g/L Na_2HPO_4, 15g/L KH_2PO_4, 2.5 g/L NaCl, 5 g/L NH_4Cl) supplemented with 0.2% Casamino acids and 0.4% glucose as carbon source was used for all experiments, except as follows. Media for Mother Machine experiments was also supplemented with 0.2 mg/mL Bovine Serum Albumin (BSA) to maintain the passivation of the PDMS (see Sec. 2.1.6). For growth rate perturbation experiments glucose was replaced with 0.4% mannose and Casamino acids with 1 mM thiamine (see Tab. 2.2 for further details). For RpoS overexpression experiments, cells were grown in LB with 125 μg/mL Carbenicillin, since the overexpression plasmid had Ampicillin resistance. For transcriptional reporters, 25 μg/mL Kanamycin or 100 ug/mL Spectinomycin was used as appropriate. In (p)ppGpp experiments with media denoted 'M9 Supp', Casamino acids were replaced with 400 μg/mL of serine, and 40 μg/mL of the remaining 19 amino acids, and the media supplemented with 2 μM $FeS0_4$, and 1 μg/mL thiamine [100, 99].

2.1.3 Reporters

Reporter plasmids were sourced from the Alon library [97] using Qiagen Miniprep kits (Qiagen, UK). Zaslaver *et al.* amplified intergenic regions between Open Reading Frames (ORF) from the *E. coli* chromosome, strain MG1655 [97] (see Fig. 2.1). They created plasmids with the intergenic regions placed upstream of the coding sequence of Green Fluorescent Protein (GFP), which we used as reporters of sigma factor activity (see Tab. 2.3). The plasmids were made available as a library of glycerol stocks of cells harbouring the plasmids, which we procured (General Electric, USA). The plasmid antibiotic resistance was changed from Kan^r to $Spec^r$, where specified, by PCR amplifying the $Spec^r$ from the pDR111 plasmid (kind gift of Prof. Rudner, see Table 2.4 for primers), then using restriction digestion of the original reporter and ligation assembly.

When necessary, cells were transformed with the appropriate reporter plasmids by using a variant of the Top10 Chemical Competence protocol (OpenWetWare) followed by standard transformation by heat shock [101]. Either an overnight culture or cells taken directly from glycerol stocks were grown up to exponential phase in LB. The cells were washed and concentrated in pre-chilled CCMB80 buffer 2-3 times (CCMB80: 10mM KOAc, 80 mM $CaCl_2{\cdot}2H_20$, 20 mM $MnCl_2{\cdot}4H_2O$, 10 mM $MgCl_2{\cdot}6H_2O$, 10% glycerol). Next the plasmid was added to the cells and the mixture incubated on ice for 20-30 minutes. After a 1 minute 42^oC heat shock, cells were allowed to recover in 1 mL LB at 37^oC for 1 hour before plating on LB agar plates with appropriate selection and left to grow overnight.

Table 2.2 Growth conditions and population growth rates for growth perturbation experiments. Sample standard deviation is calculated from the biological replicates as $\sqrt{\frac{\Sigma(x-\mu)^2}{n-1}}$, where μ is the sample mean and n the number of replicates. An error of 0.00 indicates the two replicate values of growth rate were identical up to the significant digits presented. The number of cells reported are those extracted in image analysis.

	WT		Δ*rpoS*	
Growth condition*	Biological replicates; number of cells	Growth rate (1/hr), mean ± std dev	Biological replicates; number of cells	Growth rate (1/hr), mean ± std dev
0.4% glucose, 0.2% casamino acids (37^{o}C)	4; 711	1.42 ± 0.07	3; 427	1.42 ± 0.08
0.4% glucose, 0.2% casamino acids (33^{o}C)	2; 547	0.98 ± 0.00	2; 510	1.02 ± 0.00
0.4% glucose, 0.2% casamino acids (28^{o}C)	2; 747	0.55 ± 0.02	2; 601	0.59 ± 0.01
0.4% mannose, 0.2% casamino acids (37^{o}C)	3; 720	1.20 ± 0.04	2; 453	1.23 ± 0.00
0.4% mannose, 0.2% casamino acids (33^{o}C)	2; 346	0.84 ± 0.00	2; 511	0.85 ± 0.02
0.4% mannose, 0.2% casamino acids (28^{o}C)	2; 604	0.48 ± 0.02	2; 595	0.51 ± 0.01
0.4% glucose, 1 mM thiamine (37^{o}C)	2; 896	0.74 ± 0.04	2; 536	0.74 ± 0.02
0.4% mannose, 1 mM thiamine (37^{o}C)	3; 2,719	0.49 ± 0.02	3; 2,298	0.52 ± 0.03

*M9 supplemented with the following and grown at (temperature).

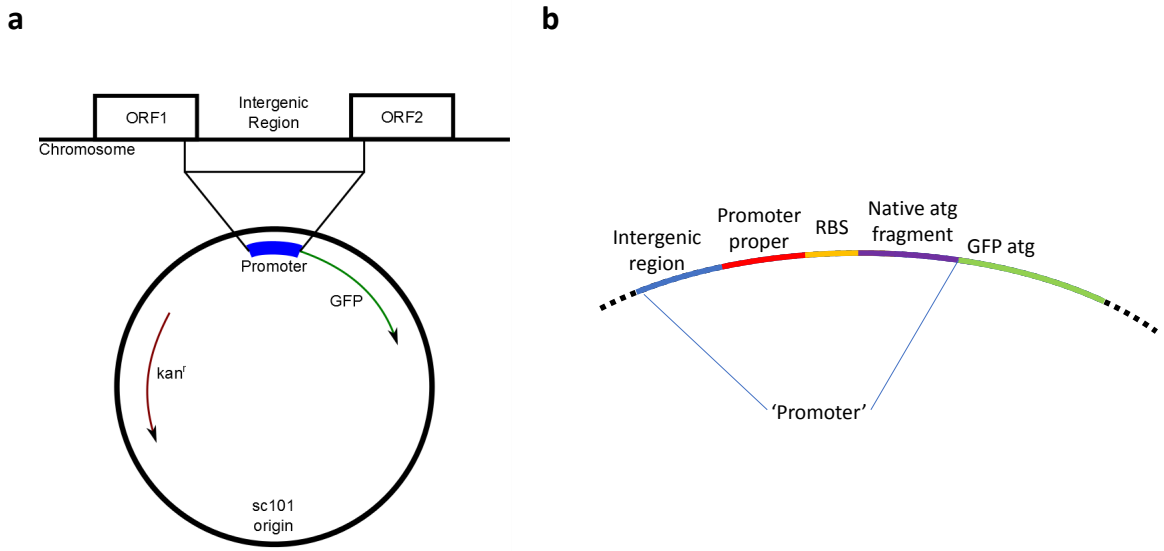

Fig. 2.1 Transcriptional reporter construct sourced from the Alon promoter library [97]. a, Regions from the *E. coli* chromosome between Open Reading Frames (ORF) were cloned into a plasmid with the Green Fluorescent Protein (GFP) coding sequence and Kanamycin resistance. b, Details of the contents of the promoter sequence derived from the chromosome.

Table 2.3 Reporter plasmids

Gene	Dominant σ-factor affinity	Other σ-factor affinity [79]	Biological Role (descriptions taken from [97])
bolA	*rpoS*	σ^{70}, σ^{N}	Alters morphology of cells under stress
blc	*rpoS*	-	Globomycin-sensitive outer membrane lipoprotein expressed at beginning of stationary phase
poxB	*rpoS*	-	pyruvate dehydrogenase/oxidase FAD and thiamine PPi binding, cytoplasmic in absence of cofactors (1st module)
rpsL	σ^{70}	*rpoS*, σ^{H}	30S ribosomal subunit protein S12
lacI	σ^{70}	-	transcriptional repressor of lactose catabolism

Table 2.4 List of primers.

Primer name	Primer description	Sequence
OP007	Chromosomal Integration, Fwd	ATAAACACGTTCGTGTCCC-GACAGGCACACAGACGGTTAGCCAC-TAATTAGAGCTCTCGAACCCCAGAGT
OP008	Chromosomal Integration, Rev	GTAAGAATAAAAAAAACGGGTCAC-CTTCTGGCGACC-CGTTTTTCTTTGCGCCT-GCAGGTCTGGACATTTA
OP015	*rpoS*-knockout, Fwd	TGAGACTGGCCTTTCTGACAGATGCT-TACTTACTCGCGGAACAGCGCTTCTG-TAGGCTGGAGCTGCTTCG
OP016	*rpoS*-knockout, Rev	CTTTTGCTTGAATGTTCCGT-CAAGGGATCACGGGTAGGAGCCACCT-TATGATTCCGGGGATCCGTCGACC
CV186	Plasmid resistance change from Kan^r to Spec^r, Fwd	AAAGATCTGATCAAGAGACAGGATGAG-GATCGTTTCGCTTGAATACATACGAAC
CV187	Plasmid resistance change from Kan^r to Spec^r, Fwd	AAAGATCTAAAATAGTGAGGAG-GATATATTTG
CV188	Plasmid resistance change from Kan^r to Spec^r, Rev	AAAGAGCTCTTATAATTTTTTTAATCT-GTTATTTAAATAG

2.1.4 Knockout construction

Knockouts strains were sourced from the Keio collection [98]. Baba *et al.* systematically knocked out nearly every gene in *E. coli*, strain BW25113 [98]. For each viable mutant they picked two isolates, available as a glycerol stock library, which we procured. The Alon library was made in strain MG1655 [97]. Thus, the knockout site with *Kan^r* was amplified by PCR and used to perform knockouts in the MG1655 *E. coli* strain. Knockouts were carried out by the commercial Red/ET Recombination system (Gene Bridges, Germany) following the recommended protocol (see Tab. 2.4 for primers). However, instead of electroporation for transforming with the Red/ET recombination plasmid and FLPe flipase plasmid we used chemical transformation. The transformation was as in Sec. 2.1.3 except the recovery was carried out at 30^{o}C and 1,000 rpm in a benchtop shaker and plates incubated at 30^{o}C as the plasmid replication ceases at 37^{o}C. Knockouts were verified by colony PCR and sequencing.

2.1.5 Chromosomal integration of reporter

Knockins were performed as above for knockouts with the Red/ET recombination system (Gene Bridges). The integrated DNA was amplified off the reporter plasmid (see Tab. 2.4 for primers). The reporter plasmids were sequenced and used as references for the integration.

2.1.6 Mother Machine microfluidic device

The Mother Machine microfluidics device was invented in the lab of Suckjoon Jun [27] (see section 1.1.3, Fig. 2.2). It consists of a feed trench (50 μm x 100 μm x 30 mm) with many channels (1.4 μm x 1.4 μm x 25 μm) attached perpendicular to the trench. These channels hold the cells and media is supplied to the cells via the trench. We used an epoxy master mould to fabricate our devices, which was a kind gift of Suckjoon Jun. The devices were fabricated by casting Sylgard 184 polydimethylsiloxane (PDMS) (Dow Corning, USA) with a ratio of 10:1 base to curing agent onto the master mould and cured overnight at 65^{o}C. The chips were then cut out and plasma bonded (Femto Plasma System, Diener, Germany) to a glass bottom dish (HBSt-5040, Wilco Wells, Netherlands). To strengthen the bonding the chips were incubated for approximately ten minutes at 65^{o}C. The chips were passivated with 20 mg/ml Bovine Serum Albumin (BSA) for approximately one hour at 37^{o}C prior to cell loading.

2.2 Data acquisition

2.2.1 Bulk culture snaps

We used an imaging protocol developed previously [38] with minor modifications. Cells were grown from glycerol stocks or from colonies on LB agar plates streaked with the glycerol stocks in M9 at 37^{o}C in a shaking incubator at 220 rpm (Innova 44, New Brunswick Scientific, UK) to late exponential phase and then diluted back into M9 to an OD of 0.01 (Optical Density, 600 nm; Ultrospec 10, Amersham Biosciences, UK). After re-growing for approximately 2 hours 20 minutes, up to early exponential phase (OD ~0.15), 0.3 μL of the cell culture was spotted onto pads of 1.5% low-melting agarose in Phosphate-Buffered Saline (PBS), see Fig. 2.3a. Cells were imaged expediently, typically within 20 minutes of leaving the incubator.

2.2.2 Bulk culture snaps of fixed cells

Cells were grown as in Sec. 2.2.1. However, after measuring the OD of the culture, 37% formaldehyde in methanol was added to the remaining culture for a final concentration of 3.7% formaldehyde. Formaldehyde was added within 6 minutes of leaving the shaking

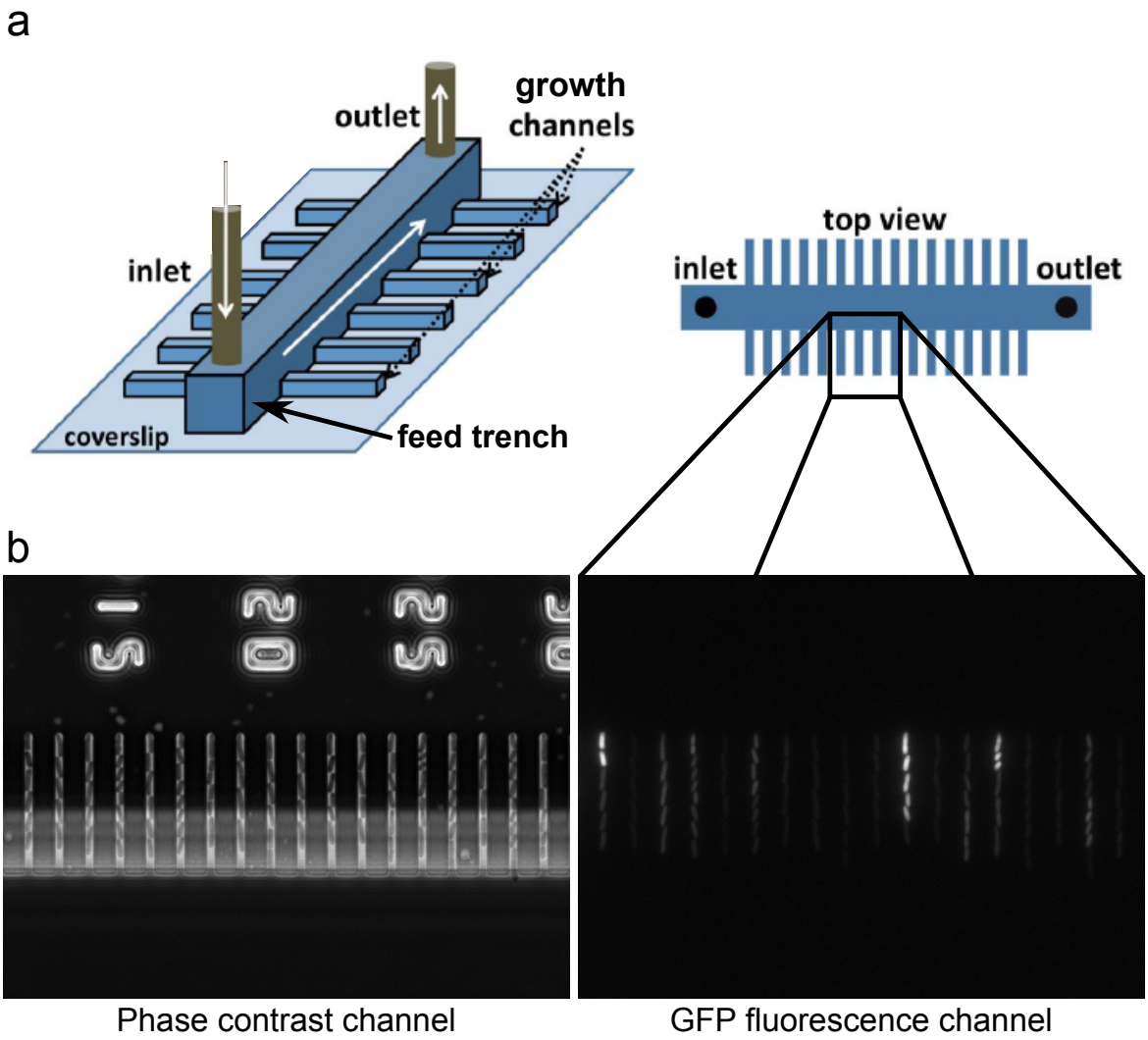

Fig. 2.2 Mother Machine schematic and sample images. a) Schematic of the Mother Machine microfluidic device, adapted from [27], with permission. The many channels hold cells that are supplied fresh media via the feed trench. b) Sample images of a single stage position in the phase contrast and GFP fluorescence channels.

incubator, and left to mix for 27 minutes. Cells were then spun at 4,500 g for 5 minutes. The pellets were washed in PBS twice with the same spinning procedure, and finally resuspended in 100 μL PBS. A 0.3 μL droplet was then spotted on agarose pads as above and imaged.

2.2.3 Population growth rate perturbation

Cells were grown as in Sec. 2.2.1. However, cells were grown from glycerol stocks using the modified media and temperature into exponential phase. Optical density measurements were taken after cells were diluted and grown up to exponential phase for imaging.

2.2.4 RpoS over-expression

Cells were streaked on LB agar plates and colonies picked into 2 mL LB. Cultures were grown into exponential phase at 37^{o}C and diluted to OD 0.01 into 10 mL LB supplemented with either IPTG or water and grown again. OD measurements were taken at intervals and cells imaged as above.

2.2.5 Mother Machine movies

Cells were grown from glycerol stocks as above. They were concentrated by centrifugation (4,000 rpm for 10 min) and injected into the Mother Machine devices. A second centrifugation step for 5 min at 4,000 rpm using a spin coater (Polos Spin150i, SPS, Netherlands) forced cells into the channels. Cells were allowed to settle in the device while being supplied with fresh media for 2 hours prior to beginning acquisition. Media was supplied at a flowrate of 1 ml/h by either a Fluigent pressure pump (MFCS-EZ, Fluigent, France) with an M-Flow sensor (Fluigent, France) or a syringe pump (Fusion 100, Chemyx, USA). Multiple stage positions, each with ten to twenty occupied channels, were imaged in time lapse every 10 minutes.

2.2.6 Agarose pad movies

The agarose pad movie protocol has been described previously [38], see Fig. 2.3a. Briefly, 1.5% low-melting agarose was melted in M9, allowed to cool, supplemented with antibiotics, and cast sandwiched between two coverslips. Cells were grown from glycerol stock overnight in M9 media, diluted to an OD of 0.01 and grown up to exponential phase. The culture was diluted to an OD of ~0.01 and ~2 μl spotted onto pads cut out from the cast agarose to a size of ~5x5 mm^2.

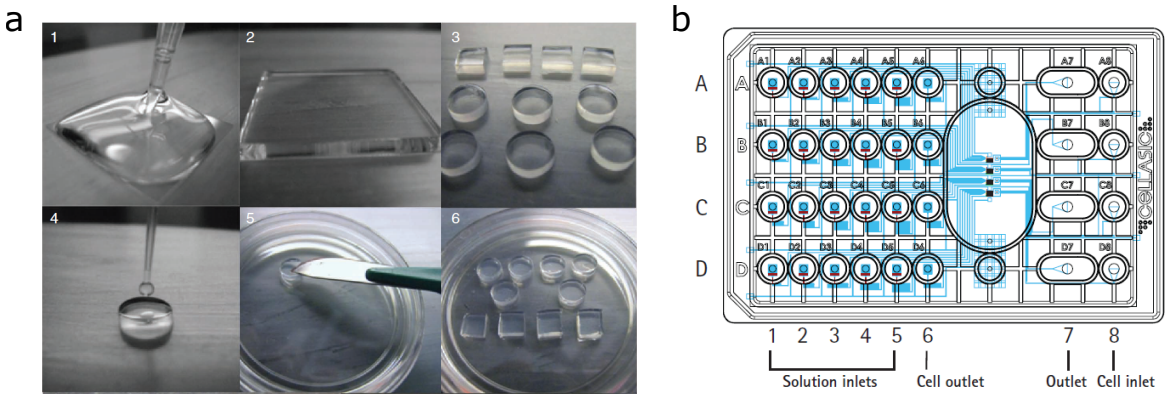

Fig. 2.3 Alternative single-cell time-lapse methods. a) The agarose pad method involves casting a low-melting agarose melted in media into pads. A droplet of cell culture is added to the pad before flipping onto a microscope slide. Figure adapted from [38], with permission. b) Schematic of the commercially available CellASIC microfluidic device, adapted from [102].

2.2.7 CellASIC movies

We loaded exponential phase cells prepared as in the agarose pad movies into the CellASIC ONIX B04A-03 microfluidic device using the manufacturer's protocol (EMD Millipore Corporation, Fig. 2.3b) [102, 103].

2.2.8 Microscopy

We used a widefield microscope with epifluorescence and phase contrast imaging modes (Nikon Ti-eclipse, Nikon, UK) equipped with the Nikon Perfect Focus (PFS) Unit. Illumination for the epifluorescence was provided by a white light LED source (SOLA SE Light Engine or Spectra X Light Engine, Lumencor, USA), transmitted by a liquid light guide (Lumencor, USA), through a fluorescence filter cube (GFP Channel: 49002-ET-EGFP, excitation: ET470/40x, dichroic: T495LP, emitter: ET525/50m; RFP Channel: 41027-Calcium Crimson, excitation: HQ580/20x, dichroic: Q595LP, Emitter: HQ630/60m, Chroma, USA), and a CFI Plan Apochromat 100x oil immersion objective (NA 1.45, Nikon). Phase contrast illumination was provided by a 100 W lamp via a condenser unit (Nikon). Images were acquired on a CoolSNAP HQ2 camera (Photometrics, USA). The sample was held in motorized stages (Nikon). The sample was incubated along with much of the microscope body using a temperature controlled, heated chamber (Solent Scientific, UK). The microscope was controlled with MetaMorph software (version 7.8.10.0, Molecular Devices, USA). Fluorescent beads (TetraSpeck microspheres, 0.5 μm, Molecular Probes, USA) were imaged as a calibration standard.

2.3 Quantifying gene expression and growth rate

2.3.1 Bulk culture single-cell gene expression

A custom MATLAB (version 2014a, Mathworks, USA) script based on the published Schnitzcells software was used for image analysis [38] (Fig. 2.4). The microscope was calibrated for each experiment with fluorescent beads to mitigate the effect of non-uniform sample illumination and daily variations in the apparatus. Cells were taken from a field of view computed from the beads to be within 80% of maximum intensity. Cells were segmented in the phase contrast channel. The mean fluorescence was then the corresponding pixels in the GFP channel normalized to cell area. A threshold was applied to exclude debris and substrate autofluorescence, which was found by inspection, was subtracted from the mean cell fluorescence. Finally, the cell fluorescence was normalized by the fluorescence of the top 2% of fluorescent beads.

2.3.2 Bulk culture growth rates

Growth rate was calculated by fitting an exponential curve to the OD measurements in the growth perturbation experiments. Growth rate was not computed for the RpoS overexpression experiments as, by inspection, cultures appeared to change their rate of growth over time.

2.3.3 Mother Machine movies image analysis

The mother cell – the cell that remained at the end of growth channels farthest from the feed trench – was isolated and tracked. The first step in the isolation process was to extract channels at each stage position. We averaged the GFP fluorescence channel images for a position over many frames, yielding a clear peak in intensity at each occupied channel location and a broad signal indicating the length of the channel (Fig. 2.5). This procedure was robust even with cells expressing background GFP, such as Δ*rpoS* harbouring P_{bolA}-*GFP*. We then used these peaks to create a box around the channel, which we subsequently used to extract the channel at each frame in both the phase and fluorescence channels (Fig. 2.5).

The mother cell was isolated for each channel and frame independently using only the phase contrast channel to avoid segmentation errors due to low fluorescence signals (Fig. 2.6a). We determined the boundary of the cells using the eigenvalues of the Hessian at each pixel (the Hessian is simply the spatial second derivative of pixel intensity, Fig. 2.6b). Applying a threshold to the resulting image yielded a crude segmentation of the cells and the surrounding PDMS (Fig. 2.6c). To exclude the PDMS we fit two lines along the channel on minima in the Hessian. We identified these points with a procedure relying on the variance of the Hessian along pixels lying perpendicular to the channel. By enforcing the fit

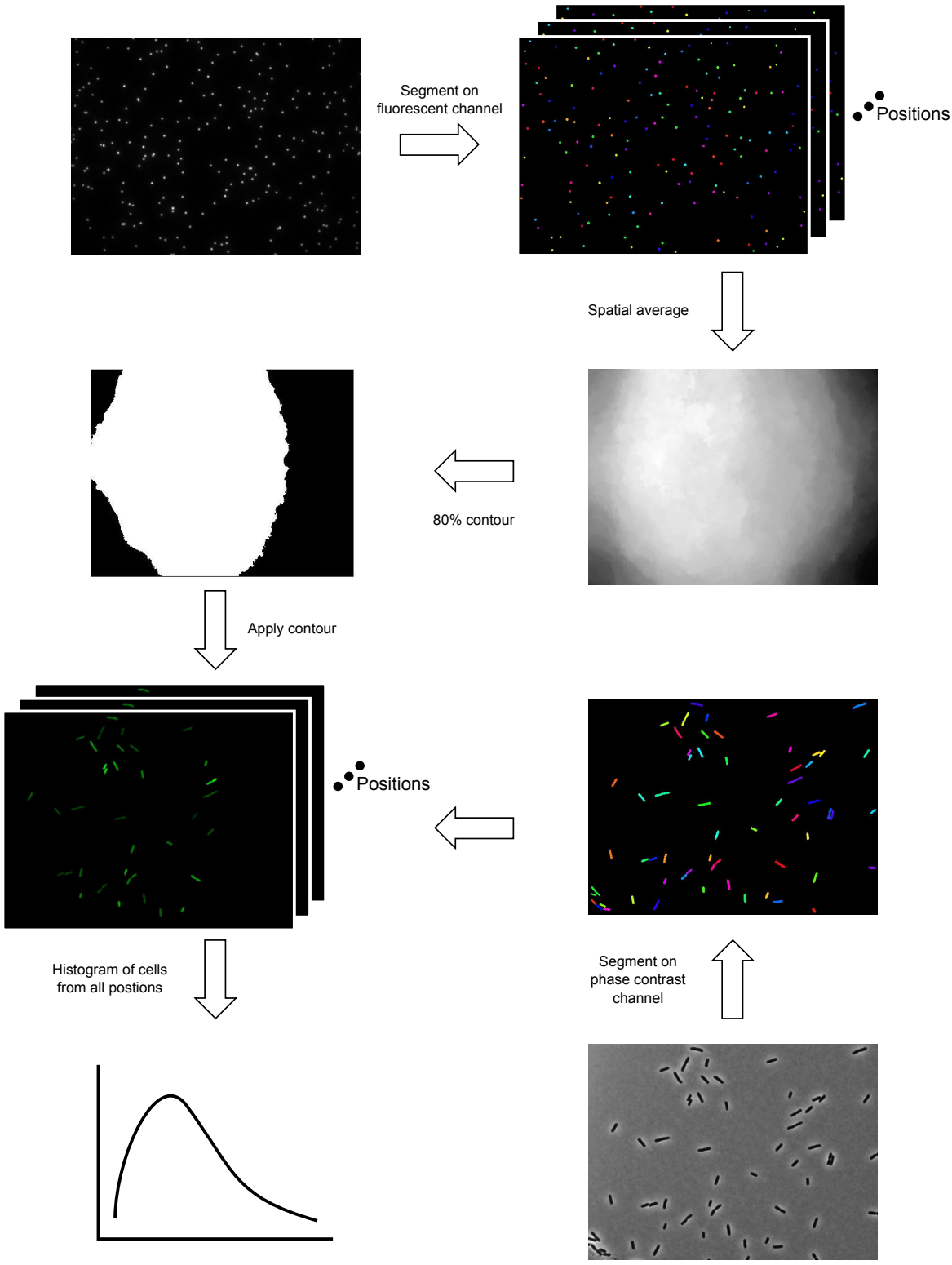

Fig. 2.4 Processing bulk culture single-cell images. Fluorescent beads were used to compensate for the flatness of the field of view of the microscope. First the beads were segmented using the fluorescence channel, clumps of beads excluded by size, and a spatial averaging of beads within 100 pixels was taken for each pixel in the image. Only cells within the 80% contour of the resulting spatially averaged beads image were used. The cells themselves were segmented using the phase contrast channel. The mean value of pixels in the fluorescence image corresponding to a cell were then used to compute histograms of fluorescence expression levels.

lines be parallel, poorly identified points were excluded (Fig. 2.6d). This yielded regions corresponding mostly to cells (Fig. 2.6e), which we could label (Fig. 2.6f). Small blobs were excluded next (Fig. 2.6g). Using the brightness of the feed trench in the phase image, we identified the cell furthest away from the trench as the mother cell (Fig. 2.6h). We fixed jaggedy borders by dilating and filling in kinked edges of the mother cell ((Fig. 2.6i, j). As only the mother cell was kept, there were no special procedures required for tracking cells in time. The image analysis was robust most of the time, but failed intermittently. Thus, every frame used in subsequent analysis was manually checked, and corrected if necessary, using the movie editing feature of the Schnitzcells package [38]. Cells that did not grow for the entire duration of the movie were discarded in this process.

2.3.4 Single-cell growth rates

We numerically computed the relative growth rate, $g = \frac{1}{l}\frac{dl}{dt}$, at each frame, where l is cell length. Throughout the thesis we refer to this relative growth rate of single cells simply as growth rate. We first computed the numerical derivative of cell length as the difference in cell length between consecutive frames ($\Delta t = 10$ minutes):

$$\frac{dl}{dt} \sim \frac{l_{t+1} - l_t}{\Delta t} \tag{2.1}$$

Growth rate at division events was calculated as the average of the growth rates from the frames immediately before and immediately after the division event. Despite the manual image curation, unphysical, negative growth rates occasionally resulted due to segmentation artefacts. These were corrected by replacing the negative values with the mean of the nearest frames with non-negative values. The numerical derivative was normalized by the initial length, l_t:

$$g \sim \frac{l_{t+1} - l_t}{\Delta t \cdot l_t} \tag{2.2}$$

and then smoothed with a moving average filter spanning five frames (Fig. 2.7b, c). The growth rate sample traces presented in figures were smoothed again with a moving average filter spanning five frames for display.

The population growth rate of mother cells was computed as $g_{pop} = ln(2)/t_D$ where t_D, the population doubling time, was found by numerically solving:

$$\frac{P_{final}}{P_{initial}} = 2 = \sum_i n_i 2^{\frac{t_D}{c_i}} \tag{2.3}$$

where P_x are the hypothetical number of cells in a population, n_i are the experimentally determined fraction of cells growing with cell cycle time c_i. We note that the Mother Machine technique over-represents slow growing cells compared to bulk culture since the slow growing cells do not have to compete with fast cells in the Mother Machine [104].

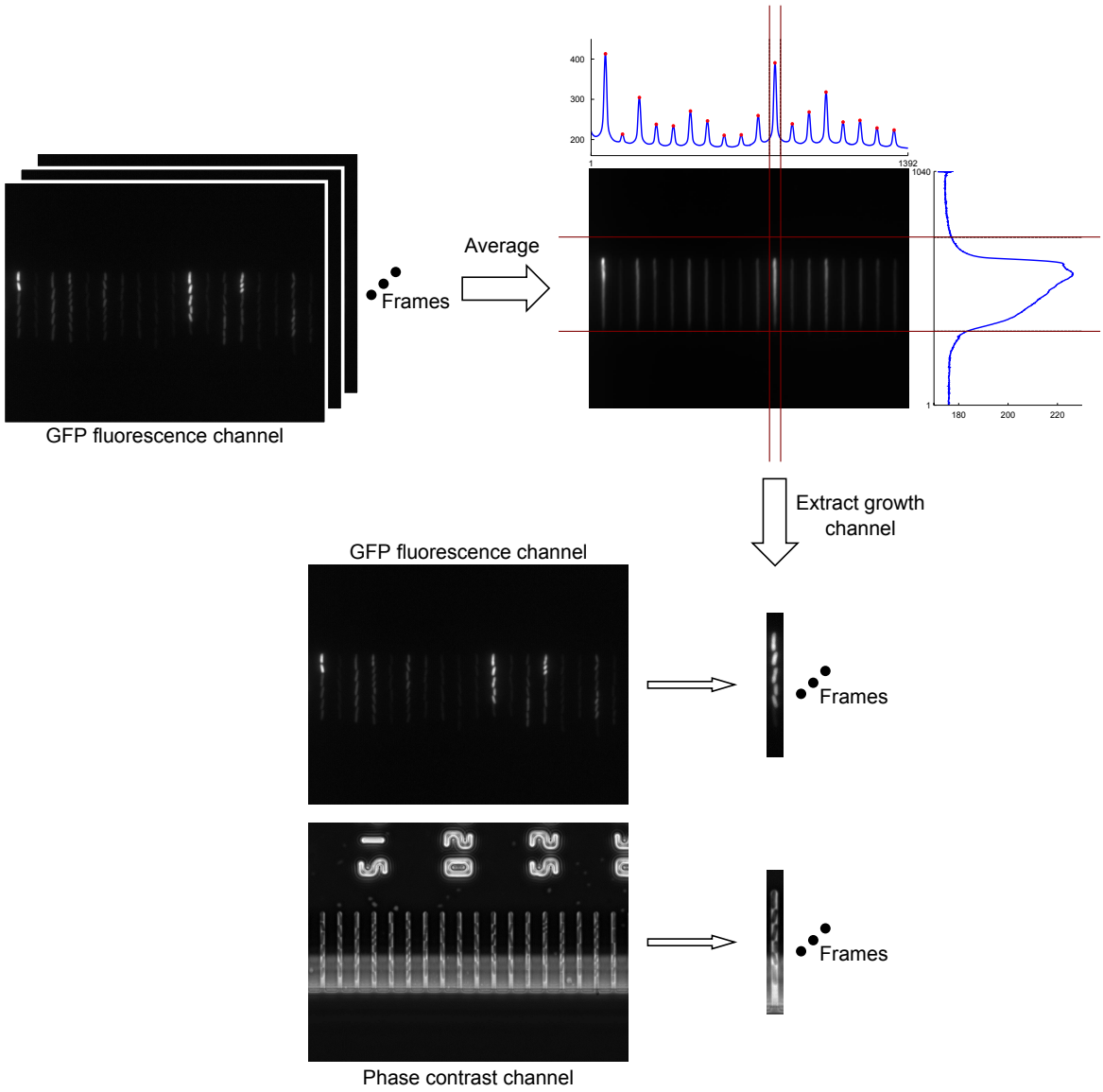

Fig. 2.5 Mother Machine image pre-processing to extract channels. For each stage position, the fluorescence channel was averaged over the course of the movie. Using the averaged image, the limits of individual channels were identified. The channels for each frame in both the fluorescence and phase contrast imaging channels were isolated using these limits.

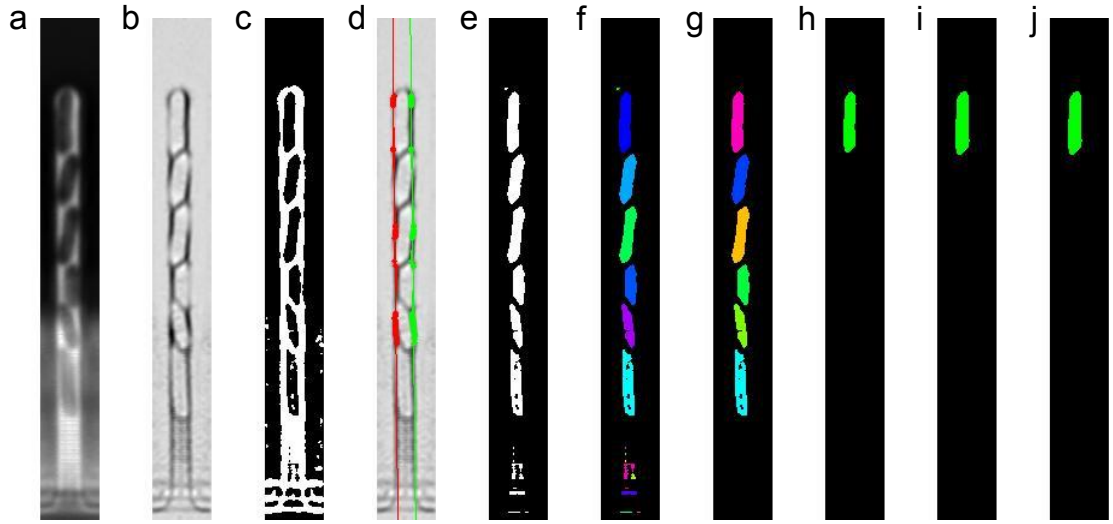

Fig. 2.6 Illustration of segmentation of mother cell. a) The original phase contrast image. b) the Hessian of the phase contrast image. c) Threshold to segment cells (colour inverted image shown for clarity). d) Procedure to exclude PDMS surrounding the cells. e) Applying the mask resulting from (d). f) Identifying regions as cells. g) Excluding small area cells as artefacts. h) Isolating the mother cell as the cell furthest away from the feed trench. The feed end of the channel appears brighter in the phase contrast image. i, j) Cleaning segmentation by dilating (i) and filling in kinked edges (j) the mother cell.

2.3.5 Promoter (RpoS) Activity

Gene expression level was calculated as in Section 2.3.1. However, for Mother Machine data calibration to beads was done using only the top 2% normalization – no cells were excluded due to position in the field of view. Promoter activity (A) is the rate of production of the gene under the control of a promoter normalized by the cell volume (V, $A = \widetilde{A}/V$) [39]:

$$\frac{dF}{dt} = \widetilde{A} - p \cdot F \tag{2.4}$$

F is the gene product, GFP in the case of the transcriptional reporters used in the thesis, and p is a constant accounting for degradation and bleaching. If the promoter is RpoS sensitive, then A is RpoS activity, and if σ^{70} sensitive, σ^{70} activity. To extract promoter activity from the observables of cell length (l) and mean fluorescence (M) per cell we note that total fluorescence is the product of mean fluorescence and cell volume:

$$F = M \cdot V \tag{2.5}$$

By the product rule:

$$\frac{dM}{dt}V + M\frac{dV}{dt} = \widetilde{A} - p \cdot M \cdot V \tag{2.6}$$

The volume of rod shaped *E. coli* cells can be approximated as the volume of a cylinder ($V = l\pi r^2$, where r is cell radius). Thus, by the product and chain rules:

$$\frac{dM}{dt}V + M\pi r^2\frac{dl}{dt} + 2M\pi lr\frac{dr}{dt} = \widetilde{A} - p\cdot M\cdot V \tag{2.7}$$

Dividing by cell volume we find:

$$\frac{dM}{dt} + \frac{M}{l}\frac{dl}{dt} + \frac{2M}{r}\frac{dr}{dt} = A - p\cdot M \tag{2.8}$$

Cell radius does not vary appreciably (see Fig. 2.7a). In fact, the majority of the variation observed is at the detection limit of the image analysis (~ 1 pixel, see Fig. 2.8a), thus, $\frac{dr}{dt} \sim 0$. Finally, rearranging we obtain promoter activity as the component of the time-derivative of the mean fluorescence corrected for by growth rate and bleaching:

$$A = M\left(\frac{1}{l}\frac{dl}{dt} + p\right) + \frac{dM}{dt} \tag{2.9}$$

We computed promoter activity numerically. The relative growth rate, $g = \frac{1}{l}\frac{dl}{dt}$, was calculated as in Sec. 2.3.4. The mean fluorescence, M, was smoothed with a moving average filter spanning five frames, and then dM/dt was calculated by taking the numerical derivative of the smoothed mean fluorescence (Fig. 2.7d, e). The promoter activity sample traces in figures were smoothed again with a moving average filter spanning five frames for display. We numerically set p = 0.1 (≡0.6/hr). Our conclusions were not sensitive to the value of p selected over the range of 0.025 to 0.4 (≡0.15/hr to 2.4/hr). Note that cell width does not correlate with promoter activity (Fig. 2.8b).

RpoS activity peaks (as in Fig. 3.8) were found by first smoothing promoter activity with a moving average filter spanning five frames and then using the built-in MATLAB function `findpeaks` to identify local maxima. For each of these maxima, the highest value of the un-smoothed promoter activity within a window of seven frames centred on each local maximum was identified as the peak.

2.3.6 Cross-correlation

The normalized cross-correlation between growth rate and promoter activity was computed as follows:

$$\bar{c}_{g-A}(\Delta t) = \sum_{t\in\text{all time}} \frac{g(t+\Delta t) - \bar{g}}{\sqrt{c_{g-g}(0)}} \cdot \frac{A(t) - \bar{A}}{\sqrt{c_{A-A}(0)}} \tag{2.10}$$

where g is growth rate, A is promoter activity, Δt, is the time difference between the two signals, overbars indicate averages over time, and c is the auto-correlation:

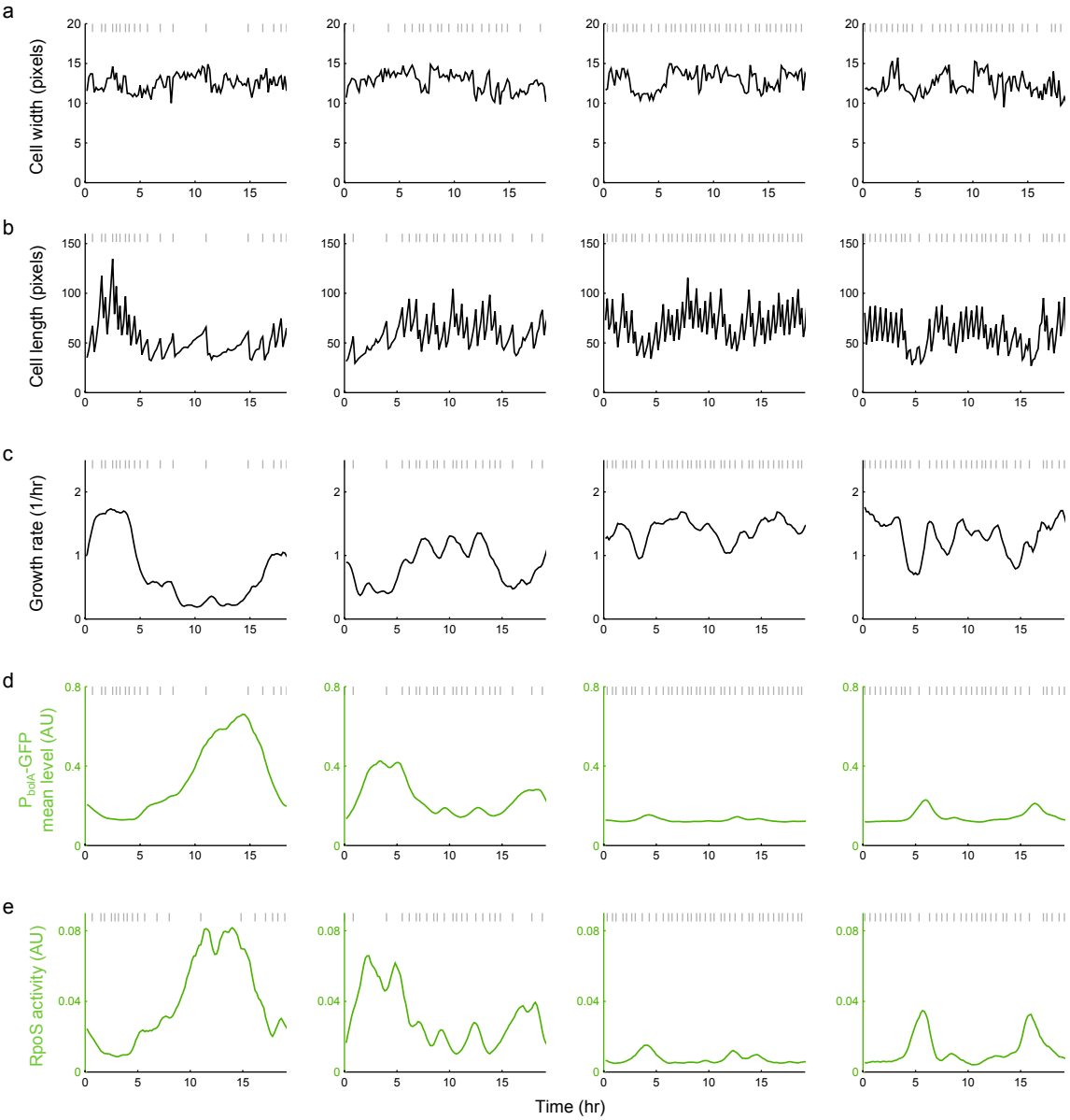

Fig. 2.7 Illustration of promoter activity computation for sample traces of the four mother cells in Fig. 3.8b. a, Cell width, $2r$. b, Cell length, l. c, Growth rate is computed as the normalised numerical derivative of cell length: $g = \frac{1}{l}\frac{dl}{dt}$. d, Mean fluorescence per cell from the P_{bolA}-*GFP* reporter, (M). e, Promoter (RpoS) activity is the rate of GFP production from the reporter due to RpoS, computed using $A = M(\frac{1}{l}\frac{dl}{dt} + p) + \frac{dM}{dt}$. All traces, except cell width and length, are smoothed with a window of five frames. Grey vertical lines indicate cell divisions.

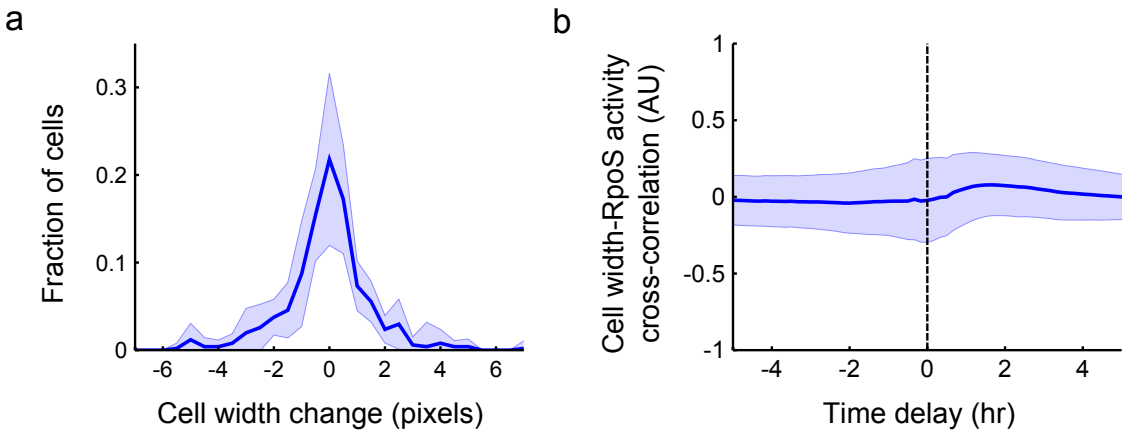

Fig. 2.8 Cell width is approximately constant in the Mother Machine experiments. a) Histogram of change in cell width between frame 59 and 60 from all movies (505 cells). The mean is ~-0.080 pixels with a standard deviation of ~1.5 pixels. b, The cell width and RpoS activity are not correlated, illustrated as a nearly constant, zero cross-correlation between these two quantities over all movies (507 mother cells from 11 technical replicates drawn from 7 biological replicates).

$$c_{a-a}(\Delta t) = \sum_{t \in \text{all time}} (a(t+\Delta t) - \bar{a}) \cdot (a(t) - \bar{a}) \tag{2.11}$$

where a is either promoter activity or growth rate.

2.4 Survival assay

2.4.1 Mother Machine assay

Cells were loaded into the Mother Machine as above. Cells were allowed to grow in fresh media for 10 hours, then exposed to 35 mM H_2O_2 for 35 minutes and then supplied with fresh media again for at least 12 hours. The media was switched with a Fluigent 2-switch or M-switch (Fluigent, France). This stress exposure time was informed by a preliminary test with fluorescent dextran (Fig. 2.9). We found that there was a lag between commanding the device to switch and the media switching in the Mother Machine chip of ~10 minutes (1 frame). The media switched to near maximal (minimal) values within 1 frame (<10 minutes) of switching to dextran (no dextran), but the full transient lasted ~2 frames. The interval of time that the fluorescence remained high was approximately the requested 35 minutes, however, shorter times would likely have not been robust. Thus, the stress exposure was set to 35 minutes.

Two 35 minute pulses of 3 to 12 mM propidium iodide were supplied with the second round of fresh media and the cells were imaged in the RFP channel to observe DNA chelation of dead cells. This approach was not robust for identifying survivors and dead cells as the dye did not penetrate all cells that appeared dead by inspection of the phase contrast

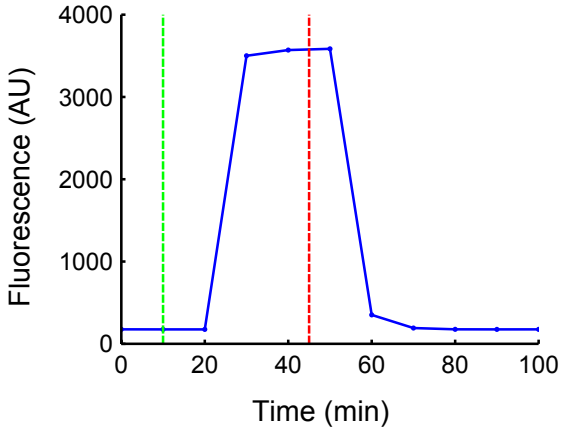

Fig. 2.9 Testing media switching in the Mother Machine. Preliminary experiment using fluorescent dextran to test the switching characteristics of Mother Machine set-up. Green (red) line indicates when device was commanded to switch to dextran (no-dextran). The duration of the high dextran fluorescence approximates the requested interval, albeit with a lag and some transients.

channel. Thus the movie for each mother cell was manually curated to determine survival using solely the phase contrast channel. If the cell began growing post-H_2O_2 treatment and before the movie ended, it was counted as a survivor. Ambiguous cases, where a judgement about whether the cell was growing or not could only be made tentatively, were excluded from the tally (*WT*, 14% of cells excluded, Δ*rpoS*, 5%). However including these cells in the survival fraction calculation, with their tentative assignments of survival, did not change the results significantly.

2.4.2 Receiver Operating Characteristic (ROC) curve

A ROC curve measures how well a binary classifier performs as the threshold of the classifier is varied. We used growth rate and rpoS activity to classify the survival of cells in the Mother Machine survival assay. The True Positive Rate (TPR) as a function of the threshold was computed as:

$$TPR(threshold) = \frac{\#\text{ surviving cells past threshold}}{\text{Total }\#\text{ surviving cells}} \tag{2.12}$$

Similarly, the False Positive Rate (FPR) was computed as:

$$FPR(threshold) = \frac{\#\text{ non-surviving cells past threshold}}{\text{Total }\#\text{ non-surviving cells}} \tag{2.13}$$

When growth rate was used as the classifier, cells passed the threshold if their growth rate was below the tested value; while for rpoS activity if it was above. The TPR was plotted against the FPR to generate the ROC curve. The optimal threshold was computed by finding the threshold that resulted in the maximum difference between the TPR and FPR. The Area

Under the Curve (AUC), computed by numerical integration of the ROC curve, is a measure of the quality of the classifier. A perfect classifier has AUC = 1, while one that is no better than random guessing has AUC = 0.5.

2.4.3 Bulk culture Colony Forming Units (CFU) assay

Cells were grown into exponential phase from glycerol stocks at either 37^{o}C or 28^{o}C and diluted into 10 mL fresh media. They were grown into exponential phase again and aliquoted into 2 mL cultures. These aliquots were exposed to either water or 26 mM H_2O_2 and incubated for a further 20 minutes. Cultures were then serially diluted in M9 and plated on LB agar plates. The colonies on the plates were counted after an overnight incubation at 37^{o}C to determine the Colony Forming Units (CFU). Survival fraction was computed as cells/mL from the stress condition divided by the cells/mL from the water condition. Averages were taken over all plates that were in the dynamic range of the assay (30 to 300 colonies per plate).

2.5 Mathematical model

The simulation was written in MATLAB. The core-algorithm code is presented below, the detailed code is available in Appendix A.

```
for k = 1 to number of simulations
    %initializing first step

    for t = 1 to Number of time steps
        %first run the rpoS Gillespie:

        while till accumulated Gillespie time does not exceeds growth clock
            %Perform standard Gillespie algorithm
        end

        %compute concentration of the molecules

        %Update growth rate using Hill function

        %adder rule:
        if added length > adder value
            %divide cell and molecules in half
        else
            %increase cell length
        end

        %store values with sampling resolution
        if mod(t,storestep) == 1
            %store simulation step
        end
    end

end
```

Chapter 3

Stochastic RpoS expression

3.1 How is RpoS distributed in single cells in exponential phase?

3.1.1 RpoS is heterogeneously distributed

The low RpoS expression observed by others in exponential phase cells [75, 77, 80] prompted our first question: How is this RpoS distributed amongst single cells? It could be that all cells have basal levels of RpoS or some cells could express the majority of the RpoS (Fig. 3.1). To answer this question we grew cells in bulk culture into exponential phase and examined aliquots of the culture with single-cell resolution under a microscope [38] (see Fig. 3.2a, Sec. 2.2.1). As a proxy for RpoS we used a transcriptional reporter with a promoter from an RpoS-responsive gene fused to GFP, P_{bolA}-*GFP*, based on a preliminary screen and literature [79, 97]. By computing histograms of mean RpoS level per cell we discovered that RpoS is heterogeneously distributed amongst single cells (Fig. 3.2b). To test the transcriptional fusion further we carried out the same liquid culture assay on an *rpoS*-knockout (Δ*rpoS*, Fig. 3.2b). The characteristic long tail of the heterogeneous *WT* distribution vanished in the knockout strain, leaving only spurious gene expression [105, 79].

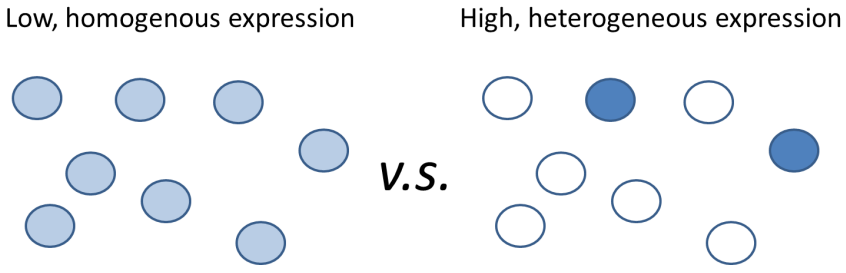

Fig. 3.1 Illustration of alternatives for RpoS distribution. The low expression of RpoS in exponential cells was measured in bulk cells. This small amount could be homogeneously distributed amongst the cells (a) or be due to a few cells with high RpoS expression (b).

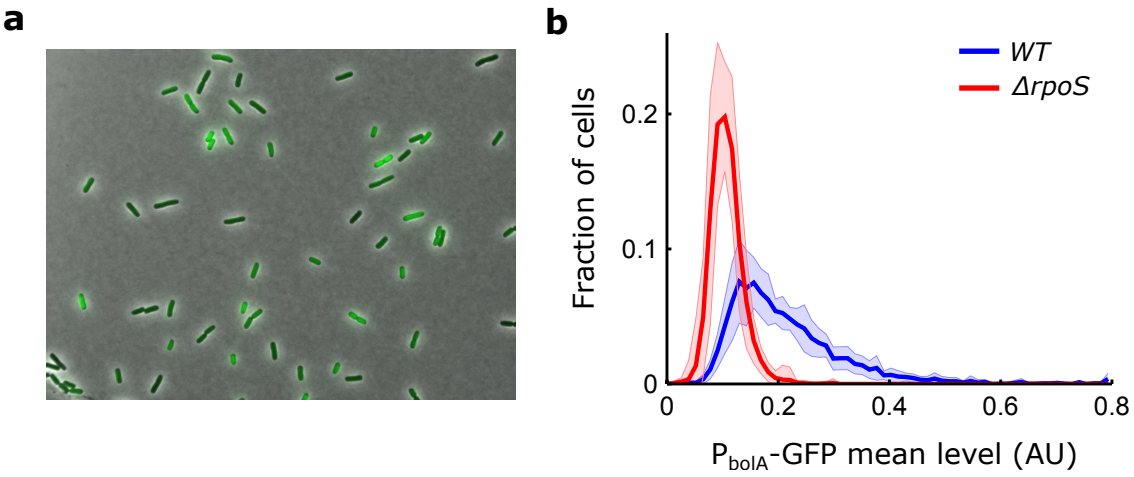

Fig. 3.2 The stress response master regulator, RpoS, is heterogeneously expressed in unstressed cells. a, Representative phase contrast and fluorescence composite image of RpoS reporter, P_{bolA}-*GFP*, in *WT*; channel ranges chosen for display. b, Histograms of mean GFP per cell (line: mean, shaded region: ± std dev) in *WT* (10 biological replicates, 4,037 cells, mean = 0.21, CV = 0.51) and Δ*rpoS* (9 bio. reps., 4,069 cells, mean = 0.11, CV = 0.27) strains. The long tail of high RpoS expression present in the *WT* is absent in the knockout.

3.1.2 Controls for imaging assay and reporters

The results observed in Fig. 3.2 could have arisen from technical sources, such as the imaging assay, plasmid segregation noise, or regulatory effects specific to the reporters as opposed to RpoS. The following controls rule this out.

Imaging assay does not induce heterogeneous stress response

Our imaging assay may have caused the heterogeneity in RpoS expression by inducing a stress response due to a sudden depletion of nutrients on the agarose pads. To control for this, we fixed cells while still in liquid culture with formaldehyde in methanol. This did not eliminate the long-tail of the WT distribution, despite potential denaturation of the GFP by methanol [106], suggesting the heterogeneity is intrinsic to the liquid culture (Fig. 3.3).

Heterogeneity of RpoS not due to plasmid segregation noise

During cell division plasmids can be unequally distributed to daughter cells [107]. The resulting difference in gene dosage may have led to heterogeneous GFP expression. To control for this effect, we chromosomally integrated the P_{bolA}-*GFP* reporter. We used three times longer fluorescent exposure times since the chromosomally integrated reporters were very dim. The *WT* chromosomally integrated reporter is qualitatively more heterogeneous than the reporter in the Δ*rpoS* background (Fig. 3.4). We quantified this with the coefficient of variation (CV). The CV of *WT* is 0.31, while that of Δ*rpoS* is 0.21. Since different exposure

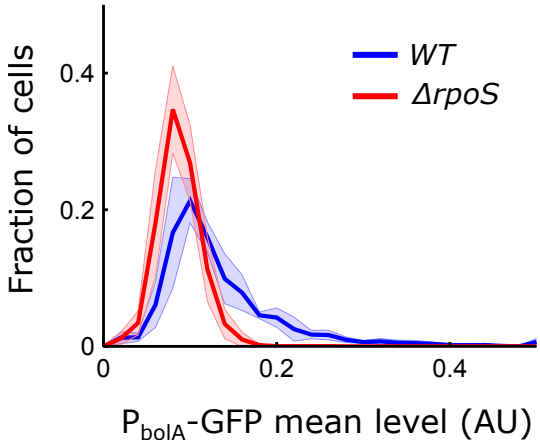

Fig. 3.3 Long tail distribution of RpoS is intrinsic to liquid culture. Fixing cells with formaldehyde while still in liquid culture does not eliminate long-tailed distribution of RpoS. Transcriptional fusion of P_{bolA}-*GFP* in *WT* (6 biological replicates, 3,012 cells, mean = 0.13 AU, CV = 0.57) and Δ*rpoS* (6 bio. reps., 3,292 cells, mean = 0.087 AU, CV = 0.28).

times were used for the chromosomal and plasmid based experiments, it was difficult to directly compare the two by overlaying histograms. However, the CVs can be compared. A similar increase in CV from Δ*rpoS* to *WT* was observed in the plasmid experiments (from 0.27 to 0.51).

To ensure we were not simply observing random dark counts of the detector, as well as to ensure the Δ*rpoS* construct had the dim reporter integrated, we measured strains with no reporter. The *WT* signal was above background (Fig. 3.4). The Δ*rpoS* signal was also above this background. This is likely due to the high homology of RpoS and σ^{70} allowing for GFP expression, as well as spurious background expression due to the promiscuity of RNA polymerases [79, 105].

Alternative reporters for RpoS and σ^{70}

The transcriptional fusions were constructed by cloning the intergenic region from the *E. coli* chromosome (Fig. 2.1a) [97]. Consequently, the DNA upstream of the GFP coding sequence contains the ribosome binding site (RBS) and the native *atg* start site of the gene from which the promoter was taken as well as additional chromosomal upstream DNA (Fig. 2.1b). All of these elements could have contributed to the heterogeneous GFP signal we observed, instead of RpoS heterogeneity. To rule this out, we tested alternative RpoS reporters and found similar behaviours (Fig. 3.5), despite these reporters deriving from genes of very different functions (Tab. 2.3) [79].

To test whether the long-tail was specific to RpoS, we examined σ^{70} reporters (Tab. 2.3) [79]. The distributions of σ^{70} levels in WT populations had less pronounced long-tails due

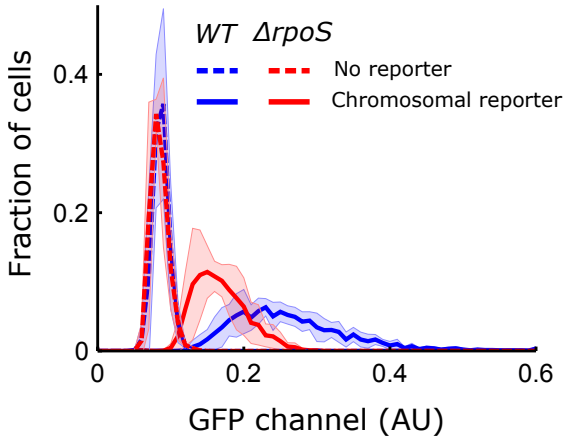

Fig. 3.4 Long-tailed RpoS distribution is not due to plasmid segregation effect. Distribution of RpoS level from bulk liquid culture measured with 3x higher exposure than for plasmid-borne reporter images: with chromosomally integrated P_{bolA}-*GFP* reporter *WT*, 4 biological replicates, 2897 cells, mean = 0.26 AU, CV = 0.31; and Δ*rpoS*, 4 biological replicates, 2039 cells, mean = 0.17 AU, CV = 0.21; *WT* with no reporter, 2 biological replicates, 1170 cells, mean = 0.087 AU, CV = 0.12; Δ*rpoS* with no reporter, 2 biological replicates, 954 cells, mean = 0.085 AU, CV = 0.15.

to the higher abundance of σ^{70} in cells and did not change significantly in Δ*rpoS* (Fig. 3.6) [79].

Translational fusion to *rpoS*

The transcriptional reporters above measure the activity of the sigma factors, but do not directly report on sigma factor expression. To measure this, we procured a chromosomally integrated, translational fusion of RpoS to mCherry, *rpoS::mCherry* (Fig. 3.7a). The *mCherry* coding sequence was inserted into the chromosome in the lab of Kenn Gerdes, leaving the translational fusion the only RpoS in the cell[1]. We found RpoS levels were heterogeneously distributed with this reporter as well (Fig. 3.7b). However, the translational fusion was not able to activate the transcriptional reporter, suggesting the fusion lacks function (Fig. 3.7c). This was likely due to steric hindrance from the mCherry protein interfering with either RpoS binding to the RNA polymerase core, or, if the RNAP holoenzyme could form, interfering with DNA binding.

3.2 RpoS pulsing produces heterogeneous population

We next investigated the mechanism by which the RpoS distribution is produced. Reasoning that the distribution is due to a dynamic equilibrium, not a fixed subpopulation, we tracked single cells over multiple generations using time-lapse microscopy and the Mother Machine

[1] Personal communication.

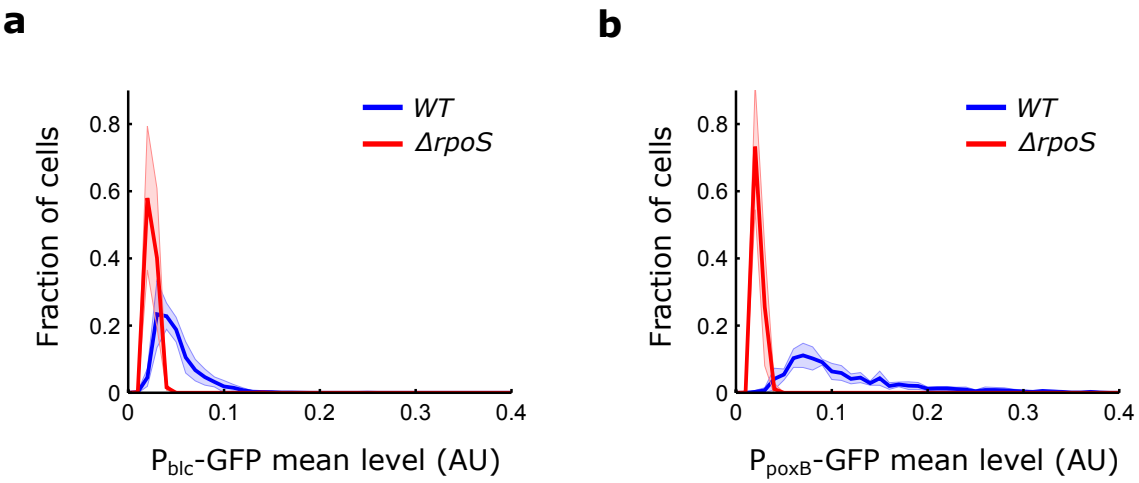

Fig. 3.5 Alternative RpoS reporters have long-tailed distributions of RpoS; the long tails vanish in the *rpoS*-knockout. a, Transcriptional fusion of P_{blc}-*GFP* in *WT* (6 biological replicates, 2,509 cells, mean = 0.050 AU, CV = 0.46) and Δ*rpoS* (4 bio. reps., 1,190 cells, mean = 0.025 AU, CV = 0.21). b, Similarly for P_{poxB}-*GFP* (*WT*: 5 bio. reps., 1,087 cells, mean = 0.12 AU, CV = 0.59; Δ*rpoS*: 7 bio. reps., 1,463 cells, mean = 0.023 AU, CV = 0.17). Lines and shaded region are mean ± std dev, respectively.

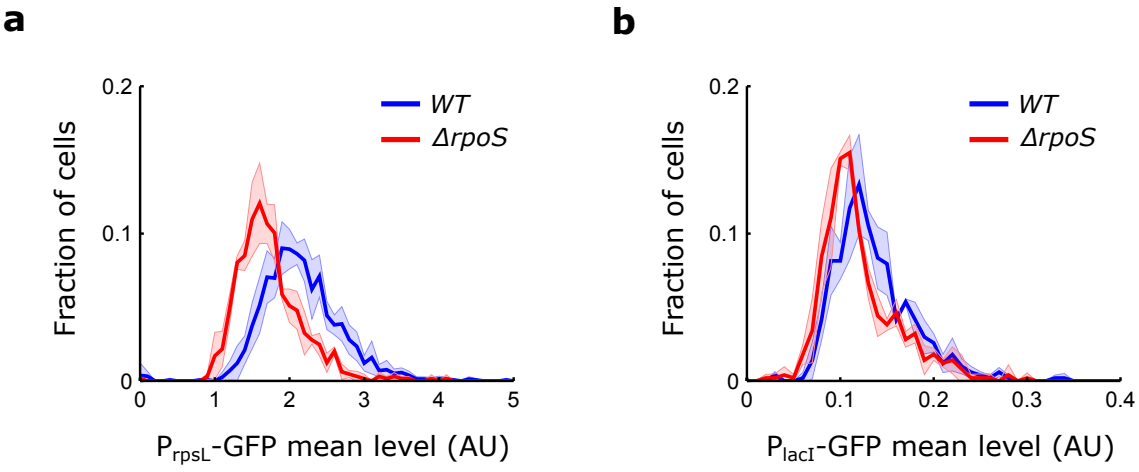

Fig. 3.6 Reporters of σ^{70} have distributions with lower coefficients of variation than RpoS reporters and distributions that are similar in WT and Δ*rpoS*. a, Transcriptional fusion of P_{rpsL}-*GFP* in *WT* (5 bio. reps., 1,576 cells, mean = 2.1 AU, CV = 0.25) and Δ*rpoS* (3 bio. reps., 647 cells, mean = 1.7 AU, CV = 0.25). b, Similarly for P_{lacI}-*GFP* in *WT* (3 bio. reps., 503 cells, mean = 0.14 AU, CV = 0.31) and Δ*rpoS* (3 bio. reps., 497 cells, mean = 0.12 AU, CV = 0.34). Lines and shaded region are mean ± std dev, respectively.

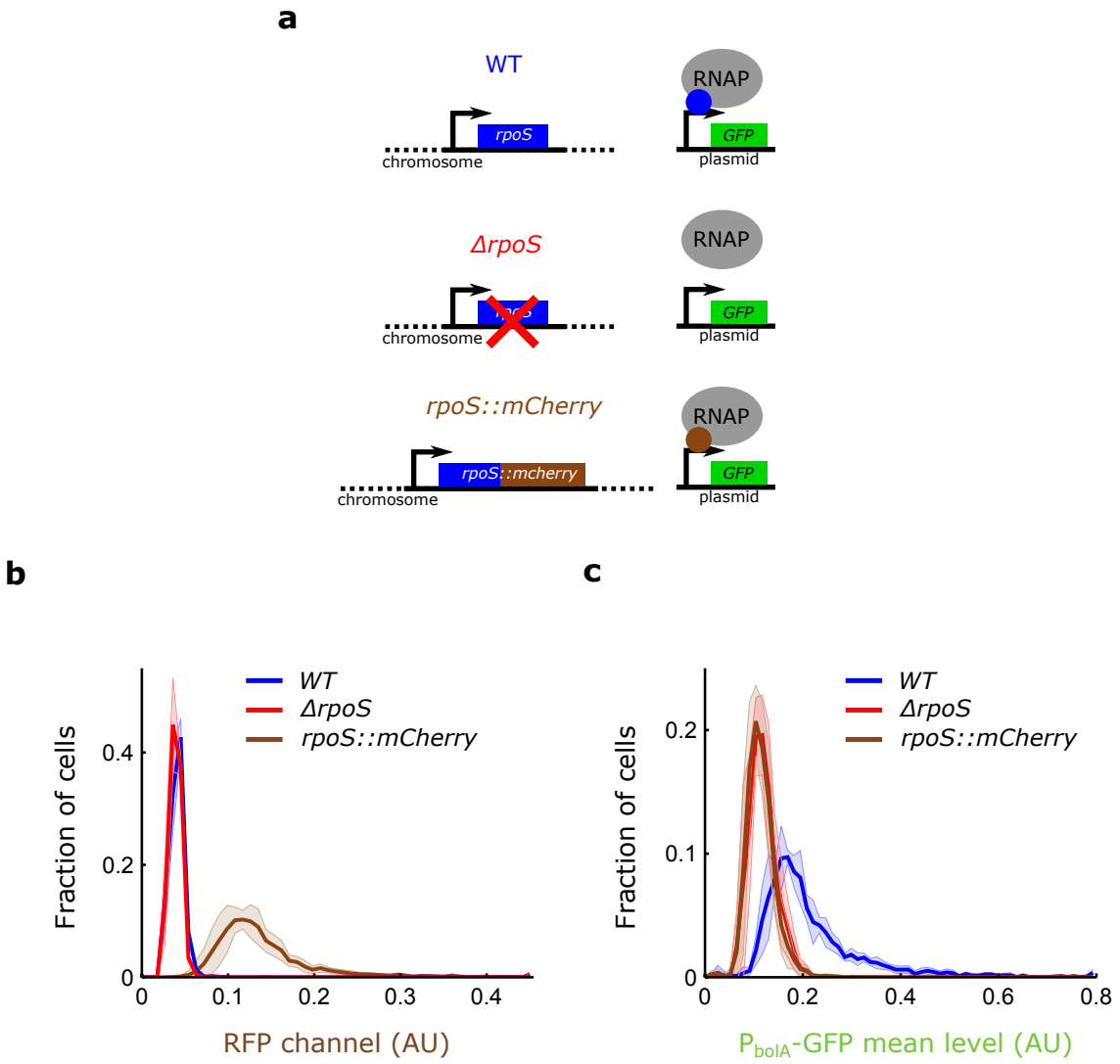

Fig. 3.7 Translational fusion of RpoS::mCherry is heterogeneously distributed, but is not functional. a, Schematic of the rpoS::mCherry strain compared to *WT* and Δ*rpoS* as found in remainder of the paper. b, c Measurements of cells in bulk culture. b, Histograms of RpoS::mCherry concentration measured as mean RFP channel fluorescence per cell compared to *WT* and Δ*rpoS* controls lacking the fluorescent construct. *WT* (5 biological replicates, 2,951 cells, mean = 0.041 AU, CV = 0.20, excluding 4 outliers), Δ*rpoS* (3 biological replicates, 1,525 cells, mean = 0.039 AU, CV = 0.16), and rpoS::mCherry (8 biological replicates, 4,949 cells, mean = 0.14 AU, CV = 0.40, excluding 27 outliers). c, Histograms of mean GFP fluorescence per cell *WT* (5 biological replicates, 3,065 cells, mean = 0.22 AU, CV = 0.51), Δ*rpoS* (3 biological replicates, 1,623 cells, mean = 0.12 AU, CV = 0.24), and rpoS::mCherry (8 biological replicates, 4,325 cells, mean = 0.11 AU, CV = 0.26). In (b, c), lines and shaded region are mean ± std dev, respectively.

microfluidic device [27] (Fig. 3.8a, Sec. 2.1.6). We found cells had heterogeneous P_{bolA}-*GFP* levels in this environment as well (Fig. 3.12e). By computing the rate of production of the mean GFP signal, we extracted the RpoS activity (see Sec. 2.3.5 for derivation and Fig. 2.7). Indeed, we found rich, dynamic RpoS activity. A small fraction of cell lineages have high RpoS activity pulses lasting multiple generations while others have a range of pulse sizes, including very small pulses (Fig. 3.8b). We also observed similar dynamics with alternative RpoS transcriptional reporters in the Mother Machine (Fig. 3.9).

Analysing the P_{bolA}-*GFP* Mother Machine data, we found a long-tailed distribution of pulse heights; supporting the idea that the long-tailed liquid culture distribution is generated by cells pulsing RpoS on to different levels (Fig. 3.8c).

3.2.1 Controls for the pulsing dynamics

RpoS pulsing not an artefact of the Mother Machine environment

The cells may have pulsed on RpoS because the Mother Machine environment was stressful - perhaps due to nutrients not reaching the mother cell from the feed trench. This is unlikely as we observed similar pulsing in two different environments (Fig. 3.10). In the first approach, media was supplied embedded in agarose pads [38] (see Methods Sec. 2.2.6). The experiment was stopped well before nutrients could be limiting; as cells would stack on top of each other within ~5 generations, preventing single-cell tracking (Fig. 3.10a). The other environment was an alternative, commercially available, CellASIC microfluidic device with media flowing around the cells [102] (Sec. 2.2.7). Here too, we observed pulsing, even in cells at the edges of microcolonies (Fig. 3.10b).

RpoS pulsing is not due to plasmid segregation noise

Using the chromosomally integrated P_{bolA}-*GFP* reporter we found a similar consistency between bulk culture and microfluidic experiments suggesting the dynamics did not arise due to plasmid segregation noise (Fig. 3.4 and 3.11a, b). The single-cell traces of growth rate and gene expression were qualitatively similar to those measured with cells harbouring the plasmid-borne reporter (Fig. 3.11a and 3.8b), as were the growth rate distributions (Fig. 3.11c) and the cross-correlation of growth with RpoS activity (Fig. 3.11d). To avoid phototoxicity effects, we used the same exposure for these experiments as those with the plasmid-borne reporter. The resulting fluorescence signal was very dim, thus we proceeded with the plasmid-based reporter.

Similar pulsing dynamics observed with translational fusion

The *rpoS::mCherry* translational fusion also had a long tail distribution of pulse heights in the Mother Machine; validating the RpoS dynamics (Fig. 3.12a-d). We further observed a

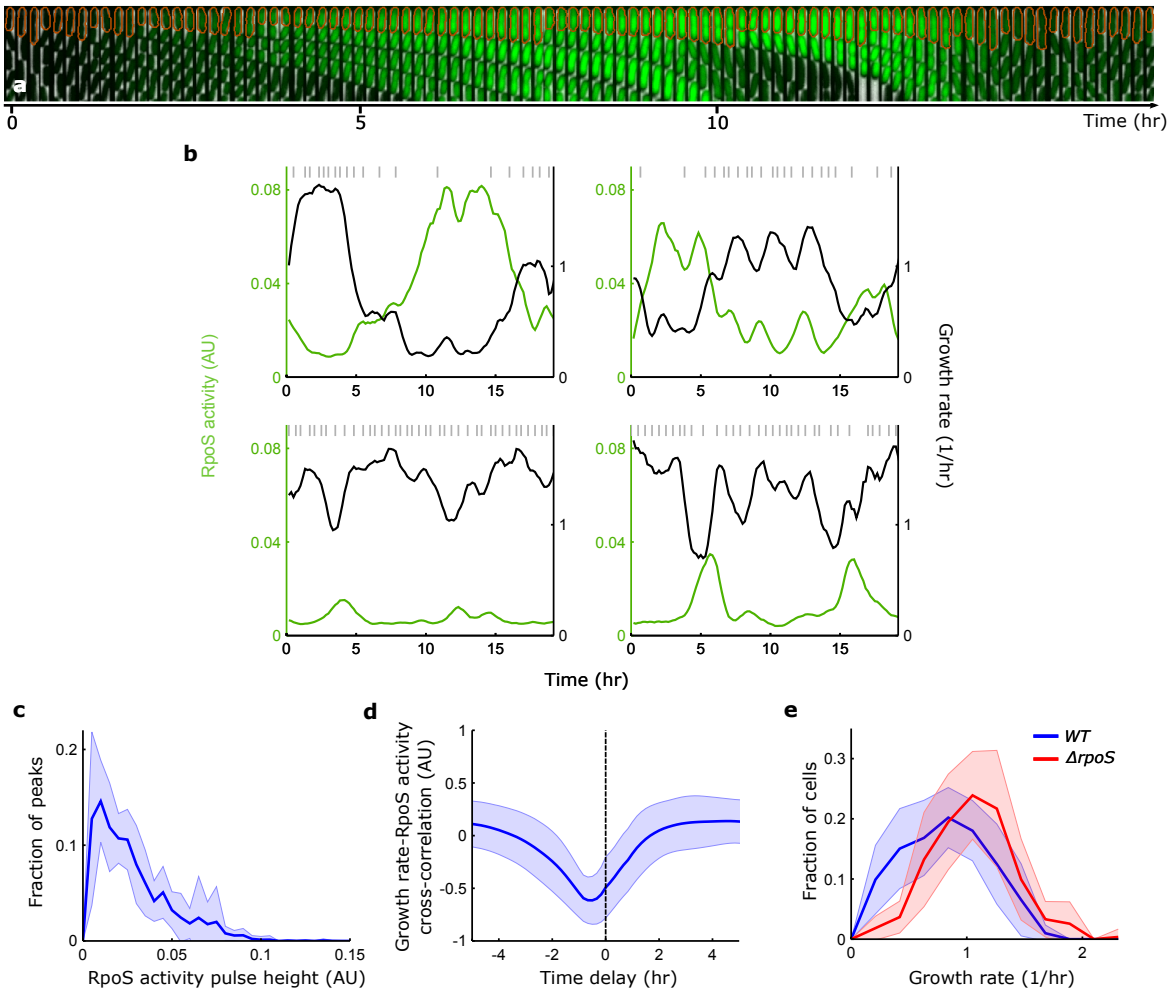

Fig. 3.8 Multi-generation RpoS and growth pulses generate heterogeneous RpoS expression. a, Sample montage of a mother cell (orange outline) in the Mother Machine pulsing on RpoS and reducing growth rate (1 frame/10 minutes). Phase contrast and fluorescence channel ranges chosen for display. b, Sample time traces of RpoS activity and growth rate for four mother cells. Grey vertical lines indicate cell divisions. c, Histogram of RpoS activity pulse height (3,608 pulses). d, Cross-correlation between growth rate and RpoS activity. e, Histogram of growth rate at one frame (59) from all movies for *WT* (505 cells) and Δ*rpoS* (272 cells). The mean ± std dev is plotted with the line and the shaded region, respectively, for *WT* (11 technical replicates drawn from 7 biological replicates, 507 mother cells) and Δ*rpoS* (10 tech. reps. drawn from 6 bio. rep., 274 mother cells).

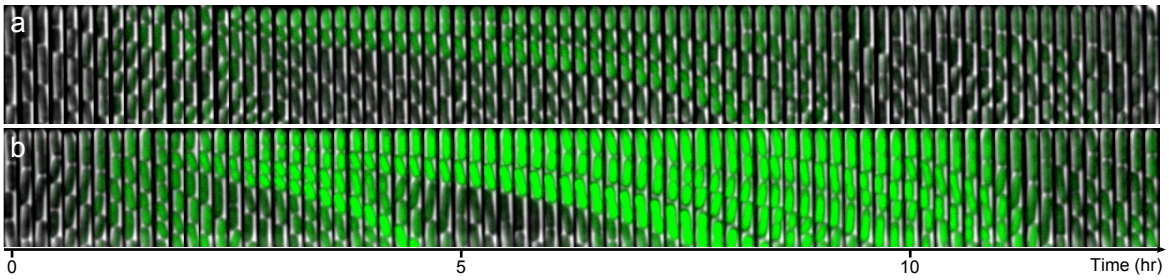

Fig. 3.9 Alternative transcriptional reporters also pulse. Sample montages of mother cells in the Mother Machine harbouring the P_{blc}-*GFP* (a) or P_{poxB}-*GFP* (b) reporters pulsing on RpoS and reducing growth rate (1 frame/10 minutes). Phase contrast and fluorescence channel ranges chosen for display.

lack of functionality of the translational fusion as a lack of transcriptional activity prompting us to continue using the transcriptional reporter (Fig. 3.12e, f).

3.3 Single-cell growth rate is also noisy

We further observed rich dynamics in the growth rate of single-cells (Fig. 3.8a,b). The sample lineages illustrate that cell growth slows down when RpoS activity is high. This relationship was quantified as a large negative value near zero time-shift in the cross-correlation of growth rate and RpoS activity (Fig. 3.8d). The strong anti-correlation suggested that growth rate should also be widely distributed, which is what we observed (Fig. 3.8e). However, the Δ*rpoS* strain also had a wide growth rate distribution suggesting growth rate is intrinsically heterogeneous [70, 71] (Fig. 3.8e).

3.3.1 Noisy growth rate driven by σ^{70}

Furthermore, σ^{70} activity was positively correlated with growth rate suggesting it is related to this intrinsic variability (Fig. 3.13a). The reporter for σ^{70}, P_{rpsL}-*GFP*, was an order of magnitude brighter than P_{bolA}-*GFP*, used to measure RpoS activity. We found growth rate distributions to follow a similar trend for *WT* and Δ*rpoS* regardless of the reporter (Fig. 3.13b). This controlled for the possibility that GFP toxicity caused the growth rate heterogeneity observed.

3.4 Conclusion and Discussion

Using single-cell microscopy of bulk cultures, and an extensive list of controls, we showed that exponential phase cells heterogeneously express RpoS. The state of high RpoS expression is produced by multi-generation pulses that are anti-correlated with growth rate.

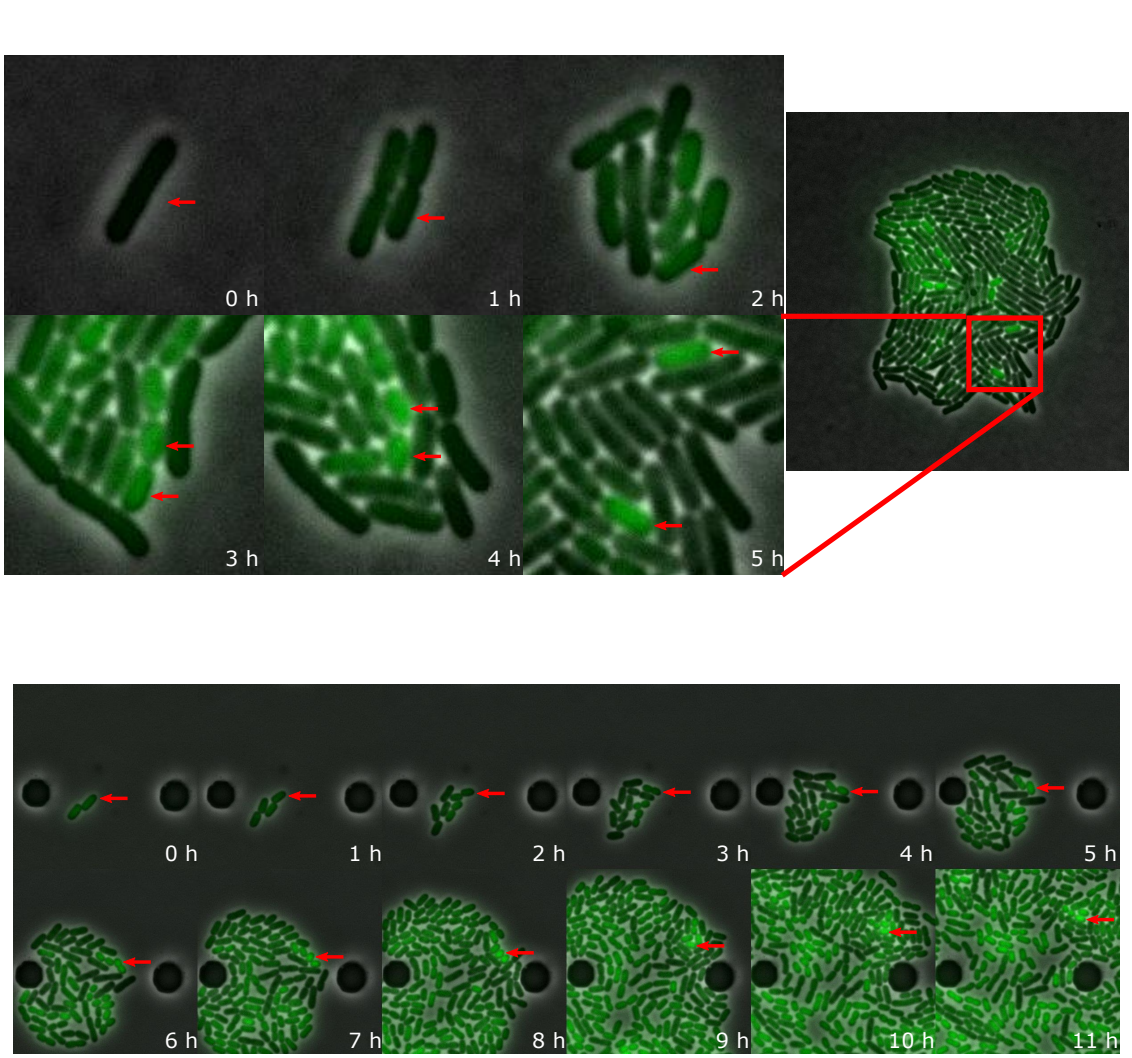

Fig. 3.10 RpoS pulsing is not an artefact of the Mother Machine microfluidic device environment. a, Sample movie montage of cells (MG1655 *WT* with P_{bolA}-*GFP*) grown on M9 agarose pads. A biological repeat showed similar effects. Red arrows indicate a lineage that grows slower than its neighbours and has high RpoS expression. A zoomed out image of the last frame illustrates the contrast in growth rates between the highlighted lineage and the remainder of the colony. b, Sample movie montage of cells (BW25113 *WT* with P_{bolA}-*GFP*) grown in the CellASIC microfluidic device. A biological repeat showed similar effects. The red arrows indicate a cell lineage that grows slower and has higher RpoS expression than its neighbours. In both (a) and (b) cells were imaged every 10 minutes and phase contrast and fluorescence channel ranges chosen for display.

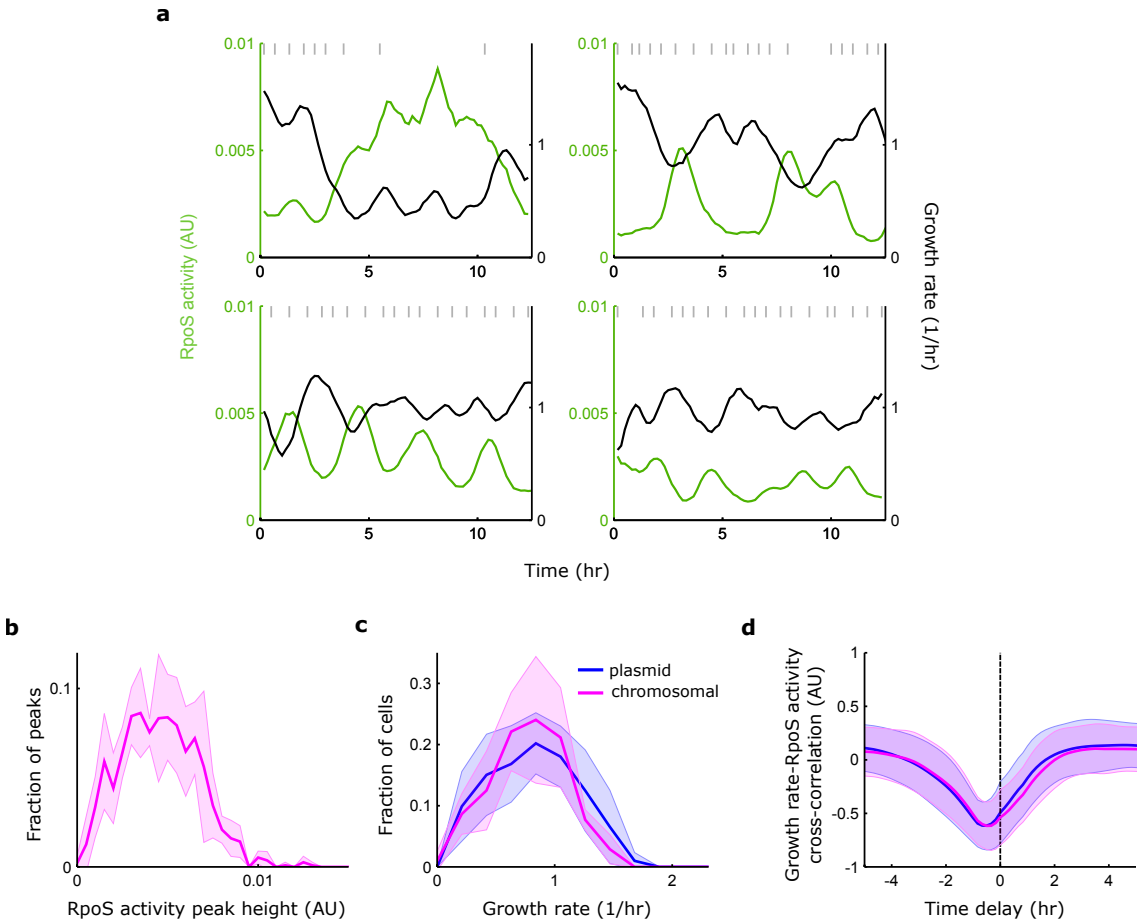

Fig. 3.11 Long-tailed RpoS distribution is not due to plasmid segregation effect, nor are the growth effects due to plasmid toxicity. a, Sample time traces of RpoS activity and growth rate for four mother cells with chromosomally integrated P_{bolA}-*GFP*. Grey vertical lines indicate cell divisions. b-d, 4 technical replicates drawn from 2 bio. reps., 106 mother cells. The plasmid data in (c, d) is reproduced from Fig. 3.8 for ease of comparison. Lines and shaded region are mean ± std dev, respectively. b, Pulse height distribution in Mother Machine experiments (990 peaks). d, Growth rate histogram at one frame (59) from all movies (104 cells). e, Cross-correlation between growth rate and RpoS activity.

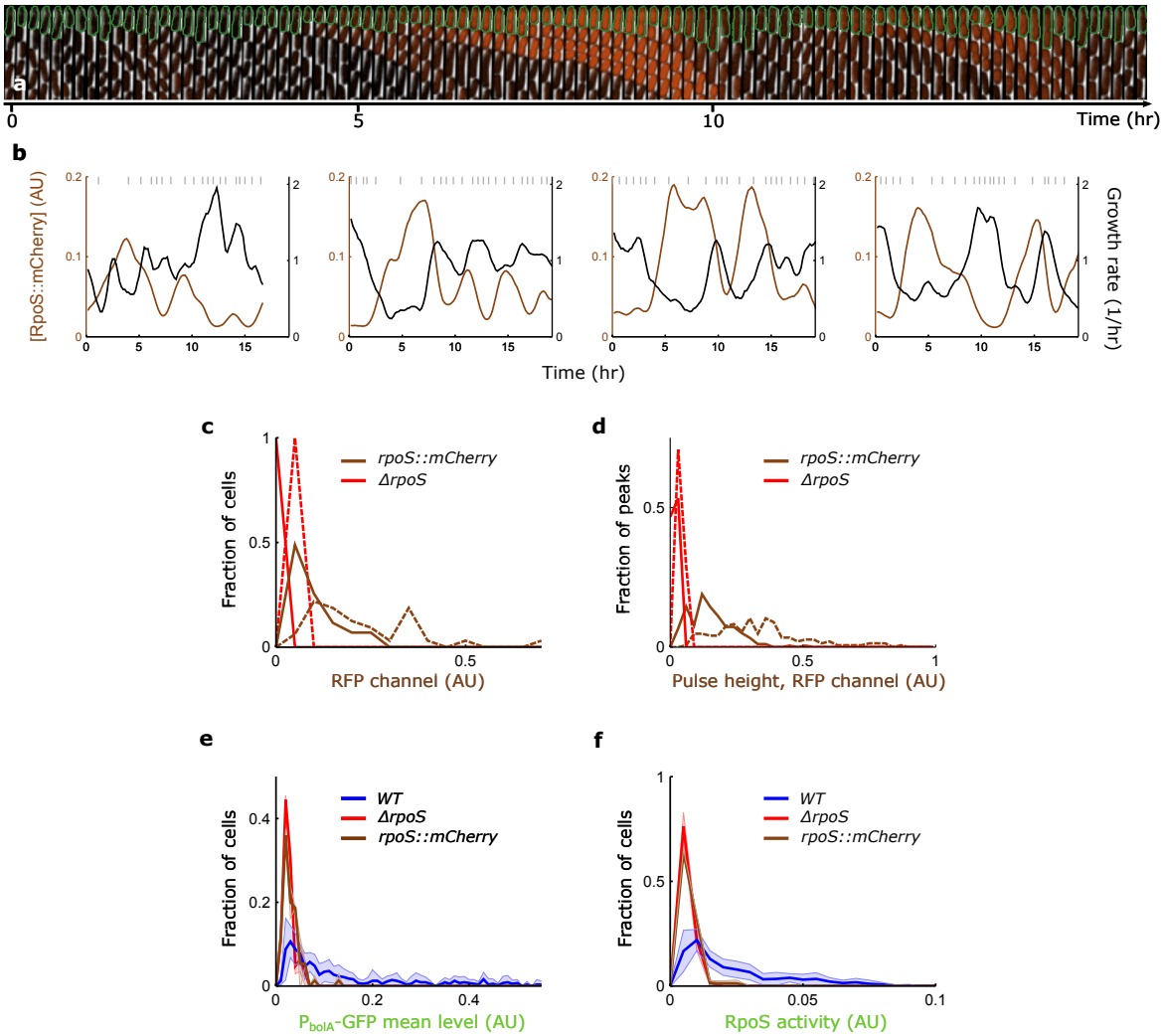

Fig. 3.12 Translational fusion also pulses in the Mother Machine. a, Sample montage of a mother cell (green outline) in the Mother Machine pulsing on RpoS::mCherry (1 frame/10 minutes; phase contrast and fluorescence channel ranges chosen for display). b, Sample time traces of RpoS::mCherry concentration and growth rate for four mother cells illustrating pulsing. Traces smoothed with a moving average filter spanning five frames, for display. c, Histograms of RpoS::mCherry concentration measured as mean RFP channel fluorescence per cell compared to Δ*rpoS* control. Δ*rpoS* (2 biological replicates shown separately due to technical discrepancy in background; dashed line: 30 cells, mean = 0.037 AU, CV = 0.21, solid line: 33 cells, mean = 0.015 AU, CV = 0.23), and *rpoS::mCherry* (2 biological replicates shown separately; dashed line: 32 cells, mean = 0.22 AU, CV = 0.67, solid line: 43 cells, mean = 0.10 AU, CV = 0.64).

(caption continued)

Fig. 3.12 caption, continued

d, Pulse height histograms of the same data in (c). Δ*rpoS* (2 biological replicates shown separately; dashed line: 202 peaks, mean = 0.040 AU, CV = 0.18, solid line: 225 peaks, mean = 0.016 AU, CV = 0.22), and *rpoS::mCherry* (2 biological replicates shown separately; dashed line: 145 peaks, mean = 0.34 AU, CV = 0.51, solid line: 179 peaks, mean = 0.15 AU, CV = 0.55). e, Mean expression from transcriptional reporter, P_{bolA}-*GFP*. *WT* (11 technical replicates drawn from 7 biological replicates, 505 cells, mean = 0.14 AU, CV = 0.98), Δ*rpoS* (2 biological replicates, 63 cells, mean = 0.026 AU, CV = 0.44), and *rpoS::mCherry* (2 biological replicates, 75 cells, mean = 0.030 AU, CV = 0.58). f, RpoS activity measured with the transcriptional reporter. *WT* (11 technical replicates drawn from 7 biological replicates, 505 cells, mean = 0.023 AU, CV = 0.82), Δ*rpoS* (2 biological replicates, 63 cells, mean = 0.0065 AU, CV = 0.32), and *rpoS::mCherry* (2 biological replicates, 75 cells, mean = 0.0073 AU, CV = 0.45). Data for (c, e, and f) were taken at one frame (59) from all movies. In (c-f), lines and shaded region are mean ± std dev, respectively.

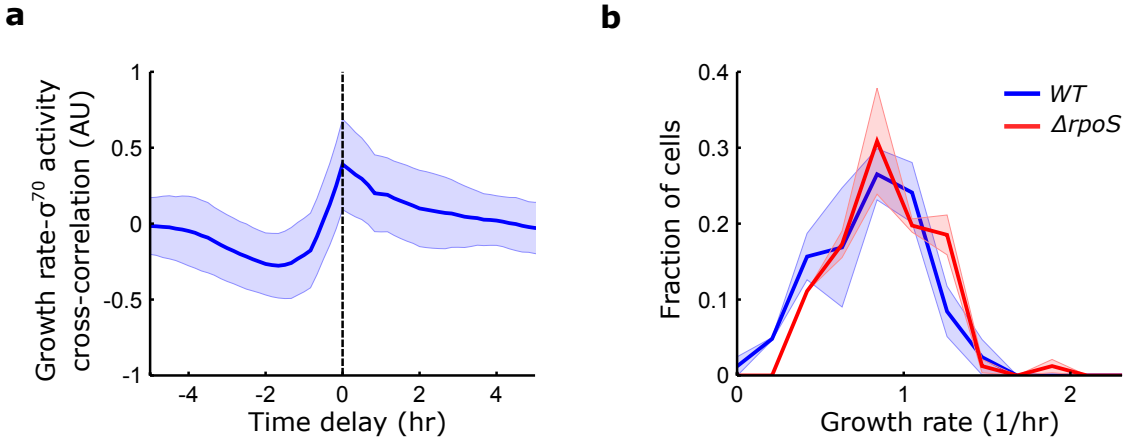

Fig. 3.13 Constitutive, σ^{70}, reporter is positively correlated with growth and high GFP expression does not affect growth rate distribution. Using P_{rpsL}-*GFP* in *WT* and Δ*rpoS*. a, Cross-correlation between growth rate and σ^{70} activity in WT cells. b, Growth rate histogram for *WT* and Δ*rpoS* from one frame (59) from all movies. *WT*: 2 biological replicates, 83 mother cells; Δ*rpoS*: 2 biological replicates, 81 mother cells. Lines and shaded region are mean ± std dev, respectively.

3.4.1 Robustness of RpoS heterogeneity

We have found the heterogeneity of RpoS to be extremely robust. We have tested that the distribution of RpoS we report was not an artefact of our culturing methods in several ways. In preliminary experiments, we serially passaged exponential phase, bulk cultures three times, and found the single-cell RpoS distribution remained heterogeneous. We have observed similar distributions of GFP from the P_{bolA}-*GFP* reporter in liquid culture snaps when two WT strains were used (MG1655 and BW25113, see Fig. 5.7 of Chap. 5). We have used two isolates of MG1655 (one a gift of Professor Kenn Gerdes) and found similar distributions (Fig. 3.7 and Fig. 5.7 of Chap. 5). We have started cultures directly from glycerol stocks and from single colonies picked from stocks streaked out on LB plates, and found similar effects. The Mother Machine data that we present is over tens of generations and the distribution of growth rates and RpoS activity is constant (as can be seen in the 'Total population' traces of Fig. 5.2b, c and Fig. 5.4b in Chapter 5, following an initial transient phase).

We also tested that our observations were not an artefact of our reporters in several ways. We used three alternative transcriptional reporters and a translational reporter, all of which showed RpoS was heterogeneous. The translational fusion was chromosomally integrated and we chromosomally integrated one of the transcriptional reporters without affecting the conclusions, ruling out plasmid segregation noise.

It was possible that the distribution of background signal was so varied that it was the source of the large heterogeneity we observed in RpoS expression. However, this was not the case, based on two pieces of evidence. First, when *rpoS* was knocked out, the distribution changed, and always decreased in heterogeneity (Fig. 3.2, 3.3, 3.4, 3.5). Second, and more strongly, the distribution of both WT and Δ*rpoS* cells with no reporter were very similar and nearly homogeneous (Fig. 3.4). This happened despite using a 3x higher exposure for the reporter-less cells compared to the cells harbouring the plasmid-borne reporter (Fig. 3.2).

3.4.2 Robustness of noisy growth

A key observation in this chapter was that the growth of *E. coli* cells is noisy. This has been observed in the past [27, 70, 44, 71] (see Fig. 1.9), however the noise we report is higher than noted previously, though still comparable. There are several reasons for this, some of which are speculative. The difference likely comes from the differences in media conditions, imaging conditions, and time resolution of data acquisition. The first work that introduced the Mother Machine used rich, LB medium [27]. Exponential phase cultures in LB medium are known to poorly express RpoS [80], which will lead to faster growth, and so lower noise (see Figure 3.8e and the results of Chapter 4). More recent work focused on noisy growth and used minimal media as used here [70]. Indeed, they found growth rates to be similarly noisy to ours, though ours were still higher (coefficient of variation of

~0.3 in Kiviet *et al.* [70], see Fig. 1.9; compared to our CV~0.4 for comparable mean growth rate of ~0.8/hr). We can speculate this difference is due to the difference in culturing and imaging conditions. By imaging their cells in the phase contrast channel about ten times more frequently than us, they likely had lower technical noise than us. They also analysed cells grown as microcolonies (similar to Fig. 3.10a), while we analysed our Mother Machine data. Growth artefacts arising from the Mother Machine have recently been revealed in a systematic study [108], which might further account for the difference in noise magnitude we report compared to Kiviet *et al.* [70]. We find it encouraging that despite the differences in techniques used the noisy growth of *E. coli* seems to be a robust biological phenomenon.

Outlook

In the next chapter we reveal a simple model that explains the observations reported in this chapter.

Chapter 4

RpoS-growth mutual inhibition

In the previous chapter we showed that RpoS activity and growth rate are dynamic, noisy, and anti-correlated. Here, we propose a coupled molecular and physiological model to explain our observations. First, we propose the intrinsic variability in growth rate arises due to stochastic molecular reactions that promote growth. Second, RpoS molecules repress growth and growth dilutes RpoS. This results in the anti-correlation between growth rate and RpoS. To show this, we use a mathematical model based on the Gillespie stochastic simulation algorithm coupled to a cell growth model. After establishing the model's ability to explain the data we perturb the experimental system to test predictions of the model.

4.1 Model implementation

For simplicity, we chose to model two molecular species, growth factor (γ) and RpoS (r). We used a stochastic Gillespie simulation for the reactions. Both were assumed to be produced by zeroth order reactions and degraded by first order reactions (Fig. 4.1). The reactions occurred in a cell, which grew at deterministic time intervals. As the cell volume increased molecule concentration was diluted. The growth rate at each deterministic time step explicitly depended on the most recent γ and RpoS concentration via the product of Hill functions (Fig. 4.1, 4.2). The Hill function for γ rose with concentration while that for RpoS decreased. This captured the promoting and repressing effects on growth rate of the two kinds of molecules, respectively. This coupled molecular and physiological simulation can be summarised as a mutual inhibition feedback between RpoS and growth rate [69] (Fig. 4.1).

4.1.1 Cell growth

We modelled a single cell growing as a function of molecular reactions occurring inside it (Fig. 4.2). A single lineage was followed, *i.e.* only one daughter cell was followed at each cell

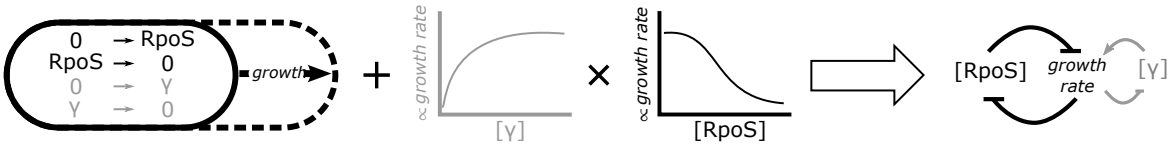

Fig. 4.1 Schematic illustration of mathematical model. Stochastic molecular reactions occur in a growing cell. The reactions are simulated with the Gillespie algorithm, while cell growth happens at deterministic time steps. Growth at each time step is dependent on molecular concentration via Hill functions. The result is a mutual inhibition between growth rate and RpoS concentration.

division. To model growth, we assumed rod-shaped cells with fixed radius and modelled growing cells by the changing length at a fixed, deterministic time interval, Δt:

$$\Delta l_i = g_{i-1} \cdot \Delta t \cdot l_{i-1} \tag{4.1}$$

where g_i and l_i are the growth rate and cell length at the i^{th} time point, respectively. Cell division was assumed to follow the adder rule [44]:

$$l_i = \begin{cases} l_{i-1} + \Delta l_i & \sum_{\text{last division}}^{i} \Delta l_k < \Delta L \\ \frac{l_{i-1}+\Delta l_i}{2} & \text{otherwise} \end{cases} \tag{4.2}$$

where ΔL is a fixed length the cell must add before it can divide.

4.1.2 Gillespie simulation of chemical reactions

The numbers of molecules in the cell were determined by a standard Gillespie stochastic simulation algorithm [47] that ran between the deterministic steps of the growth model (Fig. 4.2). Two molecular species RpoS, r, and growth factor, γ, were modelled. They were generated with zeroth order constitutive production and first order degradation reactions:

$$0 \xrightarrow{k_{rp}} r \tag{4.3}$$

$$r \xrightarrow{k_{rd}} 0 \tag{4.4}$$

$$0 \xrightarrow{k_{\gamma p}} \gamma \tag{4.5}$$

$$\gamma \xrightarrow{k_{\gamma d}} 0 \tag{4.6}$$

where k_{xp} are the production reaction rate constants and k_{xd} are the degradation reaction rate constants for species x. The reaction propensities in the Gillespie algorithm do not change with cell volume since the reactions are zeroth and first order [96].

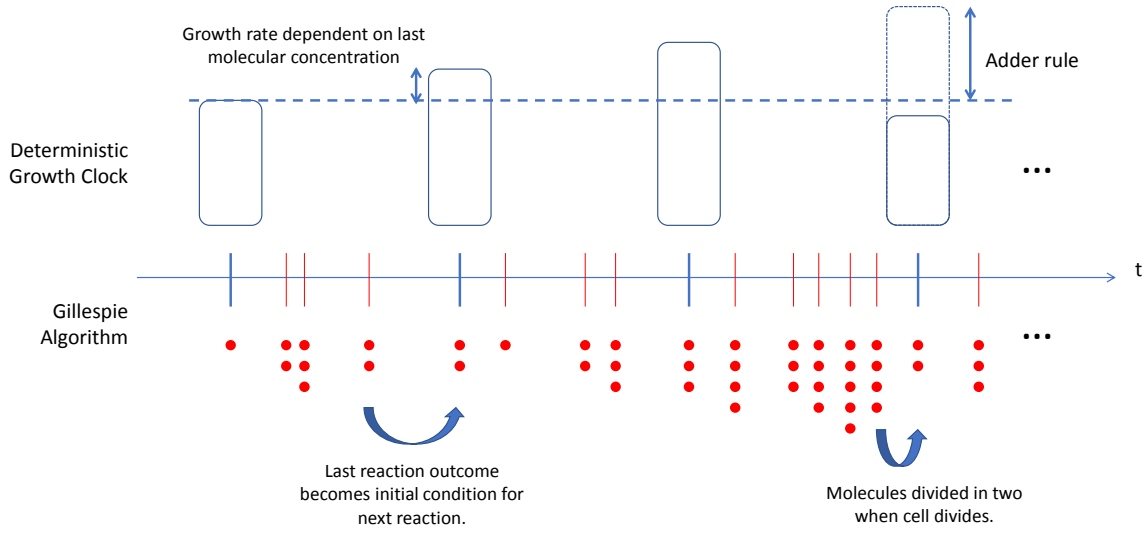

Fig. 4.2 Schematic of coupled model algorithm. The model couples a deterministic growth model with a stochastic molecular simulation. At every deterministic time point, the cell grows. The size it grows by is given by the molecule concentration present at the time. The molecule concentration is updated stochastically between growth time steps by a standard Gillespie algorithm. Cell division follows the adder rule [44], cells divide when the have added a fixed length. At division the number of molecules is divided in two.

4.1.3 Coupling the two models

At division the number of molecules were simply divided in half and rounded to the closest integer lower than the quotient:

$$species_i = \lfloor species_{i-1}/2 \rfloor \tag{4.7}$$

The concentration of the molecular species was the number of species divided by cell length (volume):

$$[species_i] = \frac{species_{i-1}}{l_{i-1}} \tag{4.8}$$

Growth rate was a product of two Hill functions of the concentration of the two molecular species generated most recently by the Gillespie algorithm:

$$g_i = g_{max} \cdot \left(\frac{1}{1 + \left(\frac{h_\gamma}{[\gamma_i]}\right)^{n_\gamma}} \right) \cdot \left(\frac{1-f}{1 + \left(\frac{h_r}{[r_i]}\right)^{n_r}} + f \right) \tag{4.9}$$

where g_{max} is the maximum growth rate; f represents the lowest growth rate can be reduced to in the limit of infinite RpoS concentration; h_γ and h_r are the values of growth factor and RpoS leading to half-maximal growth, respectively; and n_γ, n_r are the Hill coefficients. Growth factor was considered a downstream target of σ^{70} so n_γ was positive, while n_r was chosen to be negative to capture the repressive effect of RpoS on growth. Growth perturbation simulations were implemented by varying g_{max}, while all other parameters were kept constant. However, in the reduced RpoS efficacy model (Sec. 4.3.3) the parameter f was increased to keep the product $f \cdot g_{max}$ constant. See Sec. 2.5 for the pseudo code of the algorithm, and Appendix A for the complete code.

4.2 Constraining the model using experimental growth data

There were many parameters in the model (Tab. 4.1). Each chemical reaction had an associated reaction rate and the Hill functions relating molecular concentration to growth rate had several shape parameters (Fig. 4.3). As the cell grows, even if no chemical reaction occurs, the molecular concentrations change and so the growth rate in the next time step changes. The resulting molecular and growth dynamics can be non-intuitive. Thus, we used a coarse grained exploration of parameter space to find parameter values that reproduced the experimental growth rate distributions and population doubling times for Δ*rpoS* and *WT* (Fig. 3.8e).

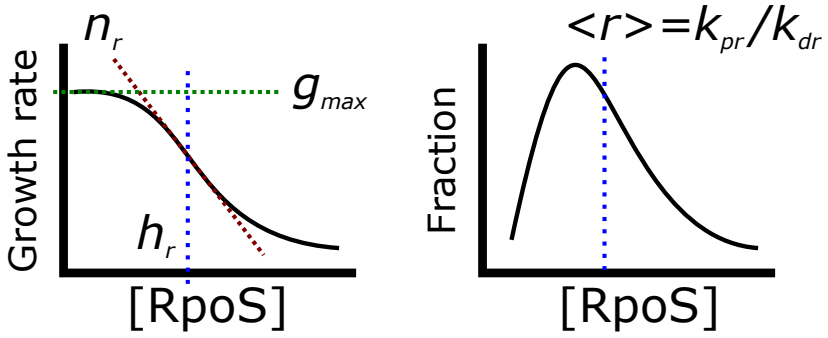

Fig. 4.3 Illustration of effect of parameters. Left, a decreasing Hill function, as used to relate RpoS concentration to growth rate (Fig. 4.1). The concentration of RpoS at which growth rate is half the maximum value (given here by g_{max}), is parametrized by h_r. The steepness of the hill function is parametrized by n_r. Right, the mean value of RpoS, $< r >$, is given by the ratio of the production (k_{pr}) and degradation rates (k_{dr}). The chemical reactions used here result in a simple birth-death process, which has a Poisson distribution [64]. However, due to the feedback between growth rate and RpoS, the distribution of RpoS concentration will not be dictated solely by the chemical reactions.

4.2.1 Constraining the γ parameters

To limit the number of parameters we had to search over, we began with no RpoS in the cells, and constrained the parameters associated with γ using the $\Delta rpoS$ data. This reduced the number of parameters to six: $k_{\gamma p}, k_{\gamma d}, g_{max}, h_\gamma$, n_γ, and ΔL. We arbitrarily chose ΔL to be 1, leaving five parameters to explore. A preliminary exploration of the parameter space suggested g_{max} should be approximately 1. Furthermore, the preliminary search revealed that a low mean value of γ, $< \gamma >= k_{\gamma p}/k_{\gamma d}$, would result in cells with no growth for extended periods of time. Thus, we limited the range of $k_{\gamma d}$ to low values in subsequent parameter exploration. Similarly, with a Hill coefficient greater than 1, the zero growth region of the Hill function would lead to stalled growth, thus, we set n_γ to 1.

We next performed a slightly finer parameter search, constrained by the preliminary findings (Fig. 4.4). We found a range of solutions that produced population doubling times (Eq. 2.3) similar to the experimental value of ~30 min. To pick a solution, we compared the histogram of simulated growth rates with the experimentally observed $\Delta rpoS$ growth rate histogram (Fig. 3.8e). After an automatic exclusion based on the squared sum of differences between the histograms, a simulation that output a histogram within the standard deviation error bars of the experimental histogram was chosen out of 3 candidates by inspection (Fig. 4.5 and Tab. 4.1).

4.2.2 Constraining the RpoS parameters

With the γ parameters set we moved on to the five parameters associated with RpoS: k_{rp}, k_{rd}, h_r, n_r, and f. For each parameter we explored four values, resulting in 1024 simulations (Fig. 4.6). For the offset, f, we tried 0, 0.01, 0.05, and 0.25. We found the low values

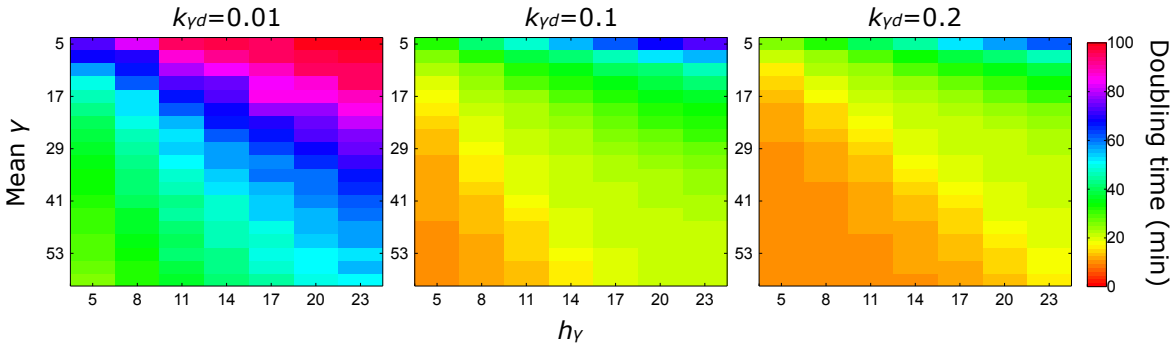

Fig. 4.4 Constraining γ parameters, doubling time heat maps. Doubling time over parameter values searched in second iteration. Doubling times resulting from 399 parameter sets varying the mean value of γ (by $k_{\gamma p} = <\gamma> \cdot k_{\gamma d}$), its degradation rate, $k_{\gamma d}$, and the half maximal concentration of the growth-γ Hill function, h_γ. For each parameter set, a single simulation of 500 hours was run and the doubling time calculated using Eqn. 2.3 on the last 250 hours.

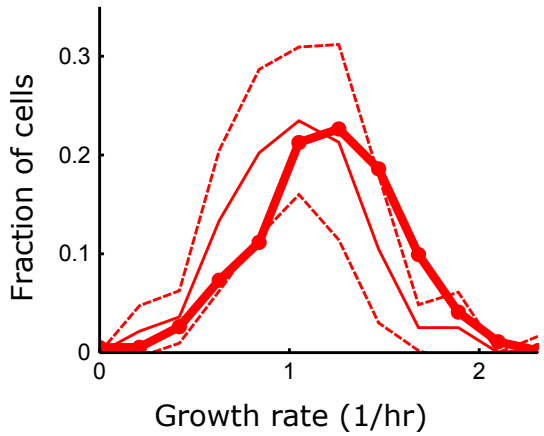

Fig. 4.5 Constraining γ parameters using experimental growth rate histograms. The final solution chosen out of those in Fig. 4.4 displayed in bold overlaid on the experimental Δ*rpoS* growth rate histogram (thin solid line) and the experimental standard deviation (dashed lines). The parameter values are listed in Table 4.1.

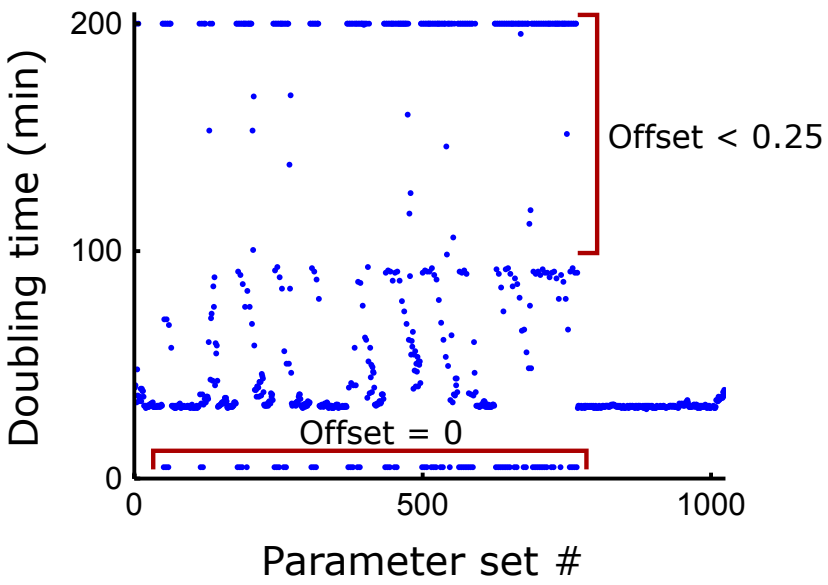

Fig. 4.6 Excluding parameter values due to unphysical growth rates. When the offset value, f, was less than 0.25 the simulations often resulted in population doubling times that were either very high or very low, indicated by the brackets. Thus, an offset of 0.25 was chosen. 1024 parameter sets were simulated in two simulation runs for 500 hours each. The doubling time was calculated using Eqn. 2.3 on the last 250 hours.

of f typically produced either very high or very low doubling times, which did not reflect our experimental observation of a *WT* doubling time similar to that of Δ*rpoS*. Thus, we proceeded with $f = 0.25$.

In the remaining 256 parameter sets, we sought a solution that produced *WT* doubling times similar to Δ*rpoS* at the same time as having a larger fraction of slow growing cells, as observed experimentally (Fig. 3.8e). Most parameter combinations that resulted in similar doubling times also had very similar growth rate histograms (Fig. 4.7 and 4.8). In particular, we compared the fraction of cells with growth rate less than 0.42/h from the two simulated strains (Fig. 4.8). When this fraction was large, the doubling time differences tended to be very large. We found only one solution in this coarse parameter exploration that satisfied our constraints of a similar doubling time between *WT* and Δ*rpoS* while having a non-negligible fraction of slow growing cells (Tab. 4.1, Fig. 4.9 and 4.10d).

4.2.3 The model captures the phenomenon at both the single-cell level as well as in summary

With the parameters set to the values found in the coarse search (Tab. 4.1), the model then produced a long-tailed distribution of RpoS pulse heights, which decreased in prominence when the negative RpoS feedback on growth rate was removed in silico (Fig. 4.10b, and compare to Fig. 3.8c). The model also captured the rich single-cell RpoS and growth

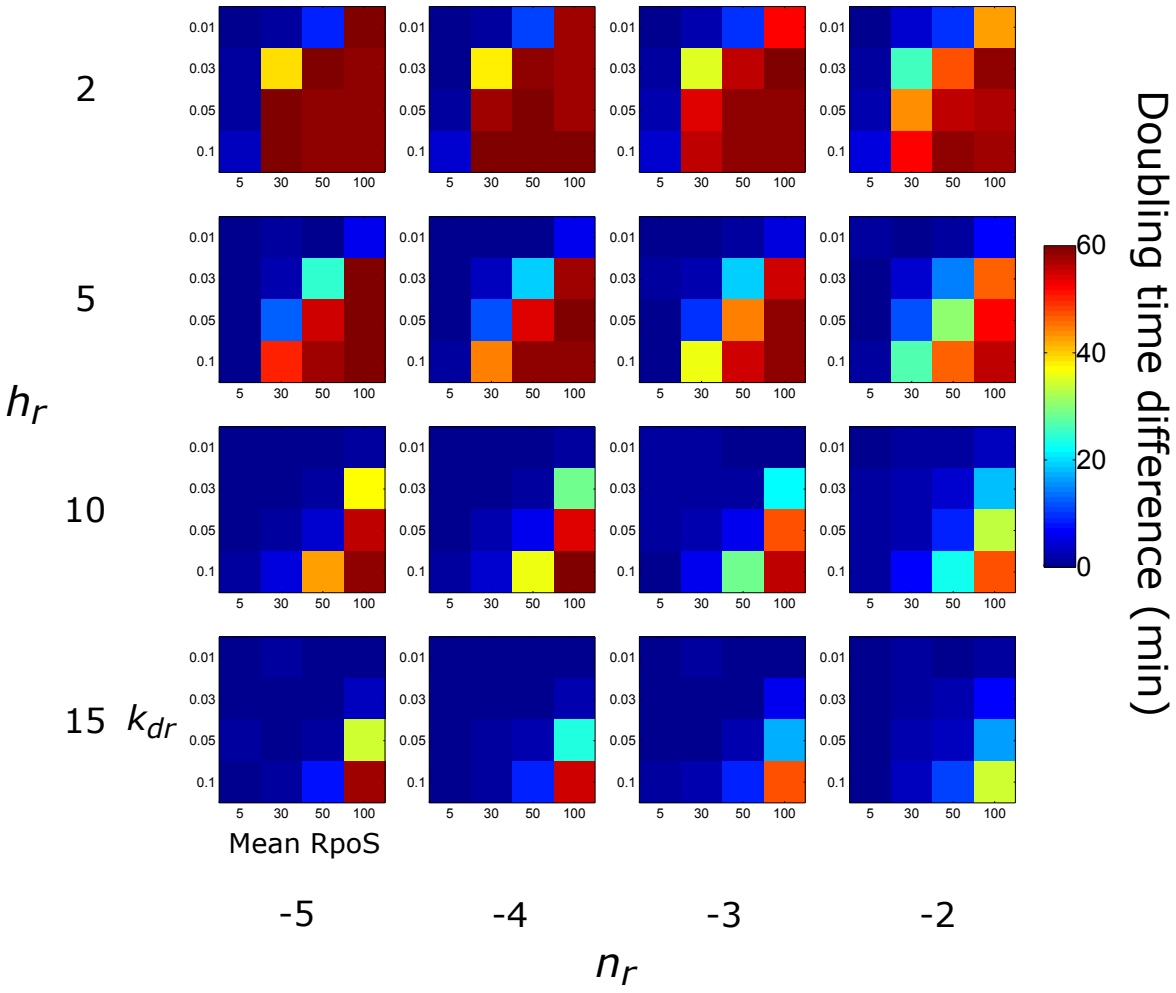

Fig. 4.7 Constraining the RpoS molecular and growth parameters, exploring doubling time difference between *WT* and Δ*rpoS*. A coarse grained exploration over the four remaining parameters after setting the offset, $f = 0.25$, resulting in 256 parameter sets (Fig. 4.6).

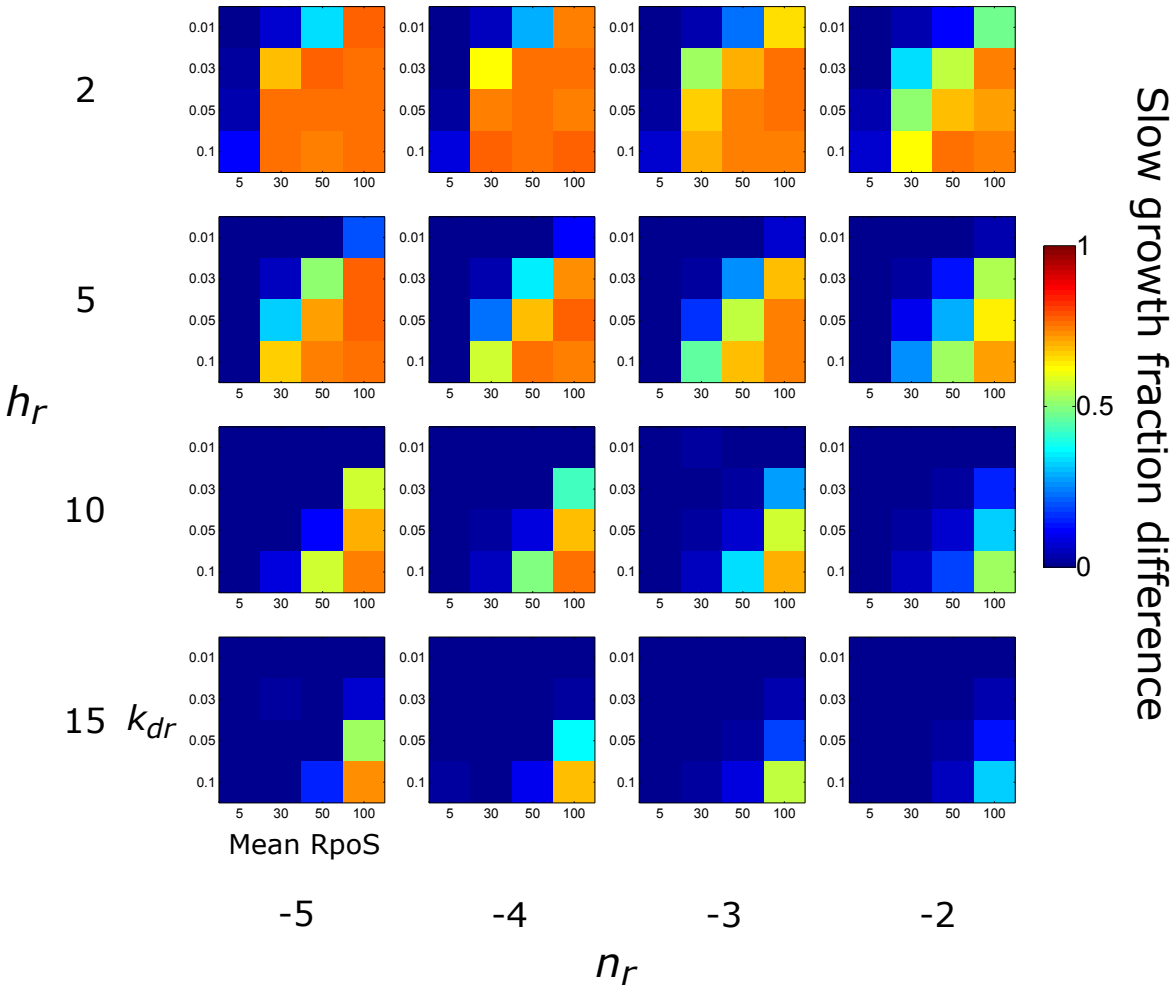

Fig. 4.8 Constraining the RpoS molecular and growth parameters, exploring slow growing fraction difference between *WT* and Δ*rpoS*. The same simulation set as in Fig. 4.7. The difference in the fraction of time cells were growing less than 0.42/hr in the last 250 hours of 500 hour simulations was compared.

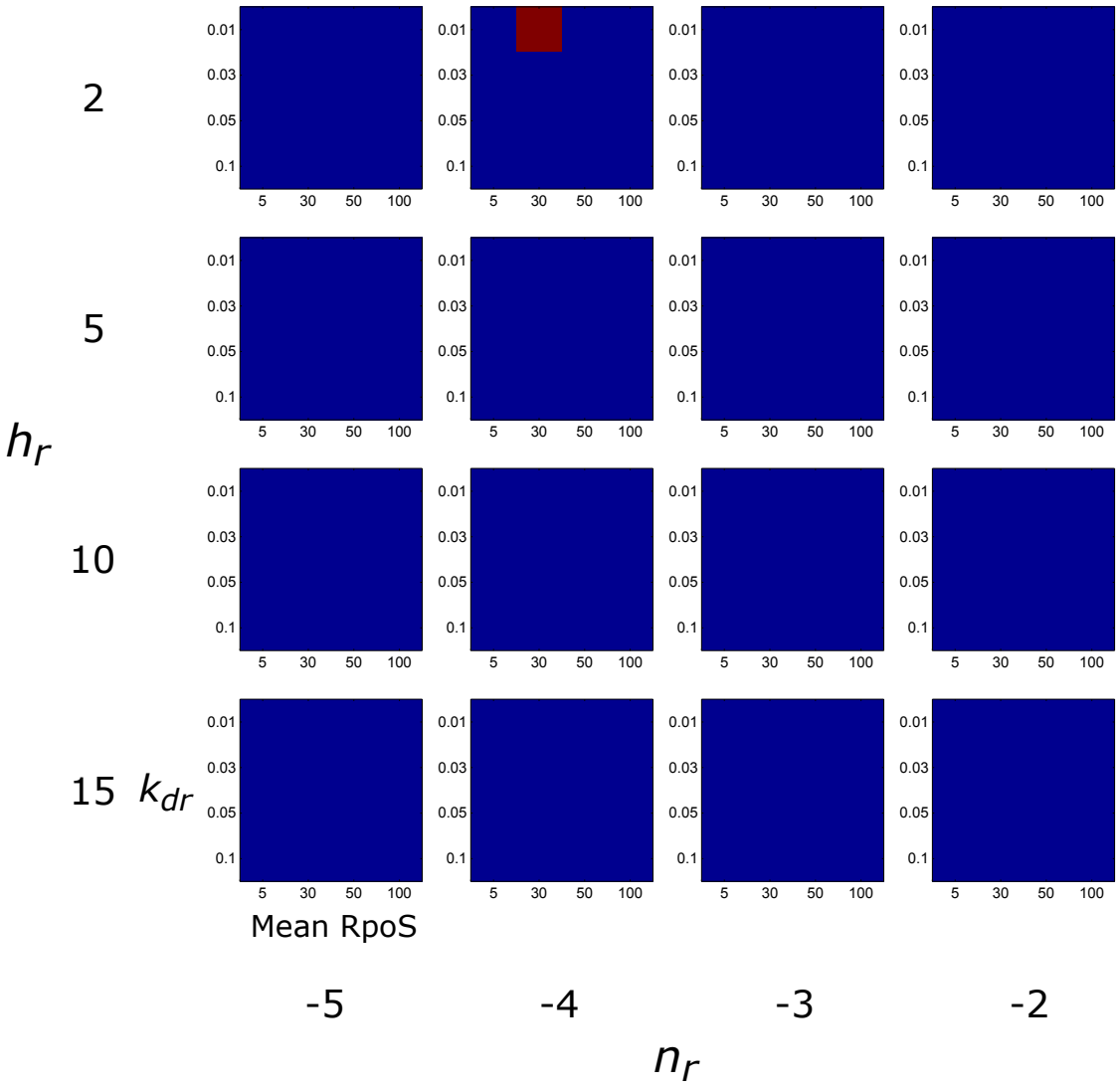

Fig. 4.9 Constraining the RpoS molecular and growth parameters by combining outputs (Fig. 4.7 and 4.8). Only one solution resulted in a *WT* doubling time similar to Δ*rpoS* while having a non-negligible fraction of slow growing cells, illustrated as the red square; the blue squares represent solutions that did not satisfy our constraints.

Table 4.1 Model parameter values found by coarse grain search that reproduced the *WT* and *rpoS*-knockout experimental growth distributions as well as the population growth rate.

Parameter	Value in model	Value in physical units	Description
		Gillespie	
$k_{\gamma p}$	2.2	13 hr^{-1}	γ zeroth order production rate constant
$k_{\gamma d}$	0.2	1.2 hr^{-1}	γ first order degradation rate constant
k_{rp}	0.3	1.8 hr^{-1}	RpoS zeroth order production rate constant
k_{rd}	0.01	0.06 hr^{-1}	RpoS first order degradation rate constant
γ_{init}	11	11 molecules	Initial value of γ
r_{init}	1	1 molecule	Initial value of RpoS
		Growth	
ΔL	1	2 μm	Length cell must grow before dividing
l_i	1	2 μm	Initial cell length
		Coupling growth and Gillespie models	
g_{max}	1.2	7.2 hr^{-1} (0.7 hr^{-1})	Maximum (average) growth rate achievable by cell
h_γ	17	17 molecules/cell	Half-maximum value for γ-growth Hill function
n_γ	1	-	Hill coefficient for γ-growth Hill function
h_r	2	2 molecules/cell	Half-maximum value for RpoS-growth Hill function
n_r	-4	-	Hill coefficient for RpoS-growth Hill function
f	0.25	-	Minimum value RpoS can reduce growth rate by
		Technical parameters	
	100 or 1,000	-	Number of simulations
	3000	500 hrs	Number of time steps
	0.005	3 s	Simulation time resolution
	1/0.005 = 200	10 min	Sampling resolution

dynamics observed (Fig. 4.10a and 3.8b), as well as the anti-correlation between growth rate and RpoS (Fig. 4.10c and 3.8e).

Moreover, the model correctly captured the effect of positive regulation of growth by a molecular species. Increasing γ concentration caused an increase in growth rate, which manifested as a positive cross-correlation between γ and growth rate (Fig. 4.10e). This corresponded well to the cross-correlation of σ^{70} and growth rate (Fig. 3.13a).

4.3 Perturbations to test model

We tested our understanding of the feedback model by perturbing population growth rate and by overexpressing RpoS.

4.3.1 RpoS overexpression reduces growth rate

Our model qualitatively predicts overexpression of RpoS will reduce growth rate due to the mutual inhibition between growth and RpoS (Fig. 4.1). To test this prediction we procured an inducible RpoS construct from the group of Prof. Herb Schellhorn [81]. They integrated expression of a T7 RNA polymerase in the chromosome of an alternative *E. coli* strain to the one we have primarily used in this thesis (see Tab. 2.1). On a plasmid they put an IPTG (isopropyl-β-D-thiogalactopyranoside) inducible P_{T7lac}-*rpoS* construct. We transformed their *WT* and Δ*rpoS* harbouring the inducible system with the P_{bolA}-*GFP* transcriptional reporter.

In preliminary experiments, we found their *WT* (*WT*+*inducible construct*) grew poorly in minimal media. In rich media its growth rate was still considerably lower than the standard strain used in this thesis. Nonetheless, continuing with the rich media we found mean RpoS expression was lower for the Δ*rpoS* than *WT* strains, and increased with IPTG concentration (Fig. 4.11a). At intervals we measured the culture density to determine population growth rates. Quantifying the growth rate was unfruitful as the cultures, by inspection, appeared to change their growth rates over time. Nonetheless, with increasing IPTG, Δ*rpoS* growth rate clearly decreased and approached that of *WT*, as predicted by our model (Fig. 4.11b).

4.3.2 Global growth rate reduction increases RpoS expression

As population growth rate is reduced, RpoS levels should increase due to decreased dilution (Fig. 4.12). We reduced population growth rate by reducing culture temperature, using reduced quality media, or combinations of the two (see Tab. 2.2) and imaged single cells from bulk cultures. Indeed, RpoS levels increased with decreasing population growth rate (Fig. 4.12).

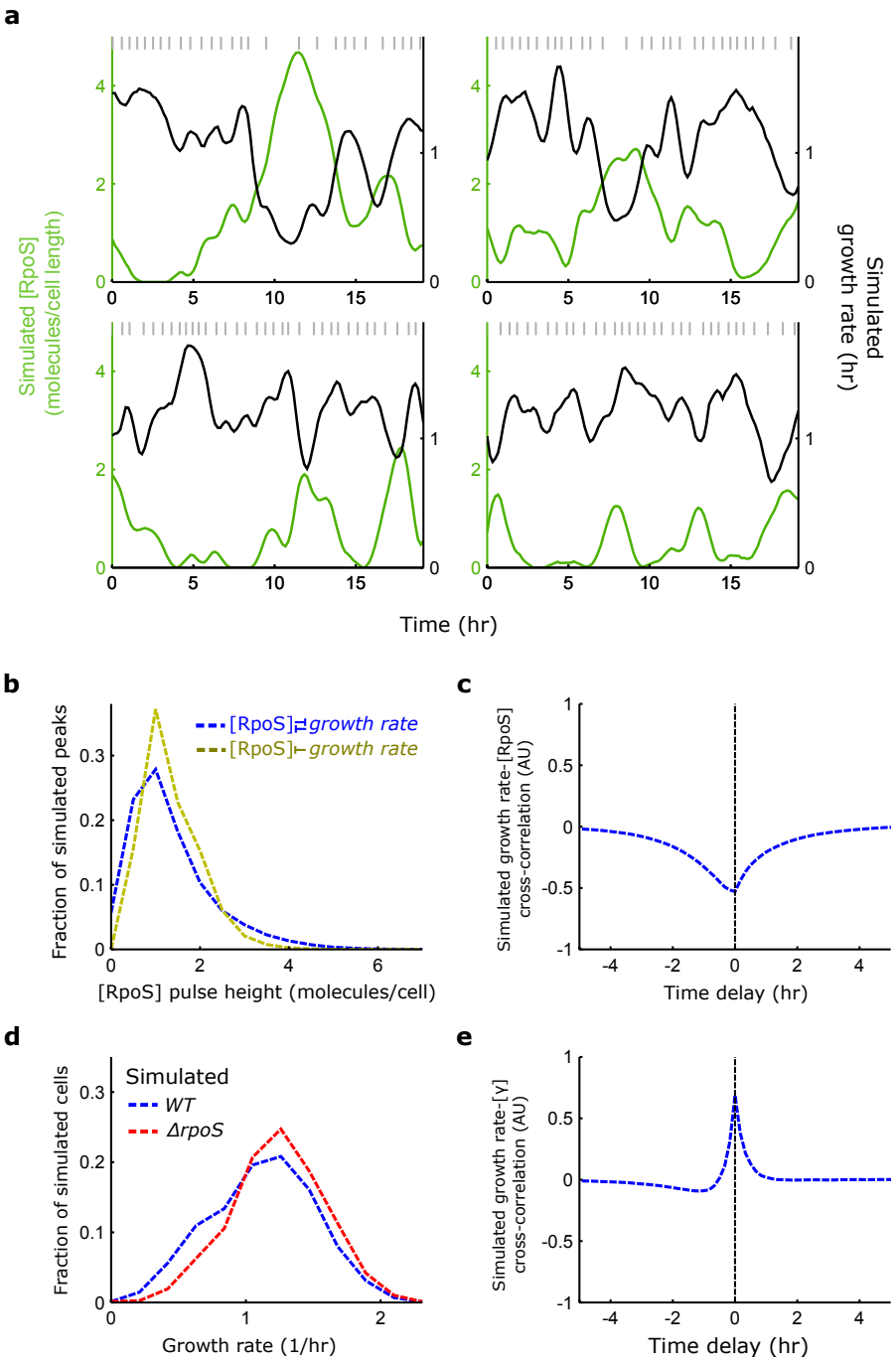

Fig. 4.10 Growth-RpoS mutual inhibition produces multi-generation RpoS pulses and heterogeneous RpoS expression. Analysis from 1,000 simulations run for 500 hours; only the last 250 hours are used to avoid initial transients in the simulation. a, Sample time traces of simulated RpoS concentration and growth rate for four cells. Traces were smoothed twice with a moving average filter spanning five frames for display. Grey vertical lines indicate cell divisions. b, Histograms of simulated RpoS concentration with and without feedback of RpoS on growth rate (88,865 and 133,126 pulses, respectively). c, Cross-correlation between simulated growth rate and RpoS concentration. d, Histograms of growth rate sampled at 24 hour intervals over all 1,000 simulations. e, Cross-correlation between simulated growth rate and γ concentration.

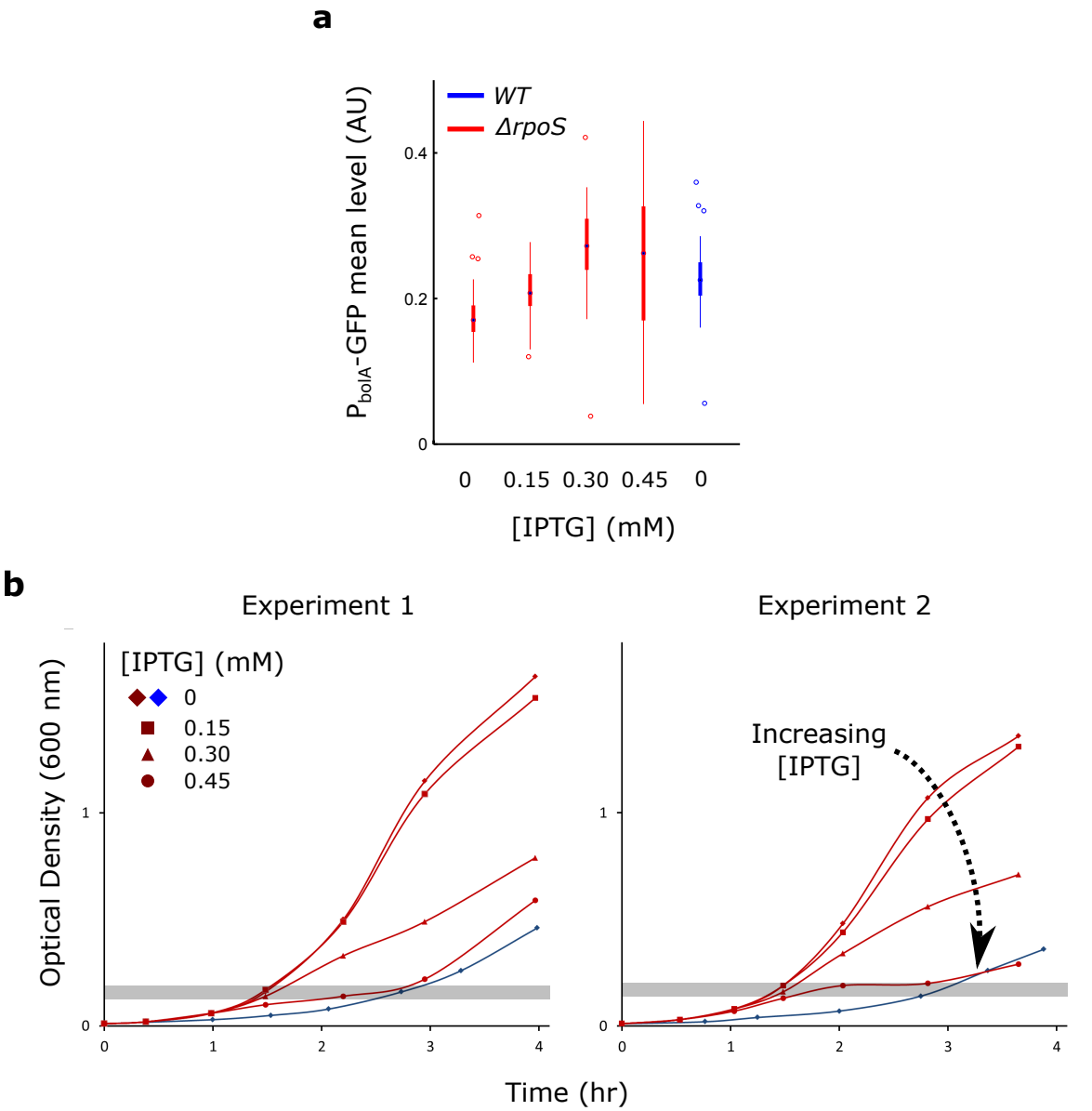

Fig. 4.11 Inducing RpoS overexpression reduces growth rate. a, Increased levels of IPTG induction produced increasing RpoS levels (box plots, median ± 25th to 75th quartiles (box) ± full distribution (whiskers) ± outliers (points); Δ*rpoS+inducible construct*: 0 mM IPTG, 136 cells, mean = 0.23 AU, CV = 0.17; 0.15 mM IPTG, 132 cells, mean = 0.21 AU, CV = 0.15; 0.30 mM IPTG, 137 cells, mean = 0.27 AU, CV = 0.19; 0.45 mM IPTG, 94 cells, mean = 0.25, CV = 0.39; WT+inducible construct: 0 mM IPTG, 115 cells, mean = 0.23 AU, CV = 0.17; data drawn from the shaded region of two experiments in (b). b, Bulk culture growth curves of Δ*rpoS+inducible construct* under IPTG induction, and *WT+inducible construct* without induction.

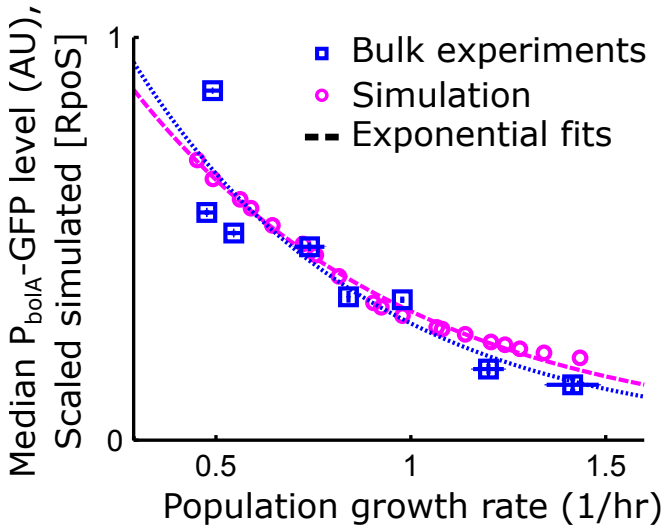

Fig. 4.12 RpoS levels increase at reduced population growth rate. Median RpoS levels in liquid culture (± std dev smaller than data point square, mean growth rate ± std dev, at least two biological replicates, see Tab. 2.2 for details) and scaled RpoS concentration from simulations as functions of population growth rate. Dashed lines are exponential fits. Scaling factor (0.32) was found by minimizing root-mean-square error between the fits over the range of observed growth rates ± 20% (0.29 to 1.6/hr).

4.3.3 RpoS efficacy decreases with population growth rate

The ability of RpoS to repress growth rate could decrease with population growth rate due to globally reduced rates of transcription [95, 109]. On the other hand, RpoS efficacy could remain constant, or even increase, allowing RpoS to control a greater portion of transcription and so repress growth more effectively (Fig. 4.13a). We used the model to distinguish between these possibilities. We modelled a reduction in population growth rate by decreasing g_{max} (Eq. 4.9). The effect of RpoS on growth rate could scale with this maximum growth rate, reflecting a constant RpoS efficacy, or remain fixed, reflecting an attenuated RpoS efficacy. We modelled the former by keeping f constant in the RpoS Hill function as g_{max} was varied. The latter was done by keeping the product $f \cdot g_{max}$ constant, thereby flattening the repressive Hill function (Fig. 4.13b).

Comparing the theory to experiments, we found RpoS efficacy reduced with population growth rate, *i.e.* RpoS was less able to repress growth at low population growth rates. Using the Mother Machine assay and reduced culture temperatures we experimentally observed the growth rate distributions of *WT* and Δ*rpoS* populations do not diverge (Fig. 4.13d). We found that the constant efficacy model overestimated the effect of RpoS on single-cell growth rate as population growth rate was reduced (Fig. 4.13c), whereas the reduced RpoS efficacy model faithfully represented reality (Fig. 4.13e). Additionally, the reduced efficacy model captured the increasing levels of RpoS at reduced population growth rates (Fig. 4.12).

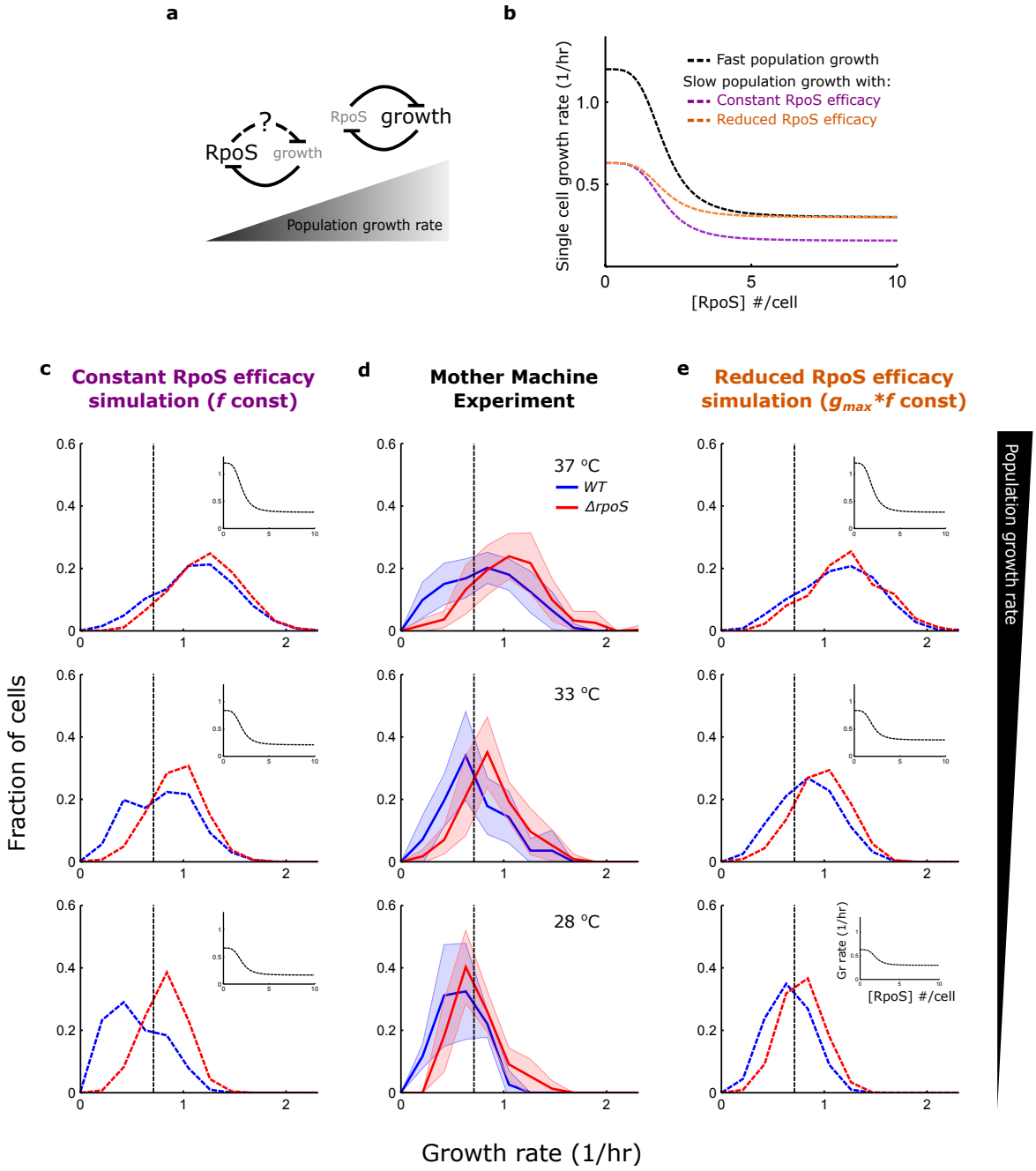

Fig. 4.13 The influence of RpoS on growth is attenuated as population growth rate decreases. a, Schematic illustrating effect of reduced population growth rate. RpoS is concentrated due to lower dilution by growth rate. However, its effect on growth rate could diminish at low population growth rate. b, Hill functions of growth rate as functions of RpoS concentration used in simulations. Fast population growth corresponds to simulation matching experimentally observed growth rate at 37^oC (d). The constant and reduced efficacy models behave differently in the large RpoS concentration limit as population growth rate is reduced. c, Growth rate histograms for simulated *WT* and Δ*rpoS* at three population growth rates achieved by keeping f constant as g_{max} was reduced.

(caption continued)

Fig. 4.13 caption, continued

Dashed black lines correspond to optimal survival threshold of 0.71/hr (Fig. 5.3 of Chapter 5). Insets: Hill functions of growth rate vs RpoS concentration. d, Experimental growth rate histograms for *WT* and Δ*rpoS* grown at three temperatures (mean ± std dev; 37^{o}C reproduced from 3.8. 33^{o}C *WT*, 5 technical replicates drawn from 3 biological replicates, 72 mother cells; Δ*rpoS*, 6 tech. reps. drawn from 3 bio. rep., 137 mother cells. 28^{o}C *WT*, 4 technical replicates drawn from 3 biological replicates, 56 mother cells; Δ*rpoS*, 4 tech. reps. drawn from 2 bio. rep., 114 mother cells). e, Growth rate histograms for simulated *WT* and Δ*rpoS* with $f \cdot g_{max}$ constant as g_{max} was reduced. Insets: same as (c). g_{max} values for the simulations were chosen such that population growth rates matched the experimentally observed population growth rates. For (c) and (e) 100 simulations were used for each condition, sampled every 24 hours, in the final 250 hours of 500 hour simulations.

4.4 Conclusion and Discussion

In this chapter we demonstrated how a mutual inhibition coupling between noisy RpoS activity and noisy growth rate could generate the RpoS pulsing behaviour reported in the previous chapter. We used the Gillespie algorithm coupled to a cell growth model to capture the phenomenon mathematically. Using a coarse grained search over the large parameter space of the model, we were able to find a parameter set that simulated the noisy RpoS and growth dynamics observed. We experimentally validated the conclusions from the model by perturbing both growth rate and RpoS expression.

4.4.1 Advantages and limitations of the model

Our model of the RpoS-growth circuit simulated single cells, each growing according to stochastic molecular reactions happening inside them. This approach allowed us to compare theory directly to experiment at the single-cell level as well as with summary statistics (Fig. 3.8 and 4.10). Despite the predictive power of our model, we note that it is a toy model. The utility of the model was to show that RpoS can pulse given a simple mutual inhibition feedback with growth rate. However, our model suffers from a large number of lumped parameters – constants that encompass many molecular details in single numbers and so become difficult to interpret. With so many parameters we also risked overfitting the data [110]. Such a phenomenological approach can still be powerful, and has been used to reveal the bacterial division rule [44], how noise propagates from gene expression to growth rate [70], and the way in which gene expression can generate bistable growth [69]. To give more meaning to the parameters, it might be useful to develop a more biochemically motivated model of the system. In this way, the number of unknown parameters might be reduced by incorporating values for biochemical parameters determined in experiments found in the literature. The number of adjustable parameters might also be reduced by incorporating recently developed bacterial growth laws based on proteome partitions that have been used to make remarkably accurate predictions of bulk culture phenotypes [111, 109, 112].

4.4.2 What is γ?

Despite the lumped nature of the parameters, our simple model makes experimentally testable predictions about the underlying molecular details. We found γ, the molecule promoting growth, degraded rapidly ($k_{\gamma d}$ ~1/hr) and was present in small molecule numbers in the cell (~5). This produced noisy growth with a growth rate distribution commensurate with experiment (Fig. 3.8e and 4.10d). Furthermore, growth rate and γ were positively correlated, similarly to the cross-correlation of σ^{70} and growth rate (Fig. 4.10e and 3.13b). These facts suggest γ is not σ^{70}, rather it is a transiently expressed molecule regulated by σ^{70}. Alternatively, γ might represent the difference in abundance of two molecular species that regulate growth. Further work may reveal the existence and identity of this molecule.

4.4.3 Ways to improve the model

Upon careful consideration, the model had two major areas of improvement. First, it ran slowly because it did not take full advantage of the Gillespie algorithm. Second, and more conceptually important, it relied on assumptions about zeroth and first order reactions that may prove to be unphysical.

Discretising time in the coupled model

We used a nested model, the outer loop being a deterministic cell growth model, the inner being a stochastic Gillespie algorithm. In preliminary work, we found the time step of the deterministic model to be important. If it was too large, we would get anomalous cell lengths, due, essentially, to missing the proper time of cell division. To solve this, we simply reduced the time step, and consequently slowed down the simulation. In doing so, we deterministically discretised time to such an extent that very few, if any, reactions happened in the Gillespie algorithm. The time-to-next-reaction that the Gillespie algorithm computes, allowing a stochastic discretisation of time, was thus wasted. Perhaps, an improved version of the model could implement growth stochastically as well. After all, growth is mediated by molecular processes. In doing so, we could once again take advantage of the stochastic discretisation of time the Gillespie algorithm provides.

Effect of growth on reaction propensities

There are two physical problems to address concerning the reaction propensities. First, there is no such thing, in chemical reality, as zeroth and first order reactions. Something does not come out of nothing, and does not become nothing. We can accept these unphysical aspects of the model, knowing that the effective reaction propensities take into account, in a lumped manner, the true physical processes occurring.

A more serious criticism of the model involves the volume-independent reaction propensities we assumed (Sec. 4.1.2). In a fixed volume it is, in fact, the case that zeroth and first order reactions are volume independent. Only at second order reactions do we encounter molecular collisions that must happen to trigger a reaction. So, second order and above reaction propensities are volume dependent [65]. Lu *et al.* showed how volume-dependent reactions propensities in the Gillespie algorithm need to be modified if the reaction volume changes, as in a growing cell [96]. Since zeroth and first order reactions are not volume dependent to begin with, we assumed they would not change in a growing cell.

However, consider the case of a cell that is double the size of its neighbour. Surely, it will have a larger capacity to produce molecules, and it might also have more molecules present to degrade other molecules. To explicitly consider this situation we might use higher order reactions, such as a second order reaction for the molecule-mediated degradation. Alternatively, we could model the situation by *lumped* zeroth and first order propensities. If we do so, the reaction propensities should be diffferent for the two cells we consider. We might skirt this issue by pointing out that if the reaction propensities are a function of *concentration* of molecules in the cell (*e.g.* ribosomes), then perhaps in steady state growth conditions, where these concentrations might remain constant as the cell grows [112], the reaction propensities might remain constant as well. Future iterations of this model should consider this volume dependence criticism more carefully.

While correcting the thesis after the *viva voce* we came across a recent paper by Thomas *et al.*, which might provide a basis for solving these problems [113]. They developed a stochastic model incorporating key molecular species (ribosomes, metabolic enzymes, *etc.*) and a detailed model of cell growth and division. They used a stochastic differential equation (Langevin) approach and so were immune to the problems with the modified Gillespie algorithm discussed above. They were able to capture the bulk growth laws previously found by Scott *et al.* [112] as well as match the noisy growth rates observed in literature [70, 71]. However, they were not able to explicitly model gene regulatory networks in their framework, as would be required to capture the growth-RpoS mutual inhibition model we proposed. Future work may allow for this exciting possibility.

Outlook

Having established the nature of the coupling between noisy growth rate and RpoS, we next turn our attention to the function of this phenotypic variability.

Chapter 5

Function of heterogeneous RpoS and noisy growth.

Here we investigate whether the noisy RpoS and growth dynamics uncovered in the previous chapters serve a function for a population of *E. coli* cells. We take advantage of the literature on the general stress response mediated by RpoS to select a stress assay. We show how RpoS expressed in the cells at the time of stress allows a subpopulation of cells to survive. Using the Mother Machine we uncover the surprising dynamics that lead to this functional phenotype.

5.1 *WT* exponential phase cells survive oxidative stress better than Δ*rpoS* cells

The RpoS regulon allows cells to survive a variety of environmental stresses, including heat, osmotic, acid, and oxidative stress [67]. Stressed *E. coli* cells are better able to survive subsequent stress, even of a different kind, by the upregulation of RpoS [77]. We sought to test the function of RpoS present in the cells absent of induction effects. To do so, we needed a stress that we could apply rapidly.

We were encouraged by a figure in the classic paper by Hennge-Aronis *et al.* that showed the first cross-protection due to RpoS (Fig. 1.7) [77]. As a control to the osmotic pre-stress, they tested cells without pre-stress against 15 mM H_2O_2 stress. It was apparent, at about 20 minutes of stress application, that *WT* cells survived better than Δ*rpoS* cells despite a lack of pre-stress (Fig. 1.7). To confirm this observation we performed a stress assay without pre-stress at three concentrations of H_2O_2. We exposed bulk, exponential phase cultures to H_2O_2 attack, and measured survival against a no-stress control with Colony Forming Units (CFUs), see Sec. 2.4.3 for details. Indeed, more than two decades later, we were able to reproduce the unnoticed trend from literature (Fig. 5.1).

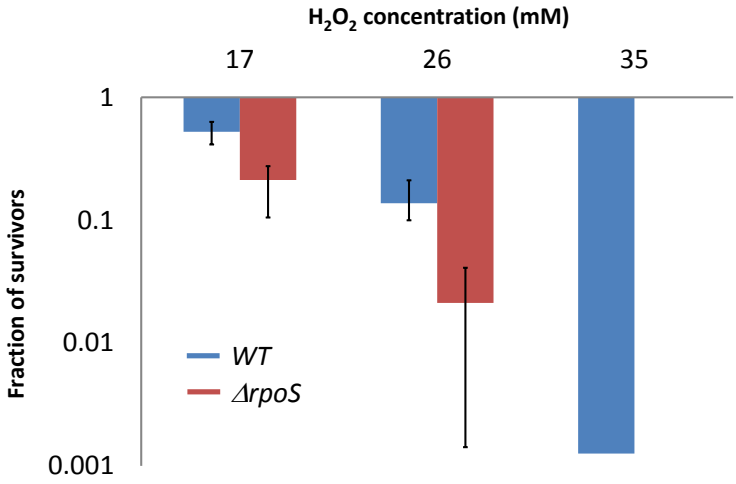

Fig. 5.1 Preliminary survival assay, varying H_2O_2 concentration. Fraction of cells surviving stress in bulk Colony Forming Units assay at three H_2O_2 concentrations applied for ~20 min (mean ± max/min; at least two biological replicates, for 17 and 26 mM H_2O_2, one experiment for 35 mM; Δ*rpoS* survival was below the detection limit of the assay when exposed to 35 mM H_2O_2).

5.1.1 Interrogating survival phenotype at the single-cell level

To understand how heterogeneous RpoS was connected to survival we turned, once again, to the Mother Machine. Reasoning that a higher H_2O_2 concentration would minimize induced-RpoS artefacts, we chose the highest H_2O_2 concentration from the bulk culture assay, as there were still survivors in the *WT*. In a preliminary test with a fluorescent dye we observed short transients when switching media (see Sec. 2.4.1 for details). Thus, we chose a longer H_2O_2 exposure time than in the bulk for the microfluidics experiment. Using the Mother Machine we allowed cells to grow in fresh media, switched to media containing 35 mM H_2O_2 for 35 minutes, and then back to fresh media (Fig. 5.2a). To assay the survival of cells after the H_2O_2 treatment, we used the phase contrast channel. If cells resumed growth, they were counted as survivors (see Sec. 2.4.1 for details). We hypothesised that cells surviving the stress treatment were those with high RpoS expression prior to the stress. As we had tracked all cells, regardless of survival, we could interrogate the RpoS and growth dynamics prior to stress application and test our hypothesis. Indeed, the population of cells that survived the stress upregulated RpoS approximately three hours prior to the stress (Fig. 5.2b), suggesting the use of the heterogeneous RpoS expression is to survive sudden stress. Consistent with literature [77], *rpoS*-knockout populations had a reduced survival fraction compared to *WT* (Fig. 5.2d).

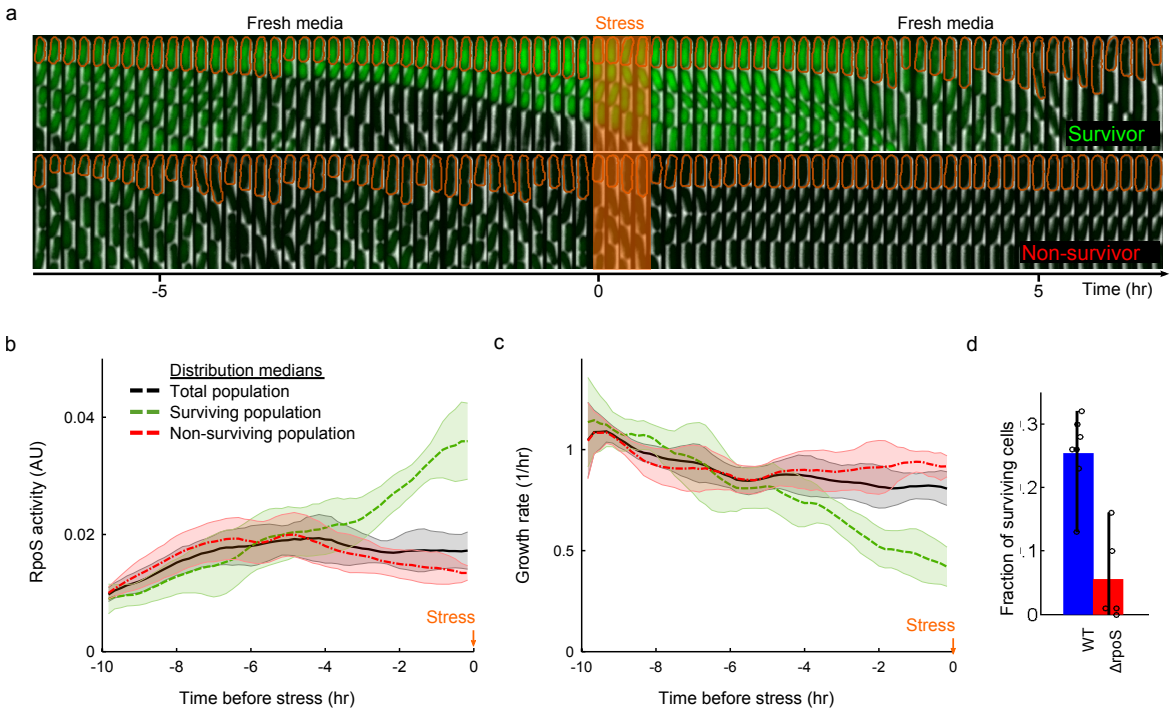

Fig. 5.2 RpoS enables survival of stress by prolonging duration of slow growing state. a, Schematic of the stress assay and sample montages of surviving (top) and non-surviving (bottom) mother cell. Mother cell outlined in orange; 1 frame/10 minutes; phase contrast and fluorescence channel ranges identical for both montages and chosen for display. Cells were grown for 10 hours in fresh media, followed by a 35 minute application of H_2O_2 stress, and fresh media once again. b, Median value of RpoS activity distributions for time points prior to stress application (t = 0), sorted according to survival (line and shaded area are mean ± std dev, 7 technical replicates drawn from 4 biological replicates; 72 surviving cells, 212 non-surviving, 284 total mother cells). c, Same as (b) for growth rate. d, Fraction of cells surviving stress in the Mother Machine assay (mean ± max/min, WT: 7 tech. reps., represented as circles, drawn from 4 bio. reps., 1,087 cells, Δ*rpoS*: 5 tech. reps. drawn from 3 bio. reps., 996 cells).

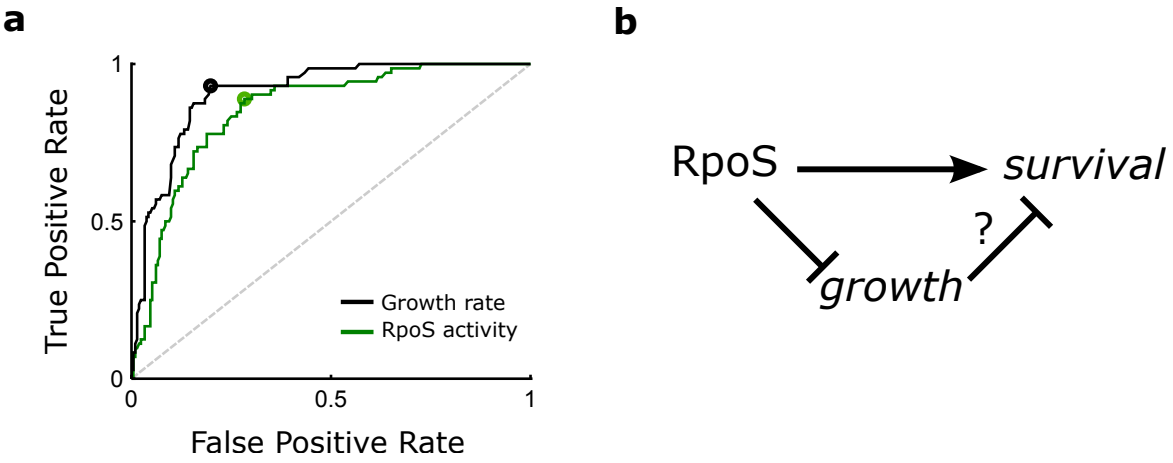

Fig. 5.3 Both RpoS activity and growth rate strongly predict survival. a, Receiver Operating Characteristic curve for growth rate (black) and RpoS activity (green) from time point preceding stress application, using data from Fig. 5.2. Grey dashed line is True Positive Rate = False Positive Rate. Circles represent locations of optimal thresholds (0.71/hr for growth rate, 0.020 AU for RpoS activity). Area Under the Curve (AUC) is 0.91 for growth rate and 0.85 for RpoS activity. b, Schematic illustrating alternative mechanisms of stress survival. High RpoS activity could directly allow cells to survive or it might first reduce growth rate, which in turn allows survival.

5.2 Surviving cells grow slower than non-surviving cells

Intriguingly, the surviving population also had reduced growth rate prior to the stress (Fig. 5.2c), which might be expected from the strong anticorrelation of RpoS activity and growth rate (Fig. 3.8d). Nonetheless, we suspected RpoS activity would be predictive of survival, and not growth. To quantify the predictive power of these two quantities we used the Receiver Operating Characteristic (ROC) curve on their values in the frame immediately prior to stress (see Sec. 2.4.2 for details). Contrary to our expectation, we found that both RpoS activity and growth rate immediately preceding stress application are strong predictors of survival (Fig. 5.3a). This suggested two alternative hypotheses; either RpoS directly causes the survival phenotype, or it acts by first reducing growth rate, which in turn allows cells to survive the stress (Fig. 5.3b).

To distinguish between these two hypotheses we return to the reduced population growth rate experiments (Fig. 4.12 and 4.13). Note as population growth rate is decreased, *WT* cells accumulate more RpoS (Fig. 4.12). On the other hand, we found that the single-cell growth rate distributions of *WT* and Δ*rpoS* do not diverge (Fig. 4.13d). In fact, the model suggests the growth rate distributions are the same (Fig. 4.13e). Thus, if RpoS directly caused survival, at lower population growth rates *WT* cells should survive much better than Δ*rpoS* cells. If RpoS acts via growth rate, the difference in survival should vanish according to the model, and become similar based on the experimental histograms. We tested this experimentally by a bulk culture Colony Forming Units (CFU) stress assay (see Sec. 2.4.3 for details) and found that RpoS acts via growth rate (Fig. 5.4a). Furthermore, we observed

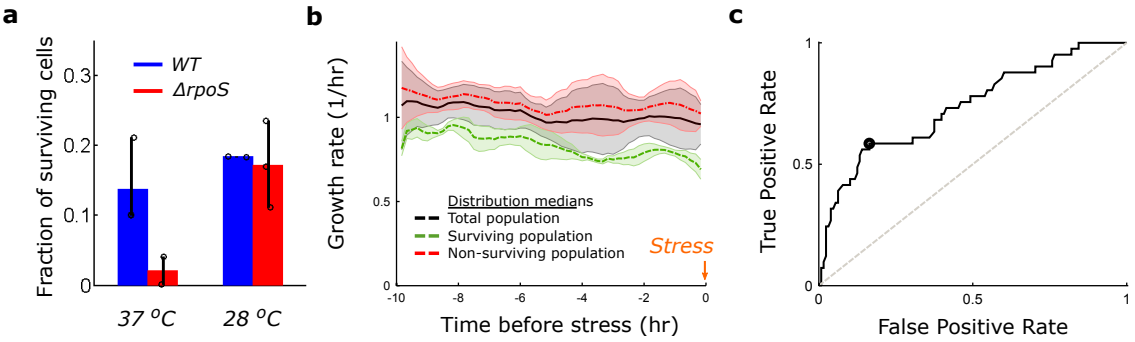

Fig. 5.4 Slow growth allows cells to survive stress. a, Fraction of cells surviving stress in bulk Colony Forming Units assay at two population growth rates produced by culturing at two temperatures (mean ± max/min; at least two biological replicates, represented as circles). The Δ*rpoS* cells that survive oxidative stress are slow growing. Cells were treated as in Fig. 5.2. b, Median value of growth rate distributions for time points prior to stress application (t = 0), sorted according to survival (mean ± std dev, 5 technical replicates drawn from 3 biological replicates, 41 surviving cells, 128 non-surviving cells, 169 total mother cells). c, Receiver Operating Characteristic curve for growth rate (optimal threshold is 0.72/hr, Area Under Curve is 0.74).

rpoS-knockout cells that survived in the Mother Machine assay at 37^{o}C also down-regulated growth prior to stress (Fig. 5.4b, c).

5.3 RpoS prolongs the slow growth state

These findings prompted the question: What is the role of RpoS at fast population growth rates? To answer this question we analysed periods when cells were growing slower than the optimal threshold for survival (Fig. 5.3a). RpoS could be acting to increase the frequency with which cells enter the slow growth, survival state; increasing the duration of time cells maintain this state; or a combination. We found the role of RpoS is to prolong the duration of these slow growth events. We observed this as a higher frequency of long duration slow growth events in *WT* compared to Δ*rpoS* (Fig. 5.5b). In contrast, the frequency with which cells attempt to grow slowly for any duration was similar for *WT* and Δ*rpoS* populations (Fig. 5.5d). The RpoS-growth feedback model captures this dynamic RpoS phenotype (Fig. 5.5c, e).

5.4 Is RpoS involved in persistence?

Although survival against antibiotics is not a classic RpoS phenotype, we were curious to know if there was a connection between our dynamic RpoS phenomenon and that of persistence – a stochastic phenotype that allows a small fraction of cells to survive antibiotic treatment [7, 8] (Sec. 1.1.2). In preliminary experiments, we exposed bulk, exponential phase cultures to carbenicillin. We found that *WT* cells survived antibiotic attack better

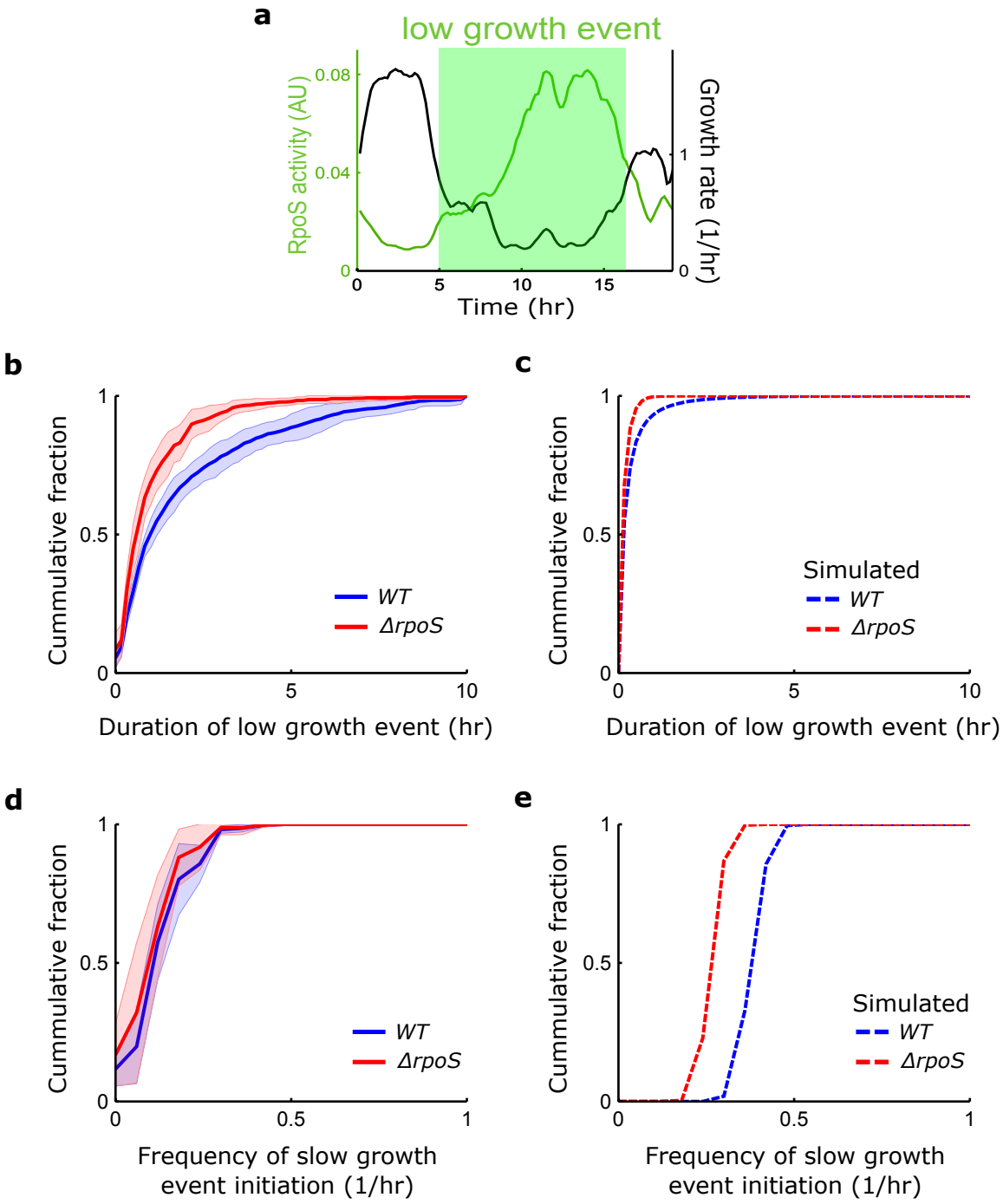

Fig. 5.5 RpoS enables survival of stress by prolonging duration of slow growing state. a, Illustration of a low growth event based on the ROC curve optimal threshold (0.71/hr, Fig. 5.3). b and c, Cumulative distribution of duration of low growth events in *WT* and Δ*rpoS* populations from experiments (b) and simulations (c). d and e, Frequency of slow growth initiation is similar between *WT* and Δ*rpoS* from experiments (d) and simulations (e). Experimental data: line and shaded area are mean ± std dev, *WT*, 11 tech. reps. drawn from 7 bio. reps., 507 mother cells, 961 (862) events; Δ*rpoS*, 10 tech. reps. drawn from 6 bio. rep., 274 mother cells, 484 (435) events. Simulation data: 1,000 simulations run for 500 hours, only the final 250 hours were used; *WT*, 96,966 (102,149) events and Δ*rpoS*, 69,992 (73,339) events. Parentheses indicate number of events for frequency plots, which are lower due to excluding events at edge of time domain.

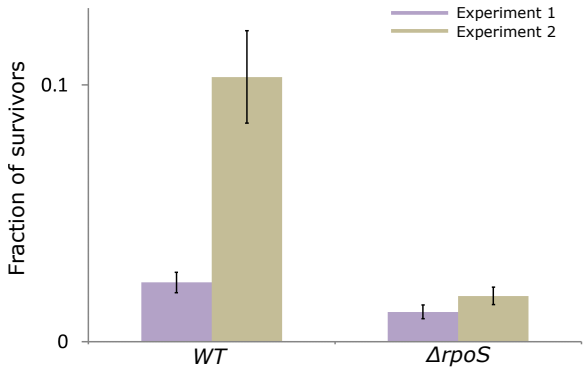

Fig. 5.6 Preliminary evidence for the role of RpoS in persistence from bulk culture survival assay. We exposed *WT* and Δ*rpoS* cultures to 100 μg/mL carbenicillin for ~1 hr and found *WT* cells survive the stress better than *rpoS*-knocout cells. Colours (purple and beige) reflect biological repeats, positions reflect genotype; error bars are computed as $\sqrt{n}/n$, where n is the number of colonies formed on the plates in the Colony Forming Units survival assay.

than Δ*rpoS* cells (Fig. 5.6). Encouraged by this we investigated a molecular mechanism associated with both persistence and RpoS.

Classically, the small molecule alarmone (p)ppGpp, has been implicated in persistence [99, 114] and found to affect RpoS expression levels [115, 116]. We wondered about the effect of (p)ppGpp on RpoS dynamics (Fig. 5.7a). The primary synthase of (p)ppGpp is RelA [117, 118]. We found a Δ*relA* mutant to have similar RpoS heterogeneity to WT (Fig. 5.7b, c). However, the primary hydrolase of (p)ppGpp, SpoT, also has residual synthetic activity [118], so we used the double mutant, Δ*relA*Δ*spoT*, to test cells devoid of (p)ppGpp. To support the growth of the sensitive double mutant we used supplemented minimal media (Methods)[100]. This caused bulk culture growth rates to increase to ~1.6/hr from the standard growth rate of ~1.4/hr, reducing RpoS expression in all strains, as expected (Fig. 5.7d, e and Fig. 4.12). We thus cultured cells at a reduced temperature of 28^oC causing growth rates to decrease to ~0.6/hr, restoring mean RpoS expression (Fig. 5.7f, g). In this condition, we found mean RpoS expression to be reduced slightly in Δ*relA*, and markedly in Δ*relA*Δ*spoT* (Fig. 5.7f, g). On the one hand, the double mutant did not reduce the mean RpoS expression to that of Δ*rpoS*, neither was RpoS heterogeneity abolished, suggesting the RpoS dynamics do not arise solely from (p)ppGpp dynamics (Fig. 5.7f). On the other hand, the marked reduction in mean RpoS suggested a possible connection of RpoS to persistence.

5.5 Conclusion and Discussion

In this chapter we took advantage of the literature on RpoS-mediate stress response to reveal a new, dynamic, RpoS-mediated survival strategy employed by *E. coli*. We showed that *WT*

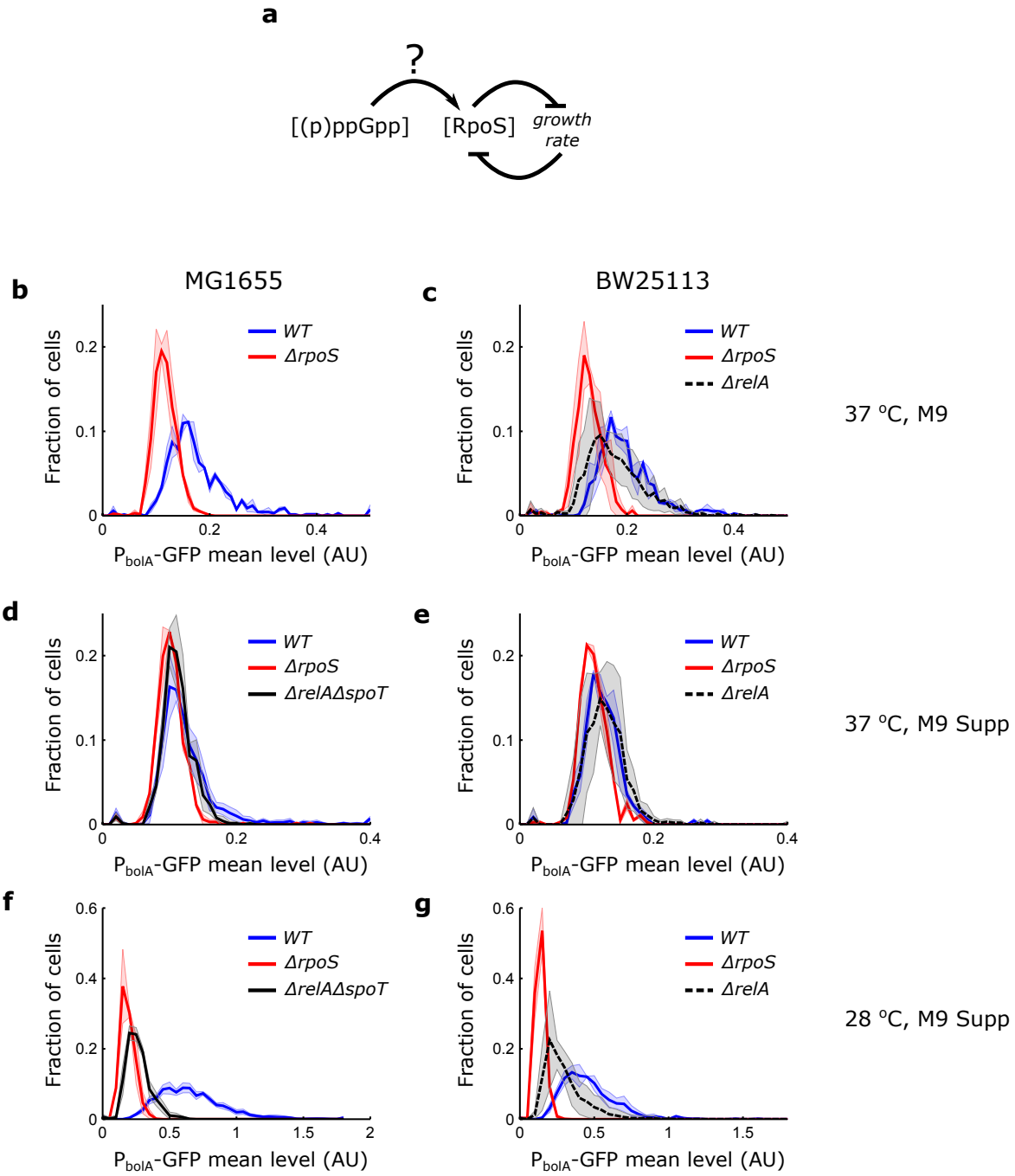

Fig. 5.7 (p)ppGpp does not abolish RpoS heterogeneity. a, Schematic illustrating the dynamic role (p)ppGpp could have on RpoS heterogeneity. b, c, Testing single-gene knockout, Δ*relA*, the primary (p)ppGpp synthase, in standard conditions. b, *WT* strain used in this work, MG1655, and Δ*rpoS::kan* harbouring reporter with kanamycin resistance replaced with spectinomycin resistance (P_{bolA}-*GFP::spec*). *WT* (2 biological replicates, 666 cells, mean = 0.18 AU, CV = 0.37) and Δ*rpoS* (2 bio. reps., 1,246 cells, mean = 0.12 AU, CV = 0.18). c, The same in the *WT* strain of the Keio collection36, BW25113. *WT* (2 bio. reps., 745 cells, mean = 0.20 AU, CV = 0.28), Δ*rpoS* (2 bio. reps., 658 cells, mean = 0.13 AU, CV = 0.21), and Δ*relA* (4 bio. reps., 1417 cells, mean = 0.18 AU, CV = 0.31).

(caption continued)

Fig. 5.7 caption, continued

d and e, The same as (b) and (c) grown at 37^{o}C in media supporting growth of the Δ*relA*Δ*spoT* double mutant in the MG1655 background [100]. d, MG1655 WT (6 bio. reps., 1974 cells, mean = 0.13 AU, CV = 0.46), Δ*rpoS* (2 bio. reps., 662 cells, mean = 0.10 AU, CV = 0.22), and Δ*relA*Δ*spoT* (4 bio. reps., 752 cells, mean = 0.11 AU, CV = 0.20). e, BW25113 WT (2 bio. reps., 452 cells, mean = 0.12 AU, CV = 0.23), Δ*rpoS* (2 bio. reps., 372 cells, mean = 0.11 AU, CV = 0.19), and Δ*relA* (6 bio. reps., 894 cells, mean = 0.13 AU, CV = 0.25). f and g, The same as (d) and (e) but grown at 28oC to restore RpoS heterogeneity and so test the double mutant Δ*relA*Δ*spoT*. f, MG1655 WT (6 bio. reps., 4307 cells, mean = 0.66 AU, CV = 0.40), Δ*rpoS* (2 bio. reps., 1488 cells, mean = 0.19 AU, CV = 0.28), and Δ*relA*Δ*spoT* (4 bio. reps., 1070 cells, mean = 0.26 AU, CV = 0.34). g, BW25113 WT (2 bio. reps., 713 cells, mean = 0.46 AU, CV = 0.40), Δ*rpoS* (2 bio. reps., 891 cells, mean = 0.14 AU, CV = 0.21), and Δ*relA* (6 bio. reps., 2738 cells, mean = 0.30 AU, CV = 0.46).

cells in exponential phase can survive oxidative stress using a bulk culture assay. Using microfluidics and time-lapse microscopy we tracked single cells to show that this survival was, in fact, due to heterogeneous RpoS activity. We next resolved the mystery of how the RpoS acted via slow growth to enable *WT* cells to survive stress better than *rpoS*-knockout cells - RpoS prolongs periods of slow growth. Finally, we presented preliminary evidence that RpoS might be linked with persistence and showed that the alarmone, (p)ppGpp, is important for our dynamic RpoS phenomenon, strengthening the persistence implication.

5.5.1 Molecular mechanism of survival

The regulon of RpoS is well studied, allowing us to speculate on the molecular mechanism underlying the oxidative stress survival phenotype. *E. coli* has two catalase genes, *katE* and *katG*, encoding hydroperoxidase (HP) I and II, respectively [67] and alkyl hydroperoxide reductase genes, *ahpCF* [119]. While *katE* expression is upregulated by RpoS, *katG* and *ahpCF* are expressed independently of RpoS [85]. We speculate that slow growing, Δ*rpoS* cells accumulate KatG and AhpCF, and so survive oxidative attack. *WT* cells would also do this. In addition, *WT* cells would express the RpoS-dependent catalase, KatE, and dynamically remain slow growing for longer than Δ*rpoS*. This extra slow growth and upregulation of *katE* might allow the enhanced survival of *WT* cells.

5.5.2 Are RpoS dynamics connected to persistence?

Our data showed that, while not essential, (p)ppGpp is important in the control of RpoS dynamics (Fig. 5.7). Indeed, RpoS has also been implicated in persister formation [114] as has slow growth [120, 121]. Exposure to antibiotics can enhance subsequent survival against acid stress, a response mediated by RpoS [122]. It may be that persisters are an extreme case of the high-RpoS, slow-growth state we have revealed. To untangle the connection between RpoS, (p)ppGpp, and persistence, an *in vivo* reporter for (p)ppGpp concentration that is independent of RpoS may be useful, although likely challenging to produce.

Furthermore, we have preliminary evidence that *WT* cells survive antibiotic attack better than Δ*rpoS* cells, the classic persistence phenotype (Fig. 5.6). It will be informative to track single cells through an antibiotic attack, as in Fig. 5.2, to see if RpoS is predictive of survival.

Chapter 6

Conclusion and Outlook

In this work, we found an instance of noisy gene expression and noisy growth coupling to produce a functional phenotype. We began with an examination of single cells drawn from bulk cultures to demonstrate the heterogeneous expression of RpoS. To unravel how this heterogeneity arose we tracked single cells over multiple generations. We found RpoS pulsing, coupled to noisy growth, generated the heterogeneity. We examined this notion further with a mathematical model of mutual inhibition between RpoS and growth, revealing how a simple feedback loop can generate the complex phenotype we observed. Finally, we showed that *E. coli* use their stress response system in this dynamic way to prepare for, and survive, sudden stressful events.

6.1 Finding the limits of the model

The regulation of *rpoS* is complex, happening at the transcriptional, translational, and post-translational levels [90]. We observed in Chapter 5 that the small molecule alarmone, (p)ppGpp had a marked effect on RpoS expression. Another potent regulator of RpoS is the protease ClpXP. RpoS is known to be actively degraded in exponential phase [75], and stabilised by a helper protein, RssB, in the transition to stationary phase [123–125] (Fig. 6.1a). In preliminary experiments we have found that cells without functional ClpXP (Δ*clpX*) have an RpoS expression distribution with a high mean that is similar in both exponential and stationary phases, consistent with literature [126] (Fig. 6.1).

Qualitatively, our growth-RpoS feedback model predicts Δ*clpX* cells should have decreased growth rates in exponential phase due to higher RpoS activity. Indeed, preliminary Mother Machine experiments indicate this is the case (Fig. 6.2a). *In silico*, we can simulate Δ*clpX* by setting the degradation rate of RpoS, $k_{rd} = 0$. Our quantitative model fails to capture the Δ*clpX* phenotype, even qualitatively (Fig. 6.2b). This is because RpoS degradation is outside the scope of our quantitative model. In literature, the degradation rate of RpoS in exponential phase cultures has been measured to be ~ 30/hr [75], while in our model

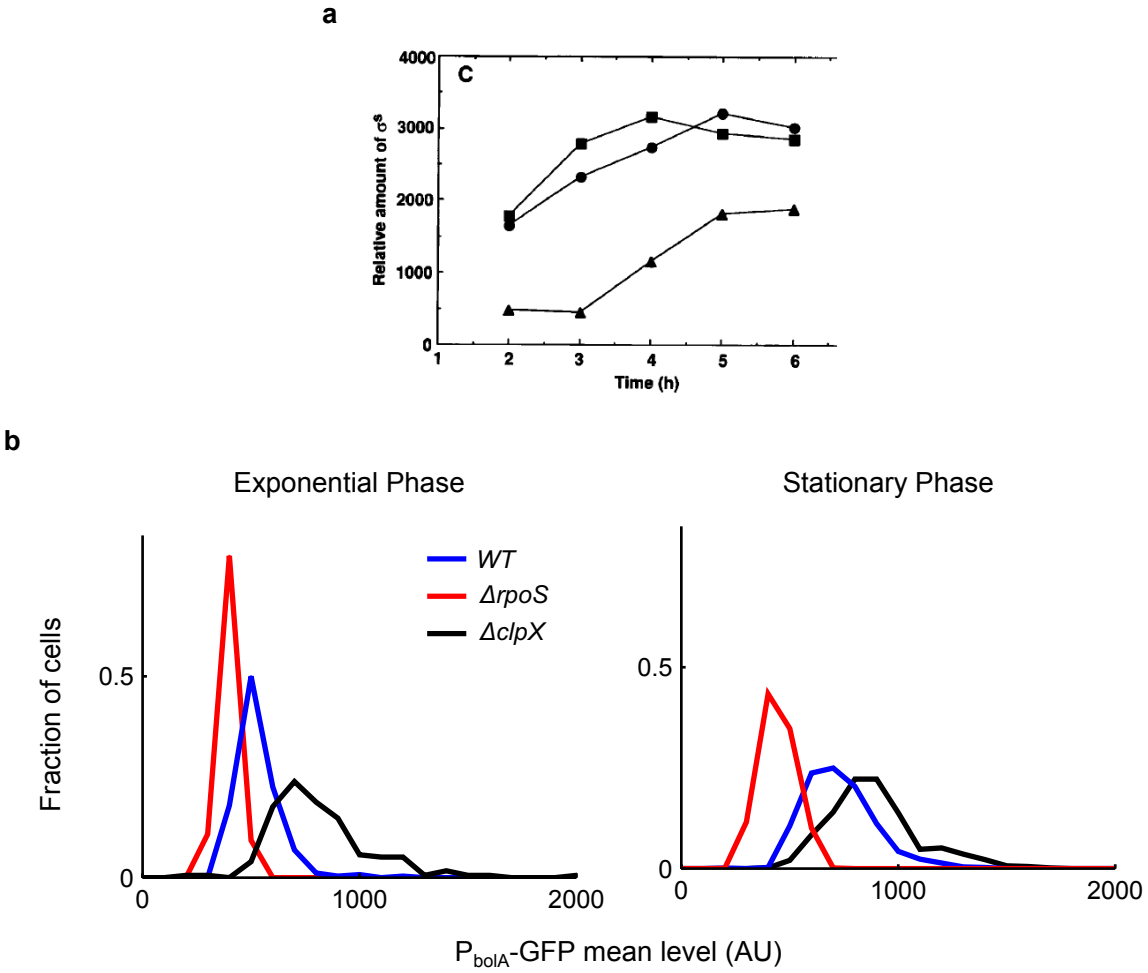

Fig. 6.1 Single-cell data reproduces ClpXP effect from bulk cultures. a) Bulk culture data reproduced, with permission, from [126]. 'Densitometric quantification' of Western blot data of RpoS in *WT* (strain AMS6) (triangles), Δ*clpP* (circles), and Δ*clpX* (squares). b) Preliminary single-cell distributions from exponential and stationary phase. Note the distributions are not normalised to calibration beads, hence the difference in scale with respect to other bulk culture single-cell data in this thesis.

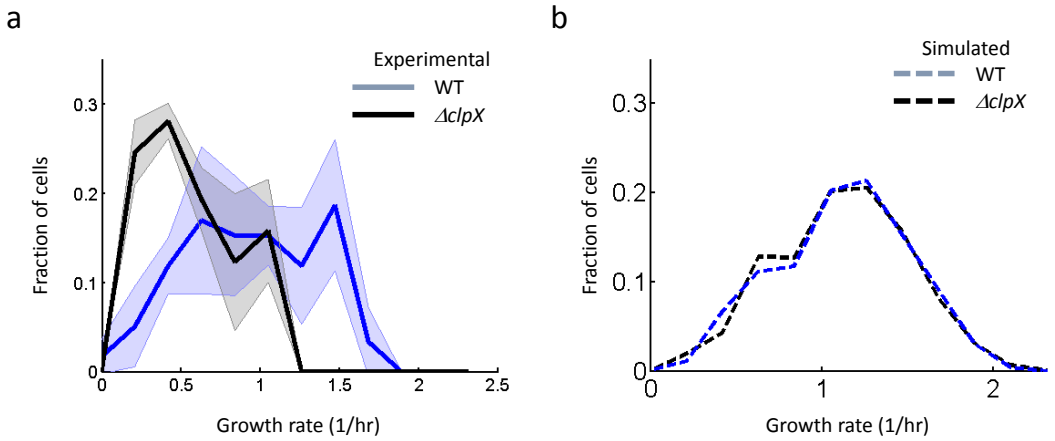

Fig. 6.2 Model fails to capture effect of depleted RpoS degradation on growth rate distribution. Preliminary growth rate histograms from experiments (a) and simulation (b). The simulation of *clpXP*-knockout was achieved with RpoS degradation set to zero ($k_{dr} = 0$).

we chose k_{dr} =0.06/hr. We effectively modelled a stabilised RpoS, present in small mean molecule number, in exponential phase. Stabilised RpoS in stationary phase has been found to have a degradation rate of <1/hr [125]. In our model, the stabilised RpoS molecules in exponential phase produce a stationary phase phenotype, slowing down growth. Instead of active degradation, dilution by a stochastic spurt of growth allows cells to exit the slow growth state in our model.

6.1.1 Finding a new parameter set

In the future, we might capture the active degradation of RpoS with an improved model. Two possibilities present themselves. One is to change the model's topology, another is to find a new set of parameters with the current topology that captures the observations we have already accounted for and further includes the new ClpXP observations. However, finding another set of parameters that captures the growth rate distributions of *WT* and Δ*rpoS* might prove challenging, as hundreds of simulations over several simulated hours must be run for each new set of parameters.

In Chapter 4 we explored parameter space coarsely over a range of values that seemed plausible. In hindsight, and with the updated information from the ClpXP investigation, an alternative approach may have been better - a gradient ascent search of parameter space. In this approach, we would start from a plausible set of parameters and run simulations

for it and small perturbations around these initial parameter values. For each of these solutions we would assess a success metric, such as the root-mean-square error between the simulated and experimental growth rate distributions. The change in parameter value that produced the greatest reduction in this error would be selected as the new initial parameter guess, around which parameter space would be explored. Perhaps such a search would yield a parameter set better able to capture reality. Such approaches in high-dimensional parameter spaces, like the one in our model, can get trapped in local minima of the success metric in parameter space, and miss the true solution. Nonetheless, a more sophisticated approach such as this should be considered in extensions of the work of this thesis.

6.1.2 Alternative molecular mechanism

Instead of finding new parameter values for the current model, in the future we might integrate additional molecular mechanisms in a new model to better capture reality. In our model, growth acts on RpoS by dilution. That is, when the cell grows, the concentration of RpoS decreases. It would be interesting to explore a model in which growth affects the degradation rate of RpoS positively (Fig. 6.3a). When growth is fast, RpoS would have a high degradation rate, with slow growth, RpoS degradation would be low. This might make the repressive feedback of RpoS on growth too strong. Perhaps a parametrisation of this model could be found that captures reality.

Another approach might be to consider sigma factor competition [127]. In the current model we lumped the repression of growth by RpoS into a negative Hill function. σ^{70} promotes growth when bound to the RNA polymerase core. If RpoS could supplant σ^{70} it might reduce growth [128]. However, σ^{70} binds the RNAP core with much greater affinity [129]. By upregulating a σ^{70} sequestering anti-sigma factor, Rsd [130, 131], RpoS may effectively compete with σ^{70}. A minimal model that incorporates sigma factor competition via an effective repression of σ^{70} by RpoS might reproduce reality better (Fig. 6.3).

6.2 Evolving the bet-hedging frequency

In vitro evolution of the stochastic RpoS bet-hedging strategy is an exciting direction for experiments in the future. The sudden stress used in this thesis constitutes a variable environment. We found the majority of cells grow rapidly when supplied with fresh media, and a subpopulation prepares for the eventuality of stress - the *E. coli* hedge their bets against these two environments. If cells were allowed to re-establish their population after the first stress, they would presumably be able to survive a second stress in a similar manner. We hypothesise the interval between stress application is related to the fraction of cells the *E. coli* bet on the adverse environment; the shorter the interval, the higher the fraction of cells in the survival state. By applying stress periodically to a bulk population, we expect

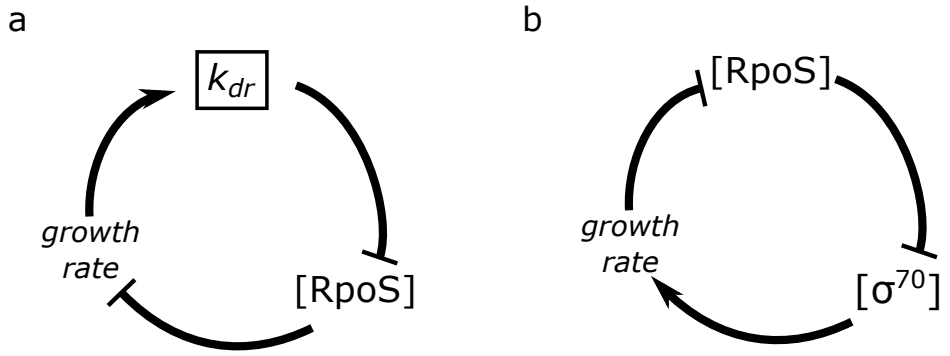

Fig. 6.3 Alternative topologies of growth-RpoS feedback loop. Growth and RpoS are in a mutual inhibition feedback loop as in the main model presented in this thesis. a, However, growth affects RpoS concentration by changing its degradation rate, k_{dr} (in addition to dilution, arrow not shown). This might more faithfully capture the degradation rates observed in literature. b, Sigma factor competition, effective model. Here, RpoS represses growth by repressing σ^{70}, which in turn is responsible for promoting growth. This is a different topology than the promoting effect of γ used in the main model (Fig. 4.1), capturing an aspect of sigma factor competition, which might lead to very different dynamics and so be better able to capture reality (Fig. 6.2).

to select a mutant strain best suited to the applied period. The nature of the mutation may reveal insights into the dynamic regulatory mechanisms of RpoS and more broadly, *E. coli* physiology. Work is under way in the lab to build the 'Oscillostat', a chemostat that generates these conditions by switching between media while maintaining a continuous culture. We anticipate exciting results from these experiments.

Outlook

We have shown bacteria can modulate their growth using heterogeneous gene expression in anticipation of an adverse environment and produced a novel toy model for analysis of such a phenomenon. We anticipate our work will have impact in the field of synthetic biology. *E. coli* is a commonly used organism in synthetic biology [132, 133], where it is standard practice to use bulk, exponential phase cultures to characterise synthetic gene circuits [134]. The cell physiology is often taken into account in deterministic models as a simple dilution effect. Our results show that exponential phase *E. coli* stochastically enter slow growth states that can last many generations with respect to the mean generation time of the population. These cells also have high RpoS activity. Thus, a subpopulation of cells may be diverting resources away from the operation of the synthetic circuit and exhibit dilution rates distinct from the population. A synthetic analogue of this phenomenon has been demonstrated previously [69], however our results apply to wild type cells, and so should be more widely applicable. Understanding the link between the coupled stochastic RpoS-growth system of this thesis and synthetic circuits promises to improve standard practice in synthetic biology. As with most creative endeavours, the most exciting outcomes

are those which we cannot foresee. We eagerly look forward to the unforeseen impact of the work presented in this thesis.

References

[1] U. Kutschera and K. J. Niklas, "The modern theory of biological evolution: an expanded synthesis," *Naturwissenschaften*, vol. 91, no. 6, pp. 255–276, 2004.

[2] R. Briggs and T. J. King, "Transplantation of living nuclei from blastula cells into enucleated frogs' eggs," *Proceedings of the National Academy of Sciences*, vol. 38, no. 5, pp. 455 – 463, 1952.

[3] J. B. Gurdon, "The Developmental Capacity of Nuclei taken from Intestinal Epithelium Cells of Feeding Tadpoles," *Journal of Embryology and Experimental Morphology*, vol. 10, no. 4, pp. 622 – 640, 1962.

[4] R. Woltereck, "Weitere experimentelle Untersuchungen über Artveränderung, speziel über das Wesen quantitativer Artunterschiede bei Daphniden.e," *Verhandlungen der deutschen zoologischen Gesellschaft*, vol. 19, pp. 110–173, 1909.

[5] K. Abley, J. C. W. Locke, and H. M. O. Leyser, "Developmental mechanisms underlying variable, invariant and plastic phenotypes," *Annals of Botany*, vol. 117, no. 5, pp. 733–748, 2016.

[6] Y.-J. Eun, P.-Y. Ho, M. Kim, S. LaRussa, L. Robert, L. D. Renner, A. Schmid, E. Garner, and A. Amir, "Archaeal cells share common size control with bacteria despite noisier growth and division," *Nature Microbiology*, vol. 3, no. 2, pp. 148–154, 2018.

[7] J. Bigger, "Treatment of Staphylococcal infections with penicillin by intermittent sterilisation," *The Lancet*, vol. 244, no. 6320, pp. 497–500, 1944.

[8] N. Q. Balaban, J. Merrin, R. Chait, L. Kowalik, and S. Leibler, "Bacterial Persistence as a Phenotypic Switch," *Science*, vol. 305, no. 5690, pp. 1622 – 1625, 2004.

[9] M. Arnoldini, I. A. Vizcarra, R. Peña-Miller, N. Stocker, M. Diard, V. Vogel, R. E. Beardmore, W.-D. Hardt, and M. Ackermann, "Bistable Expression of Virulence Genes in Salmonella Leads to the Formation of an Antibiotic-Tolerant Subpopulation," *PLOS Biology*, vol. 12, no. 8, p. e1001928, 2014.

[10] Y. Wakamoto, N. Dhar, R. Chait, K. Schneider, F. Signorino-Gelo, S. Leibler, and J. D. McKinney, "Dynamic Persistence of Antibiotic-Stressed Mycobacteria," *Science*, vol. 339, no. 6115, 2013.

[11] A. Solopova, J. van Gestel, F. J. Weissing, H. Bachmann, B. Teusink, J. Kok, and O. P. Kuipers, "Bet-hedging during bacterial diauxic shift.," *Proceedings of the National Academy of Sciences of the United States of America*, vol. 111, no. 20, 2014.

[12] J. Narula, A. Kuchina, F. Zhang, M. Fujita, G. M. Süel, and O. A. Igoshin, "Slowdown of growth controls cellular differentiation.," *Molecular systems biology*, vol. 12, no. 5, p. 871, 2016.

[13] F. Schreiber, S. Littmann, G. Lavik, S. Escrig, A. Meibom, M. M. M. Kuypers, and M. Ackermann, "Phenotypic heterogeneity driven by nutrient limitation promotes growth in fluctuating environments," *Nature Microbiology*, vol. 1, p. 16055, 2016.

[14] S. F. Levy, N. Ziv, and M. L. Siegal, "Bet Hedging in Yeast by Heterogeneous, Age-Correlated Expression of a Stress Protectant," *PLoS Biology*, vol. 10, no. 5, p. e1001325, 2012.

[15] M. Acar, J. T. Mettetal, and A. van Oudenaarden, "Stochastic switching as a survival strategy in fluctuating environments," *Nature Genetics*, vol. 40, p. 471, 2008.

[16] S. L. Spencer, S. Gaudet, J. G. Albeck, J. M. Burke, and P. K. Sorger, "Non-genetic origins of cell-to-cell variability in TRAIL-induced apoptosis," *Nature*, vol. 459, p. 428, 2009.

[17] H. M. Meyer, J. Teles, P. Formosa-Jordan, Y. Refahi, R. San-Bento, G. Ingram, H. Jönsson, J. C. W. Locke, and A. H. K. Roeder, "Fluctuations of the transcription factor ATML1 generate the pattern of giant cells in the Arabidopsis sepal," *eLife*, vol. 6, p. e19131, 2017.

[18] J. K. Graham, M. L. Smith, and A. M. Simons, "Experimental evolution of bet hedging under manipulated environmental uncertainty in Neurospora crassa," *Proceedings of the Royal Society B: Biological Sciences*, vol. 281, no. 1787, 2014.

[19] S. Stern, C. Kirst, and C. I. Bargmann, "Neuromodulatory Control of Long-Term Behavioral Patterns and Individuality across Development," *Cell*, vol. 171, no. 7, pp. 1649–1662.e10, 2017.

[20] D. L. Venable, "Bet hedging in a guild of desert annuals," *Ecology*, vol. 88, no. 5, pp. 1086–1090, 2007.

[21] S. Cortijo, Z. Aydin, S. Ahnert, and J. C. Locke, "Widespread inter-individual gene expression variability in arabidopsis thaliana," *Molecular Systems Biology*, vol. 15, no. 1, p. e8591, 2019.

[22] B. M. C. Martins and J. C. W. Locke, "Microbial individuality: how single-cell heterogeneity enables population level strategies," *Current Opinion in Microbiology*, vol. 24, pp. 104–112, 2015.

[23] T. Philippi and J. Seger, "Hedging one's evolutionary bets, revisited," *Trends in Ecology & Evolution*, vol. 4, no. 2, pp. 41–44, 1989.

[24] G. Manina, N. Dhar, and J. D. McKinney, "Stress and Host Immunity Amplify Mycobacterium tuberculosis Phenotypic Heterogeneity and Induce Nongrowing Metabolically Active Forms," *Cell Host & Microbe*, vol. 17, no. 1, pp. 32–46, 2015.

[25] A. J. Grimbergen, J. Siebring, A. Solopova, and O. P. Kuipers, "Microbial bet-hedging: the power of being different," *Current Opinion in Microbiology*, vol. 25, pp. 67–72, 2015.

[26] M. B. Elowitz, A. J. Levine, E. D. Siggia, and P. S. Swain, "Stochastic Gene Expression in a Single Cell," *Science*, vol. 297, no. 5584, pp. 1183 – 1186, 2002.

[27] P. Wang, L. Robert, J. Pelletier, W. L. Dang, F. Taddei, A. Wright, and S. Jun, "Robust growth of Escherichia coli.," *Current biology*, vol. 20, no. 12, pp. 1099–103, 2010.

[28] T. M. Norman, N. D. Lord, J. Paulsson, and R. Losick, "Memory and modularity in cell-fate decision making," *Nature*, vol. 503, p. 481, 2013.

[29] J. Park, M. Dies, Y. Lin, S. Hormoz, S. E. Smith-Unna, S. Quinodoz, M. J. Hernández-Jiménez, J. Garcia-Ojalvo, J. C. W. Locke, and M. B. Elowitz, "Molecular Time Sharing through Dynamic Pulsing in Single Cells," *Cell Systems*, 2018.

[30] T. J. Rudge, F. Federici, P. J. Steiner, A. Kan, and J. Haseloff, "Cell Polarity-Driven Instability Generates Self-Organized, Fractal Patterning of Cell Layers," *ACS Synthetic Biology*, vol. 2, no. 12, pp. 705–714, 2013.

[31] J. Sheats, B. Sclavi, M. Cosentino Lagomarsino, P. Cicuta, and K. D. Dorfman, "Role of growth rate on the orientational alignment of Escherichia coli in a slit," *Royal Society Open Science*, vol. 4, no. 6, 2017.

[32] T. Long, K. C. Tu, Y. Wang, P. Mehta, N. P. Ong, B. L. Bassler, and N. S. Wingreen, "Quantifying the Integration of Quorum-Sensing Signals with Single-Cell Resolution," *PLOS Biology*, vol. 7, no. 3, p. e1000068, 2009.

[33] R. D. Whitaker, S. Pember, B. C. Wallace, C. E. Brodley, and D. R. Walt, "Single Cell Time-resolved Quorum Responses Reveal Dependence on Cell Density and Configuration," *Journal of Biological Chemistry*, vol. 286, no. 24, pp. 21623–21632, 2011.

[34] A. Z. Rosenthal, Y. Qi, S. Hormoz, J. Park, S. H.-J. Li, and M. B. Elowitz, "Metabolic interactions between dynamic bacterial subpopulations," *eLife*, vol. 7, p. e33099, 2018.

[35] A. Prindle, J. Liu, M. Asally, S. Ly, J. Garcia-Ojalvo, and G. M. Süel, "Ion channels enable electrical communication in bacterial communities," *Nature*, vol. 527, p. 59, 2015.

[36] A. Novick and M. Weiner, "Enzyme induction as an all-or-none phenomenon," *Proceedings of the National Academy of Sciences*, vol. 43, no. 7, pp. 553 – 566, 1957.

[37] J. P. Junker and A. van Oudenaarden, "Every Cell Is Special: Genome-wide Studies Add a New Dimension to Single-Cell Biology," *Cell*, vol. 157, no. 1, pp. 8–11, 2014.

[38] J. W. Young, J. C. Locke, A. Altinok, N. Rosenfeld, T. Bacarian, P. S. Swain, E. Mjolsness, and M. B. Elowitz, "Measuring single-cell gene expression dynamics in bacteria using fluorescence time-lapse microscopy," *Nature protocols*, vol. 7, no. 1, pp. 80–88, 2012.

[39] J. C. W. Locke, J. W. Young, M. Fontes, M. J. H. Jiménez, and M. B. Elowitz, "Stochastic Pulse Regulation in Bacterial Stress Response," *Science*, vol. 334, no. 6054, pp. 366 – 369, 2011.

[40] J. W. Young, J. C. W. Locke, and M. B. Elowitz, "Rate of environmental change determines stress response specificity," *Proceedings of the National Academy of Sciences*, vol. 110, no. 10, pp. 4140–4145, 2013.

[41] L. Potvin-Trottier, S. Luro, and J. Paulsson, "Microfluidics and single-cell microscopy to study stochastic processes in bacteria," *Current Opinion in Microbiology*, vol. 43, pp. 186–192, 2018.

[42] S. Cookson, N. Ostroff, W. L. Pang, D. Volfson, and J. Hasty, "Monitoring dynamics of single-cell gene expression over multiple cell cycles," *Molecular Systems Biology*, vol. 1, no. 1, 2005.

[43] G. Ullman, M. Wallden, E. G. Marklund, A. Mahmutovic, I. Razinkov, and J. Elf, "High-throughput gene expression analysis at the level of single proteins using a microfluidic turbidostat and automated cell tracking," *Philosophical Transactions of the Royal Society B: Biological Sciences*, vol. 368, no. 1611, 2013.

[44] S. Taheri-Araghi, S. Bradde, J. T. Sauls, N. S. Hill, P. A. Levin, J. Paulsson, M. Vergassola, and S. Jun, "Cell-Size Control and Homeostasis in Bacteria," *Current Biology*, vol. 25, no. 3, pp. 385–391, 2015.

[45] Y. Tanouchi, A. Pai, H. Park, S. Huang, R. Stamatov, N. E. Buchler, and L. You, "A noisy linear map underlies oscillations in cell size and gene expression in bacteria," *Nature*, vol. 523, p. 357, 2015.

[46] L. Potvin-Trottier, N. D. Lord, G. Vinnicombe, and J. Paulsson, "Synchronous long-term oscillations in a synthetic gene circuit," *Nature*, vol. 538, p. 514, 2016.

[47] D. T. Gillespie, "Exact stochastic simulation of coupled chemical reactions," *The Journal of Physical Chemistry*, vol. 81, no. 25, pp. 2340–2361, 1977.

[48] C. V. Rao and A. P. Arkin, "Stochastic chemical kinetics and the quasi-steady-state assumption: Application to the Gillespie algorithm," *The Journal of Chemical Physics*, vol. 118, no. 11, pp. 4999–5010, 2003.

[49] M. S. Samoilov, G. Price, and A. P. Arkin, "From Fluctuations to Phenotypes: The Physiology of Noise," *Science's STKE*, vol. 2006, no. 366, 2006.

[50] N. Friedman, L. Cai, and X. S. Xie, "Linking Stochastic Dynamics to Population Distribution: An Analytical Framework of Gene Expression," *Physical Review Letters*, vol. 97, no. 16, p. 168302, 2006.

[51] Y. Taniguchi, P. J. Choi, G.-W. Li, H. Chen, M. Babu, J. Hearn, A. Emili, and X. S. Xie, "Quantifying E. coli Proteome and Transcriptome with Single-Molecule Sensitivity in Single Cells," *Science*, vol. 329, no. 5991, pp. 533 – 538, 2010.

[52] R. Milo, P. Jorgensen, U. Moran, G. Weber, and M. Springer, "BioNumbers—the database of key numbers in molecular and cell biology," *Nucleic Acids Research*, vol. 38, no. suppl_1, pp. D750–D753, 2010.

[53] R. P. Feynman, R. Leighton, M. Sands, M. A. Gottlieb, and R. Pfeiffer, "The Feynman Lectures on Physics," 2013.

[54] P. W. Anderson, "More Is Different," *Science*, vol. 177, no. 4047, pp. 393 – 396, 1972.

[55] N. V. Timoféeff-Ressovsky, K. G. Zimmer, and M. Delbrück, "On the Nature of Gene Mutation and Gene Structure," *Nachrichten von der Gesellschaft der Wissenschaften zu Gottingen*, 1935.

[56] E. Schrödinger, *What is life?* Cambridge University Press, 1944.

[57] J. D. Watson and F. H. C. Crick, "Molecular Structure of Nucleic Acids: A Structure for Deoxyribose Nucleic Acid," *Nature*, vol. 171, p. 737, 1953.

[58] M. H. F. Wilkins, A. R. Stokes, and H. R. Wilson, "Molecular Structure of Nucleic Acids: Molecular Structure of Deoxypentose Nucleic Acids," *Nature*, vol. 171, p. 738, 1953.

[59] R. E. Franklin and R. G. Gosling, "Molecular Configuration in Sodium Thymonucleate," *Nature*, vol. 171, p. 740, 1953.

[60] A. Turing, "The chemical basis of morphogenesis," *Philosophical Transactions of the Royal Society of London. Series B, Biological Sciences*, vol. 237, no. 641, pp. 37 – 72, 1952.

[61] R. Goldstein, "Coffee stains, cell receptors, and time crystals: Lessons from the old literature," *Physics Today*, vol. 71, no. 9, pp. 32–38, 2018.

[62] A. L. Hodgkin and A. F. Huxley, "A quantitative description of membrane current and its application to conduction and excitation in nerve," *Bulletin of Mathematical Biology*, vol. 52, no. 1, pp. 25–71, 1990.

[63] A. J. Lotka, "Analytical Note on Certain Rhythmic Relations in Organic Systems," *Proceedings of the National Academy of Sciences*, vol. 6, no. 7, pp. 410 – 415, 1920.

[64] L. S. Tsimring, "Noise in biology," *Reports on Progress in Physics*, vol. 77, no. 2, p. 26601, 2014.

[65] D. T. Gillespie, "A general method for numerically simulating the stochastic time evolution of coupled chemical reactions," *Journal of Computational Physics*, vol. 22, no. 4, pp. 403–434, 1976.

[66] SRI International, "EcoCyc E. coli Database," *ecocyc.org*, 2018.

[67] A. Battesti, N. Majdalani, and S. Gottesman, "The RpoS-Mediated General Stress Response in Escherichia coli," *Annual Review of Microbiology*, vol. 65, no. 1, pp. 189–213, 2011.

[68] A. Ishihama, "Building a complete image of genome regulation in the model organism Escherichia coli," *The Journal of General and Applied Microbiology*, vol. 63, no. 6, pp. 311–324, 2017.

[69] C. Tan, P. Marguet, and L. You, "Emergent bistability by a growth-modulating positive feedback circuit," *Nature Chemical Biology*, vol. 5, no. 11, pp. 842–848, 2009.

[70] D. J. Kiviet, P. Nghe, N. Walker, S. Boulineau, V. Sunderlikova, and S. J. Tans, "Stochasticity of metabolism and growth at the single-cell level," *Nature*, vol. 514, no. 7522, p. 376–379, 2014.

[71] A. S. Kennard, M. Osella, A. Javer, J. Grilli, P. Nghe, S. J. Tans, P. Cicuta, and M. Cosentino Lagomarsino, "Individuality and universality in the growth-division laws of single E. coli cells," *Physical Review E*, vol. 93, no. 1, p. 12408, 2016.

[72] P. C. Loewen, B. L. Triggs, C. S. George, and B. E. Hrabarchuk, "Genetic mapping of katG, a locus that affects synthesis of the bifunctional catalase-peroxidase hydroperoxidase I in Escherichia coli.," *Journal of Bacteriology*, vol. 162, no. 2, pp. 661–667, 1985.

[73] M. F. Christman, R. W. Morgan, F. S. Jacobson, and B. N. Ames, "Positive control of a regulon for defenses against oxidative stress and some heat-shock proteins in Salmonella typhimurium," *Cell*, vol. 41, no. 3, pp. 753–762, 1985.

[74] P. C. Loewen and R. Hengge-Aronis, "The Role of the Sigma Factor sigmas (KatF) in Bacterial Global Regulation," *Annual Review of Microbiology*, vol. 48, no. 1, pp. 53–80, 1994.

[75] R. Lange and R. Hengge-Aronis, "Identification of a central regulator of stationary-phase gene expression in Escherichia coli," *Molecular Microbiology*, vol. 5, no. 1, pp. 49–59, 1991.

[76] H. E. Schellhorn and H. M. Hassan, "Transcriptional regulation of katE in Escherichia coli K-12.," *Journal of Bacteriology*, vol. 170, no. 9, pp. 4286–4292, 1988.

[77] R. Hengge-Aronis, R. Lange, N. Henneberg, and D. Fischer, "Osmotic regulation of rpoS-dependent genes in Escherichia coli.," *Journal of Bacteriology*, vol. 175, no. 1, pp. 259–265, 1993.

[78] M. R. Mulvey and P. C. Loewen, "Nucleotide sequence of katF of Escherichia coli suggests KatF protein is a novel sigma transcription factor.," *Nucleic Acids Research*, vol. 17, no. 23, pp. 9979–9991, 1989.

[79] B.-K. Cho, D. Kim, E. M. Knight, K. Zengler, and B. O. Palsson, "Genome-scale reconstruction of the sigma factor network in Escherichia coli: topology and functional states," *BMC Biology*, vol. 12, no. 1, p. 4, 2014.

[80] T. Dong and H. E. Schellhorn, "Control of RpoS in global gene expression of Escherichia coli in minimal media," *Molecular Genetics and Genomics*, vol. 281, no. 1, pp. 19–33, 2009.

[81] G. Chen and H. E. Schellhorn, "Controlled induction of the RpoS regulon in Escherichia coli, using an RpoS-expressing plasmid," *Canadian Journal of Microbiology*, vol. 49, no. 12, pp. 733–740, 2003.

[82] J. Hurwitz, "The Discovery of RNA Polymerase," *Journal of Biological Chemistry*, vol. 280, no. 52, pp. 42477–42485, 2005.

[83] R. R. Burgess, A. A. Travers, J. J. Dunn, and E. K. F. Bautz, "Factor Stimulating Transcription by RNA Polymerase," *Nature*, vol. 221, p. 43, 1969.

[84] P. C. Loewen, "Isolation of catalase-deficient Escherichia coli mutants and genetic mapping of katE, a locus that affects catalase activity.," *Journal of Bacteriology*, vol. 157, no. 2, pp. 622–626, 1984.

[85] P. C. Loewen, J. Switala, and B. L. Triggs-Raine, "Catalases HPI and HPII in Escherichia coli are induced independently," *Archives of Biochemistry and Biophysics*, vol. 243, no. 1, pp. 144–149, 1985.

[86] R. G. Groat, J. E. Schultz, E. Zychlinsky, A. Bockman, and A. Matin, "Starvation proteins in Escherichia coli: kinetics of synthesis and role in starvation survival.," *Journal of Bacteriology*, vol. 168, no. 2, pp. 486 – 493, 1986.

[87] E. Touati, E. Dassa, and P. L. Boquet, "Pleiotropic mutations in appR reduce pH 2.5 acid phosphatase expression and restore succinate utilisation in CRP-deficient strains of Escherichia coli," *Molecular and General Genetics MGG*, vol. 202, no. 2, pp. 257–264, 1986.

[88] D. E. Jenkins, J. E. Schultz, and A. Matin, "Starvation-induced cross protection against heat or H2O2 challenge in Escherichia coli.," *Journal of Bacteriology*, vol. 170, no. 9, pp. 3910–3914, 1988.

[89] K. Tanaka, Y. Takayanagi, N. Fujita, A. Ishihama, and H. Takahashi, "Heterogeneity of the principal sigma factor in Escherichia coli: the rpoS gene product, sigma 38, is a second principal sigma factor of RNA polymerase in stationary-phase Escherichia coli," *Proceedings of the National Academy of Sciences*, vol. 90, no. 17, pp. 3511 – 3515, 1993.

[90] R. Lange and R. Hengge-Aronis, "The cellular concentration of the sigma S subunit of RNA polymerase in Escherichia coli is controlled at the levels of transcription, translation, and protein stability.," *Genes & Development*, vol. 8, no. 13, pp. 1600–1612, 1994.

[91] K. Tanaka, S. Kusano, N. Fujita, A. Ishihama, and H. Takahashi, "Promoter determinants for Escherichia coli RNA polymerase holoenzyme containing sigma 38 (the rpoS gene product).," *Nucleic Acids Research*, vol. 23, no. 5, pp. 827–834, 1995.

[92] J. E. Lane-Claypon, "Multiplication of Bacteria and the Influence of Temperature and some other Conditions thereon," *The Journal of hygiene*, vol. 9, no. 2, pp. 239–248, 1909.

[93] R. E. Buchanan, "Life Phases in a Bacterial Culture," *The Journal of Infectious Diseases*, vol. 23, no. 2, pp. 109–125, 1918.

[94] S. Cooper, "On the fiftieth anniversary of the Schaechter, Maaløe, Kjeldgaard experiments: implications for cell-cycle and cell-growth control," *BioEssays*, vol. 30, no. 10, pp. 1019–1024, 2008.

[95] M. Schaechter, O. MaalOe, and N. O. Kjeldgaard, "Dependency on Medium and Temperature of Cell Size and Chemical Composition during Balanced Growth of Salmonella typhimurium," *Journal of General Microbiology*, vol. 19, no. 3, pp. 592–606, 1958.

[96] T. Lu, D. Volfson, L. Tsimring, and J. Hasty, "Cellular growth and division in the Gillespie algorithm," *IEE Proceedings - Systems Biology*, vol. 1, no. 1, pp. 121–128, 2004.

[97] A. Zaslaver, A. Bren, M. Ronen, S. Itzkovitz, I. Kikoin, S. Shavit, W. Liebermeister, M. G. Surette, and U. Alon, "A comprehensive library of fluorescent transcriptional reporters for Escherichia coli," *Nature Methods*, vol. 3, no. 8, pp. 623–628, 2006.

[98] T. Baba, T. Ara, M. Hasegawa, Y. Takai, Y. Okumura, M. Baba, K. A. Datsenko, M. Tomita, B. L. Wanner, and H. Mori, "Construction of Escherichia coli K-12 in-frame, single-gene knockout mutants: the Keio collection," *Molecular Systems Biology*, vol. 2, 2006.

[99] A. Harms, C. Fino, M. A. Sørensen, S. Semsey, and K. Gerdes, "Prophages and Growth Dynamics Confound Experimental Results with Antibiotic-Tolerant Persister Cells," *mBio*, vol. 8, no. 6, 2017.

[100] K. Potrykus, H. Murphy, N. Philippe, and M. Cashel, "ppGpp is the major source of growth rate control in E. coli," *Environmental Microbiology*, vol. 13, no. 3, pp. 563–575, 2010.

[101] T. Knight, "TOP10 chemically competent cells," *openwetware.org/wiki*, 2013.

[102] EMD Millipore Corporation, "CellASIC ONIX B04A-03 Microfluidic Bacteria Plates," 2014.

[103] P. J. Lee, T. A. Gaige, and P. J. Hung, "Dynamic cell culture: a microfluidic function generator for live cell microscopy," *Lab on a Chip*, vol. 9, no. 1, pp. 164–166, 2009.

[104] P. Thomas, "Single-cell histories in growing populations: relating physiological variability to population growth," *bioRxiv doi: 10.1101/100495*, 2017.

[105] J. T. Wade and D. C. Grainger, "Spurious transcription and its impact on cell function," *Transcription*, vol. 9, no. 3, pp. 182–189, 2018.

[106] W. W. Ward, C. W. Cody, R. C. Hart, and M. J. Cormier, "Spectrophotometric identity of the energy transfer chromophores in Renilla and Aequorea green-fluorescent protein," *Photochemistry and Photobiology*, vol. 31, no. 6, pp. 611–615, 1980.

[107] J. Paulsson and M. Ehrenberg, "Noise in a minimal regulatory network: plasmid copy number control," *Quarterly Reviews of Biophysics*, vol. 34, no. 1, pp. 1–59, 2001.

[108] D. Yang, A. D. Jennings, E. Borrego, S. T. Retterer, and J. Männik, "Analysis of Factors Limiting Bacterial Growth in PDMS Mother Machine Devices ," *Frontiers in Microbiology*, vol. 9, 2018.

[109] S. Klumpp, Z. Zhang, and T. Hwa, "Growth rate-dependent global effects on gene expression in bacteria," *Cell*, vol. 139, pp. 1366–1375, 2009.

[110] J. Mayer, K. Khairy, and J. Howard, "Drawing an elephant with four complex parameters," *American Journal of Physics*, vol. 78, no. 6, pp. 648–649, 2010.

[111] S. Klumpp and T. Hwa, "Growth-rate-dependent partitioning of RNA polymerases in bacteria," *Proceedings of the National Academy of Sciences*, vol. 105, pp. 20245–20250, 2008.

[112] M. Scott, C. W. Gunderson, E. M. Mateescu, Z. Zhang, and T. Hwa, "Interdependence of Cell Growth and Gene Expression: Origins and Consequences," *Science*, vol. 330, no. 6007, pp. 1099 – 1102, 2010.

[113] P. Thomas, G. Terradot, V. Danos, and A. Y. Weiße, "Sources, propagation and consequences of stochasticity in cellular growth," *Nature Communications*, vol. 9, no. 1, p. 4528, 2018.

[114] J. L. Radzikowski, S. Vedelaar, D. Siegel, Á. D. Ortega, A. Schmidt, and M. Heinemann, "Bacterial persistence is an active σS stress response to metabolic flux limitation.," *Molecular Systems Biology*, vol. 12, no. 882, 2016.

[115] A. Bougdour and S. Gottesman, "ppGpp regulation of RpoS degradation via anti-adaptor protein IraP," *Proceedings of the National Academy of Sciences*, vol. 104, no. 31, pp. 12896 – 12901, 2007.

[116] M. F. Traxler, V. M. Zacharia, S. Marquardt, S. M. Summers, H.-T. Nguyen, S. E. Stark, and T. Conway, "Discretely calibrated regulatory loops controlled by ppGpp partition gene induction across the 'feast to famine' gradient in Escherichia coli," *Molecular Microbiology*, vol. 79, no. 4, pp. 830–845, 2010.

[117] S. Metzger, G. Schreiber, E. Aizenman, M. Cashel, and G. Glaser, "Characterization of the relA1 mutation and a comparison of relA1 with new relA null alleles in Escherichia coli.," *Journal of Biological Chemistry*, vol. 264, no. 35, pp. 21146–21152, 1989.

[118] H. Xiao, M. Kalman, K. Ikehara, S. Zemel, G. Glaser, and M. Cashel, "Residual guanosine 3',5'-bispyrophosphate synthetic activity of relA null mutants can be eliminated by spoT null mutations.," *Journal of Biological Chemistry*, vol. 266, no. 9, pp. 5980–5990, 1991.

[119] L. C. Seaver and J. A. Imlay, "Alkyl Hydroperoxide Reductase Is the Primary Scavenger of Endogenous Hydrogen Peroxide in Escherichia coli ," *Journal of Bacteriology*, vol. 183, no. 24, pp. 7173–7181, 2001.

[120] N. Chowdhury, B. W. Kwan, and T. K. Wood, "Persistence Increases in the Absence of the Alarmone Guanosine Tetraphosphate by Reducing Cell Growth," *Scientific Reports*, vol. 6, p. 20519, 2016.

[121] J. Feng, D. A. Kessler, E. Ben-Jacob, and H. Levine, "Growth feedback as a basis for persister bistability," *Proceedings of the National Academy of Sciences*, vol. 111, no. 1, pp. 544 – 549, 2014.

[122] K. Mitosch, G. Rieckh, and T. Bollenbach, "Noisy Response to Antibiotic Stress Predicts Subsequent Single-Cell Survival in an Acidic Environment," *Cell Systems*, vol. 4, no. 4, pp. 393–403.e5, 2018.

[123] A. Muffler, D. Fischer, S. Altuvia, G. Storz, and R. Hengge-Aronis, "The response regulator RssB controls stability of the sigma(S) subunit of RNA polymerase in Escherichia coli.," *The EMBO Journal*, vol. 15, no. 6, pp. 1333–1339, 1996.

[124] L. A. Pratt and T. J. Silhavy, "The response regulator SprE controls the stability of RpoS.," *Proceedings of the National Academy of Sciences of the United States of America*, vol. 93, no. 6, pp. 2488–2492, 1996.

[125] H. I. Zgurskaya, M. Keyhan, and A. Matin, "The σS level in starving Escherichia coli cells increases solely as a result of its increased stability, despite decreased synthesis," *Molecular Microbiology*, vol. 24, no. 3, pp. 643–651, 1997.

[126] T. Schweder, K. H. Lee, O. Lomovskaya, and A. Matin, "Regulation of Escherichia coli starvation sigma factor (sigma s) by ClpXP protease.," *Journal of Bacteriology*, vol. 178, no. 2, pp. 470–476, 1996.

[127] A. Farewell, K. Kvint, and T. Nyström, "Negative regulation by RpoS: a case of sigma factor competition," *Molecular Microbiology*, vol. 29, no. 4, pp. 1039–1051, 1998.

[128] M. Mauri and S. Klumpp, "A Model for Sigma Factor Competition in Bacterial Cells," *PLoS Computational Biology*, vol. 10, no. 10, 2014.

[129] H. Maeda, N. Fujita, and A. Ishihama, "Competition among seven Escherichia coli σ subunits: relative binding affinities to the core RNA polymerase," *Nucleic Acids Research*, vol. 28, no. 18, pp. 3497–3503, 2000.

[130] M. Jishage and A. Ishihama, "A stationary phase protein in Escherichia coli with binding activity to the major σ subunit of RNA polymerase," *Proceedings of the National Academy of Sciences*, vol. 95, no. 9, pp. 4953–4958, 1998.

[131] M. Jishage and A. Ishihama, "Transcriptional Organization and In Vivo Role of theEscherichia coli rsd Gene, Encoding the Regulator of RNA Polymerase Sigma D," *Journal of Bacteriology*, vol. 181, no. 12, pp. 3768–3776, 1999.

[132] M. B. Elowitz and S. Leibler, "A synthetic oscillatory network of transcriptional regulators," *Nature*, vol. 403, p. 335, 2000.

[133] T. S. Gardner, C. R. Cantor, and J. J. Collins, "Construction of a genetic toggle switch in Escherichia coli," *Nature*, vol. 403, p. 339, 2000.

[134] P. K. Grant, N. Dalchau, J. R. Brown, F. Federici, T. J. Rudge, B. Yordanov, O. Patange, A. Phillips, and J. Haseloff, "Orthogonal intercellular signaling for programmed spatial behavior.," *Molecular systems biology*, vol. 12, no. 1, p. 849, 2016.

Appendix A

Code for stochastic model

Below is the detailed code of the coupled Gillespie and growth simulator. The inputs and outputs are named in a self explanatory manner.

```
function [grO,cellLO,rpoSnO,rpoScO,sig70nO,sig70cO,cyc] = ...
    GillGrSim_v4_NoDetailsSampled(kdrpoS,krpoS,kdsig70,ksig70,sinit,...
    rinit,gmax,adderVal,nrpoS,rpoSHalf,nsig70,sigHalf,offset,...
    numsims,numtimes,timestep,storestep)
%% Admin Parameters
numtimesInternal = numtimes/timestep;
numstore = ceil(numtimesInternal/storestep);

if storestep == 1
    storeAllFlag = 1;
else
    storeAllFlag = 0;
end

grO = zeros(numsims, numstore);
cellLO = zeros(numsims, numstore);
rpoSnO = zeros(numsims, numstore);
sig70nO = zeros(numsims, numstore);
rpoScO = zeros(numsims, numstore);
sig70cO = zeros(numsims, numstore);

%% Running simulation
clear simulation
for k = 1:numsims
    %initializing first step:
```

```
    cellL = 1;
    rpoS = rinit;
    sig70 = sinit;
    totalAdded = 0;
    tlast = 1;
    cycn = 1;
    savestep = 1;

    for t = 1:numtimesInternal
        %% first run the rpoS Gillespie:
        Gt = 0;
        while Gt<timestep
            %calculate propensity vector
            a = [ksig70 sig70*kdsig70 krpoS rpoS*kdrpoS];
            acum = cumsum(a);
            a0 = sum(a);

            %generate random numbers
            r1 = rand(1);
            r2 = rand(1);

            %when will the next reaction happen:
            tnext = log(1/r1)/a0;

            %Check if Gillespie time exceeds growth time?
            Gt = Gt+tnext;
            if Gt<timestep

                %which reaction will occur:
                if r2*a0 <= acum(1)
                    sig70 = sig70 + 1;
                elseif r2*a0 <= acum(2)
                    if sig70 ~=0;
                        sig70 = sig70 -1;
                    end
                elseif r2*a0 <= acum(3)
                    rpoS = rpoS + 1;
                elseif r2*a0 <= acum(4)
                    if rpoS ~=0;
```

```
                    rpoS = rpoS -1;
                end
            end

        end
    end

    %% concentration of the molecules
    rpoSc = rpoS/cellL;
    sig70c = sig70/cellL;

    %% Update growth rate
    gr = (gmax/(1+(sigHalf/sig70c)^nsig70))*...
        ((1-offset)/(1+(rpoSHalf/rpoSc)^nrpoS)+offset);


    %% update length of cell and rpoS concentration
    addLength = gr*cellL*timestep;
    %adder rule:
    if totalAdded >= adderVal
        cellL = (cellL + addLength)/2;
        totalAdded = 0;
        rpoS = floor(rpoS/2);
        sig70 = floor(sig70/2);
        cyc(k).cyc(cycn) = (t-tlast)*timestep;
        tlast = t;
        cycn = cycn+1;
    else
        cellL = cellL + addLength;
        totalAdded = totalAdded + addLength;
    end

    %store values every storestep'th iteration of simulation
    if mod(t,storestep) == 1 || storeAllFlag == 1
        grO(k,savestep) = gr;
        cellLO(k,savestep) = cellL;
        rpoSnO(k,savestep) = rpoS;
        sig70nO(k,savestep) = sig70;
        rpoScO(k,savestep) = rpoS/cellL;
```

```
104             sig70cO(k,savestep) = sig70/cellL;
105             savestep = savestep + 1;
106         end
107     end
108 
109 end
110 
111 %catch when there is no growth
112 if ~exist('cyc')
113     cyc(1).cyc(1) = 0;
114 end
```